SOLID STATE ELECTROCHEMICAL STUDIES AND ASSESSMENT OF III-V COMPOUND SEMICONDUCTOR SYSTEMS

By

SUDHANSHU MISRA

A DISSERTATION PRESENTED TO THE GRADUATE SCHOOL
OF THE UNIVERSITY OF FLORIDA IN PARTIAL FULFILLMENT
OF THE REQUIREMENTS FOR THE DEGREE OF
DOCTOR OF PHILOSOPHY

UNIVERSITY OF FLORIDA

1998

ACKNOWLEDGEMENTS

I would like to thank my research supervisor, Dr. Timothy J. Anderson, for his guidance and support all throughout this doctoral research. I am also grateful to Dr. Ursula R. Kattner at National Institute of Standards and Technology, Gaithersburg, for her valuable input during the optimizations and calculations performed in this study. It was a pleasure and a learning experience working on experiments on Sb-Te System with Dr. Yves Feutelais associated with Laboratoire de Chimie Minerale II, Faculte de Pharmacie at Chatenay-Malabry in France. I am thankful to Dr. Ranga Narayanan and Dr. Mark E. Orazem for their constant interest and involvement in the experiments conducted during this research.

TABLE OF CONTENTS

page

ACKNOWLEDGEMENTS iii

ABSTRACT v

CHAPTERS

1 INTRODUCTION 1

Phase Diagrams and Their Importance to Compound Semiconductors 1
Typical Phase Diagrams of III-V Systems 3
Thermodynamic Information From Phase Diagrams 8
Solid State Activity Measurements 10
Solid Electrolytes 11
Principle of Electrochemical Cells 12

2 EXPERIMENTAL STUDIES 16

Description of Apparatus and Measurement Techniques 16
Experimental Results in Binary Systems 25
Ga-As System 25
Standard Gibbs Energy of Formation of GaAs (s) 28
In-As System 33
Activity of In Along the In-rich Liquidus 40
Standard Gibbs Energy of Formation of InAs (s) 41
Sb-Te System 49
Activity of Sb in Sb-Te Melts 53
Experimental Results in Ternary Systems 61
Activity of Ga in In-rich Ternary Liquid $Ga_xIn_yAs_{1-x-y}$ Solutions 62
Activity of GaAs (s) in the Pseudobinary Section GaAs-InAs 66

3 ASSESSMENT STUDIES..... 73

Assessment Procedure (Lukas Program)..... 73
Assessment of Binary Systems..... 77
Ga-As Assessment..... 77
In-As Assessment..... 83
In-Sb Assessment.....105
Ga-Sb Assessment.....124
Assessment of Ternary Systems.....133
Ga-Sb-As Assessment.....133
In-Sb-As Assessment.....139

4 CONCLUSIONS.....151

REFERENCES.....154

BIOGRAPHICAL SKETCH.....171

Abstract of Dissertation Presented to the Graduate School of the University of Florida in Partial Fulfillment of the Requirements for the Degree of Doctor of Philosophy

SOLID STATE ELECTROCHEMICAL STUDIES AND ASSESSMENT OF III-V COMPOUND SEMICONDUCTOR SYSTEMS

By

Sudhanshu Misra

December 1998

Chairman: Dr. Timothy J. Anderson
Major Department: Chemical Engineering

Thermodynamic properties have been determined for compound semiconductors by solid state electrochemical technique and used successfully in making assessments to the available data on these systems. The measurement technique used a solid electrolyte and two custom designed unique cell configurations to maintain stable open circuit electromotive force (emf) values, and minimize volatile V-component (-As, -Sb) loss due to vaporization during the experimental stage.

The experimental data on Gibbs energy data for the binary systems Ga-As, In-As and Sb-Te are the first of their kind and are very important for a good understanding of their thermodynamic properties and their alloys. In addition to these systems, In-Sb and Ga-Sb systems were also assessed. The assessments of the III-V binary systems were used as start points for thermodynamic predictions into the two ternary systems, namely

Ga-Sb-As and In-Sb-As. Solid state emf measurements were also conducted on the ternary Ga-In-As to understand the thermodynamic characteristics in the pseudobinary section of the GaAs-InAs phase diagram. The experiments confirmed the presence of a miscibility gap in the $Ga_xIn_{1-x}As$ solid phase.

CHAPTER 1
INTRODUCTION

Phase Diagrams and Their Importance to Compound Semiconductors

Phase diagrams are graphical representations of the relations between state parameters and the delineation of phase fields within this parameter space. Phase diagrams are useful in selecting initial compositions and subsequent processing conditions for thermal processes including the separation and purification of materials since phase diagrams are a graphical representation of the conditions of phase equilibria. Extensive thermodynamic information can be extracted from them. A thermodynamic description of a phase is related to the interaction of the species and the structure of the phase at the molecular level. Thus phase diagrams can be calculated from known thermodynamic phase functions and, conversely, thermodynamic properties and phase structure characteristics can be obtained from phase equilibria data.

Since temperature, pressure and concentration are typically measurable and controllable state parameters in many processes; the Gibbs energy is the important thermodynamic function, the value of this function being a minimum at equilibrium for constant temperature, pressure and overall composition. Graphically, the compositions of two phases in equilibrium at a certain temperature and pressure is determined by the common tangent to the two curves representing the concentration-dependent Gibbs energy of each phase. This is a graphical interpretation of the equilibrium condition that

the chemical potentials of the species in the coexisting phases are equal. It is noted that the pressure dependence in solid-liquid phase equilibria problems is often assumed negligible for pressures less than 10^7 MPa.

Of interest to the present study are the class of semiconductors constituted by the elements from the Groups III and V columns of the periodic table, and termed III-V compound semiconductors. These compounds exhibit extended miscible substitutional solid solutions when mixed on the same sublattice, thereby allowing the semiconductor device designer control of the lattice parameter and electrical or optical characteristics of the material to conform to the required device specification. The increased number of elements in III-V compounds as opposed to the elemental nature of Si, however, make their property characterization and processing technology more difficult.

The attractive characteristics of compound semiconductors include the possibility of direct bandgap energy and the concomitant high electron mobility. As a result, these materials are important in high speed electronic and optoelectronic device applications. Furthermore, these materials offer a broad selection of optical and electrical properties that are often superior to those of elemental Si. Group III-V compounds have been used in a wide range of applications as the host semiconductor material, including high-speed, optoelectronic and integrated optical devices [Hei78, Sew75 and Yos75]. In particular, (In, Ga) Sb and (In, Ga) As form important constituents in the solid solutions used for long wavelength photodetectors, light emitting diodes, diode lasers and heterogeneous bipolar transistors. Moreover, the semiconductor InSb has the lowest bandgap energy (E_g = 0.18 eV) and highest room temperature electron mobility ($\mu_n = 10^5$ cm^2/V-s) of any III-V compound semiconductor [Wel52, Wel53 and Bre54].

The processes for fabrication of compound semiconductor devices often require near equilibrium contact between solid and liquid phases (e.g., bulk crystal growth, liquid phase epitaxy) or between solid and vapor phases (e.g., chemical vapor deposition, rapid thermal annealing). Phase diagram and thermodynamic property functions are important in specifying the necessary boundary conditions in the analysis of such device processing steps. It is observed that the optical and electrical properties of compound semiconductors are sensitive to the processing conditions. As an example, variations in the melt stoichiometry during bulk crystal growth or in the vapor phase III/V input molar ratio during CVD significantly changes the electrical properties of the grown material. This implies that extremely accurate thermodynamic properties and phase relations are sometimes necessary for their meaningful application to process analysis.

Typical Phase Diagrams of III-V Systems

A typical III-V binary phase diagram is shown in Figure 1-1. It is noted that pure solid elements show negligible solubility of the other element and each half of the phase diagram is termed simple eutectic. In this phase diagram, the eutectic towards the Group III-rich region of the phase diagram is shown as being nearly degenerate, which means that the eutectic composition is so close to pure Group III component that it cannot be depicted in the figure. The eutectic composition is determined in the first order by the differences between the compound and pure component melting temperatures, and modified by the liquid solution behavior and component thermodynamic properties. For example, the relatively close melting temperatures of GaSb and Sb produces a eutectic composition that is relatively rich in Ga. The eutectic compositions in the Group V-rich

portion of the III-As or III-P phase diagrams, however, can be experimentally difficult to determine because of the experimental problems encountered by high vapor pressures.

The upper curve in Figure 1-1 stretching across the limits of the phase diagram is the liquidus curve which is a boundary of the two-phase region (liquid + AB) and separates the pure liquid phase from the two-phase region. The vertical line drawn at the composition 0.5 atom fraction of the phase diagram represents the position of the essentially stoichiometric compound AB (i.e., a line compound). In actuality the compound AB in III-V systems is a solid solution phase with negligible extent of solubility, and, when comparing this boundary to other phase boundaries, AB is treated as a line compound. Although the solid solution extent of the line compound has negligible influence on the other boundary positions, the extent is of utmost importance to the semiconducting properties. Any deviation in the ideal stoichiometry of the III-V compound $A_{0.5}$ $B_{0.5}$ in this region of solid solution (typically of the order 10^{-3} to 10^{-5} mole fraction) is the result of native point defects. Many of these defects are ionic and can significantly change the impurity behavior and electrical and optical properties of these materials. Thus, by being able to accurately describe the thermodynamics of these solid solutions it is possible to predict bulk phase equilibria as well as the stability and extent of solid solution.

Figure 1-2(a) shows a typical III-III'-V ternary phase diagram, where A and B are the group III elements. The vertical plane through the elements A and C is the binary III-V limit, while a similar plane through the points B and C is the binary III'-V limit. Both the binary phase diagrams are of the type just discussed and as shown in Figure 1-1. The

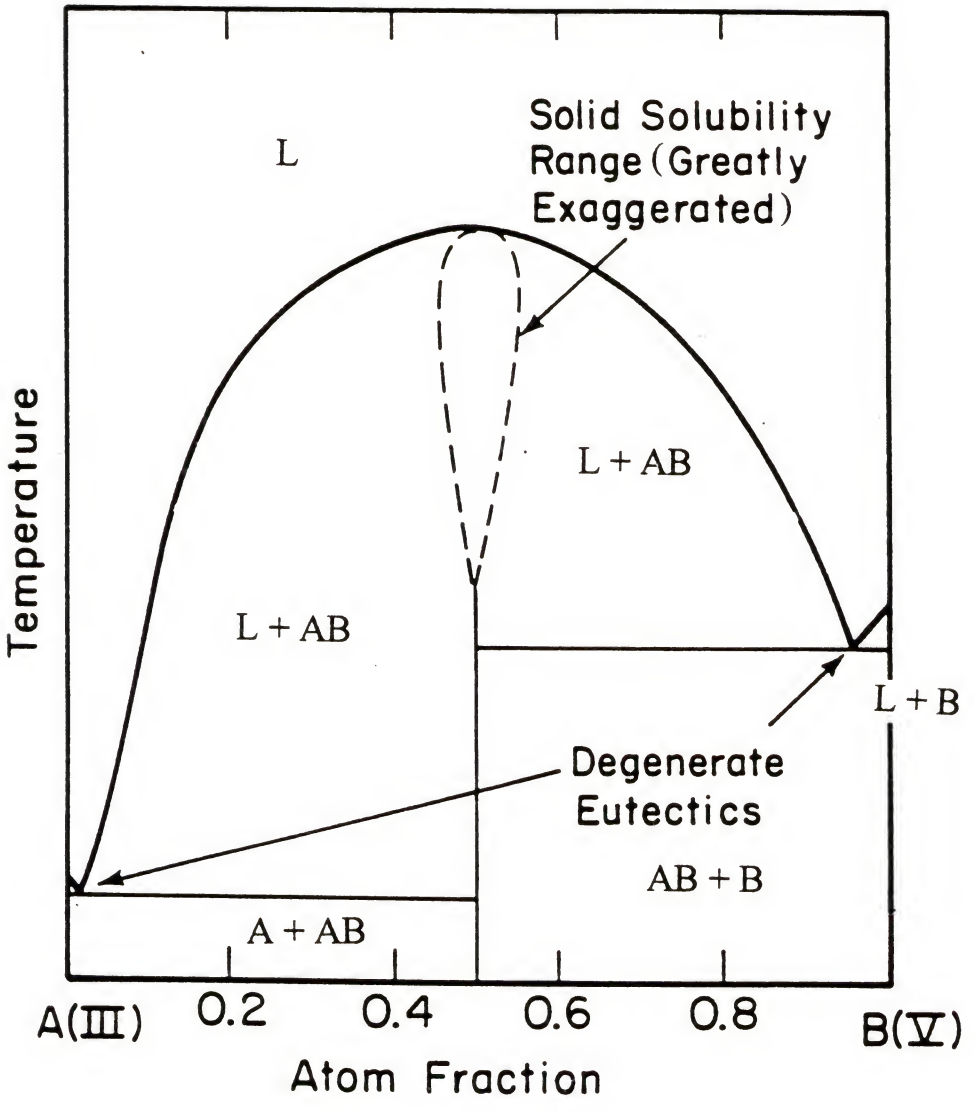

Figure 1-1. Schematic III-V binary phase diagram.

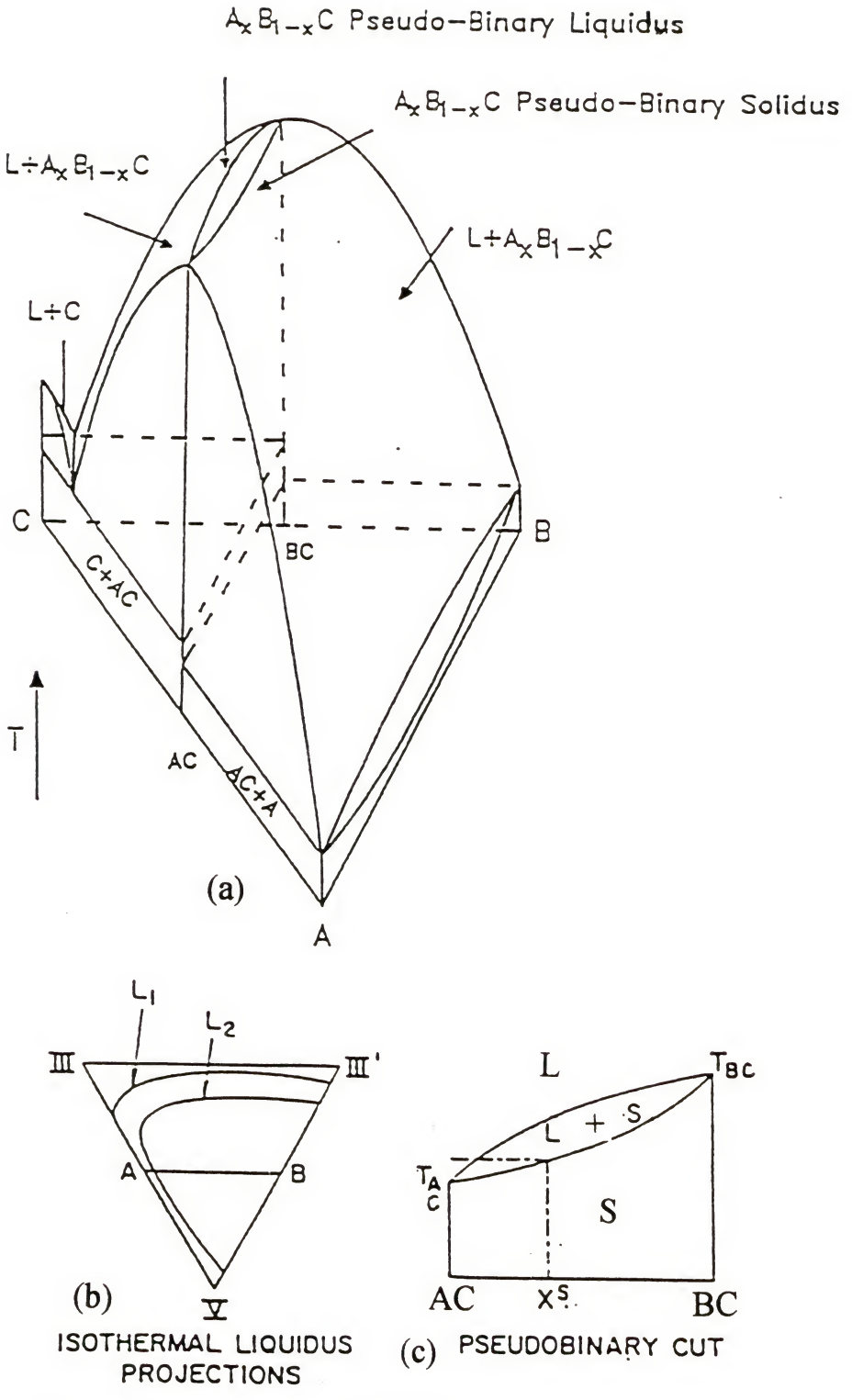

Figure 1-2(a). Schematic III-III'-V ternary phase diagram,
(b). Isothermal liquidus projections L1 and L2,
(c). Pseudobinary AC-BC phase diagram.

vertical plane passing through the points A and B represents the III-III' binary systems which exhibit a range of phase diagram types. The surface enveloping the entire ternary diagram is the liquidus surface, which denotes the upper temperature limit of the two phase (liquid +solid phase/pure element) region. The eutectic valley located in the Groups III/III'-rich region of the phase diagram is almost degenerate, while the region in the phase diagram towards the Group V-rich (i.e., As, Sb, P) is not well characterized owing to problems associated with the high vapor pressures of Group V elements at those conditions of temperature and composition.

As in the case of binary phase diagrams, the vertical lines at the $x_V = 0.5$ composition in the binary subsystems A-C and B-C are the locations of the line compound phases, IIIV and III'V respectively. The vertical plane passing through the compounds AC and BC includes a region of solid solution between IIIV and III'V, and is termed the pseudobinary cut. When the ternary phase diagram is cut by a vertical plane through AC and BC and viewed from the side, the typical pseudobinary phase diagram is seen as comprising three regions sandwiching a 'cigar' shaped two-phase region representing solid-liquid equilibrium (isomorphous phase diagram). The phase above the two-phase region is the ternary liquid solution of fixed $x_V = 0.5$, while that below the lower curve of the two phase region is the pseudobinary solid solution. An understanding of the correlation between structural properties, band structures, and the phase diagram will aid in evaluating these alloys for use in long wavelength IR material (LWIR), lasers, photodetectors, and other device applications.

The systems of specific interest to this study are the binary Group III (Ga, In) arsenides and antimonides, and the associated ternaries (Ga-In-As, Ga-Sb-As and In-Sb-

As). The binary sytem Sb-Te is also addressed in this study because of its application as an eraseable optical storage and recording media. The motivation of this research is to provide accurate thermodynamic information for the liquid and solid phases of these technologically important semiconductor systems. This information will be helpful to understand the interactions in the alloys at the molecular level, and to identify the design parameters (e.g., temperature, pressure, compositions, molar flow ratios, growth conditions) at the macroscopic level for material processing. Accurate thermodynamic properties are essential in selection of starting materials (source) and in the estimation of extents of chemical reactions. Of particular importance are the solid-gas phase reactions that occur during chemical vapor deposition (CVD) and their manifestation in a CVD phase diagram. These are guiding tools for establishing the boundaries of process operation to achieve certain film properties.

Thermodynamic Information From Phase Diagrams

Phase diagrams can be thought of as graphical solutions of the conditions of phase equilibria and metaphorically as storage media of thermodynamic properties. It is often the case that several experimental determinations of different thermochemical properties and phase diagrams exist. The relationships of thermodynamics provide a means to check the consistency of the experimental thermochemical and phase diagram data. This methodology of performing consistency tests by the process of comparing predictions based on one set of data (e.g., phase diagram) to experimental data based on other sets (e.g., enthalpy or Gibbs energy data) and vice versa, has been illustrated by Aselage [Ase85].

Compound semiconductors of interest in this study pose a situation where phase diagram data is readily avaliable in literature, however thermodynamic properties such as vapor pressure and enthalpy data is not so accurately available. For this reason, estimates have been made by numerous authors to calculate thermodynamic properties from phase diagram data. Such estimates coupled with little experimental data on these systems render the understanding of the thermodynamic properties difficult. The large uncertainities involved in such estimates make it challenging to reliably perform experiments for measurements of thermodynamic properties.

The data by Hoshino et al. [Hos65] on In-Sb system indicate that the In-Sb solution is not subregular as earlier assumed, and the concentration dependence of the exchange energy is nonlinear. Regular solution behavior was assumed in the In-As solutions near the melting temperature of InAs [Kar75]. In the Ga-Sb system, the experimental values of excess heat and entropy of solutions have not been well represented. The current predictions on the heat of mixing differed from the data given by Predel and Stein [Pre71] and Gambino and Bros [Gam75] by the order of 2 kJ/mol. The excess entropy differed from the data of Bergman et al. [Ber74] by about 2.5 J/mol-K. The values of heat and entropy of formation of solid InAs, GaAs and GaSb have not been theoretically well represented [Glu72, Luk77, Pan72, Gor75, Yam88 and Fol58]. In particular, the data on In-As and Ga-As in the As-rich segment of the phase diagram is lacking, and the values that are available are subject to significant dispersion when compared with each other. Tmar et al. [Tma84] addressed the discrepancy in data for In-As and Ga-As systems due to lack of information on gaseous phase composition and the species contribution to the total pressure in the gaseous phase. Both As_2 and As_4 are the

main constituents of the vapor phase, depending upon the location in the phase diagram. The authors calculated partial pressure of As_2 and As_4 based upon total pressure measurements of Rau [Rau75], enthalpy of fusion data of Kaufman et al. [Kau81], and the data of Drowart et al. [Dro78] for the energy of dissociation of As_4 into As_2. Such calculations revealed that any uncertainity with the dissociation enthalpy has negligible impact on the phase diagram optimization, while has a serious impact on the absolute partial pressures of As_2 and As_4 species calculated above the In-As and Ga-As systems. In all such cases direct measurement of Gibbs energy data is desirable. Such is possible by emf measurements in semiconductor alloys using galvanic cells, the cells being associated with a functional error in the order of 0.1 to 0.3 %.

Calculations have also been performed for activity coefficients of Sb and Te in Sb-Te alloys [Gla69, Gho89], however no experimental data exist. Furthermore, the Sb-Te system is associated with extremely small excess entropy of mixing, which indicates the predominance of entropy increase on mixing due to chemical interactions over the decrease due to the resulting ordering. In view of insufficient thermochemical data on these technologically important compound semiconductor systems, an attempt is made in the present work to perform experiments and assessments to obtain the most consistent set of thermodynamic data in order to characterize these sytems fully.

Solid State Activity Measurements

The use of solid electrolytes in galvanic cells has been a common method to measure the equilibrium properties of electrode materials. The critical issues in solid state ionics are material stability, transport processes, and interfacial phenomena. The

application of solid electrolytes to the measure Gibbs energies in compound semiconductor systems is discussed next.

Solid Electrolytes

The solid electrolyte used in this study is a solid solution between Y_2O_3 and ZrO_2. The yttria stabilizes the material in a fluorite crystal structure, and thus is termed yttria stabilized zirconia (YSZ). It exhibits abnormally high oxygen ion conductivity. The fluorite structure is a face-centered-cubic arrangement of cations with the oxygen atoms occupying the tetrahedral sites. Such a structure has a large number of octahedral interstitial voids. In YSZ, the size of the O^{-2} ion is sufficiently larger than the metal cation to permit easy diffusion of O^{-2} ions through the crystal structure. The presence of 8 to 10 wt % Y_2O_3 is essential to stabilize the flourite phase in zirconia for use at temperatures below 1500°C.

The conductivity mechanism of YSZ is based upon its defect structure. The most common defect types are the Schottky defects (vacancy pairs) and Frenkel defects (vacancy-interstitial pairs). The total electrical conductivity, σ, through the YSZ is the sum of the effects due to the concentrations of ionic and electronic (electrons and holes) defects in the solid, and is given by

$$\sigma = \sum_i c_i q_i \mu_i + n q_e \mu_e + p q_h \mu_h \qquad (1.1)$$

where c is the ionic defect concentration, q is the charge, μ is the mobility, and n and p are the electron and hole concentrations, respectively. The subscripts i, e and h represent ions, electrons and holes, respectively. Useful application of solid electrolytes requires the

electron and hole conductivity to be considerably less than the total conductivity. That is the case in YSZ that oxygen ion conductivity is essentially the only mechanism.

Principle of Electrochemical Cells

The activity of component A in a binary A-B solution was determined in an electrochemical cell of the type:

$$A, AO_y//YSZ//A_yB_{1-y}, AO_y \qquad (I)$$

In the experimental measurements presented here, two types of measurements were made. In one configuration component activities in solution were determined and in the other the Gibbs energy of compound formation was measured.

The reference electrode consists of a two phase mixture of A and its stable oxide AO_x, while the working electrode contains the solution A_yB_{1-y} and the most stable oxide AO_x. The half cell reactions and the overall rections are:

$$A\ (pure) + x\ O^{-2} = AO_x + 2x\ e^- \qquad (Ia)$$

$$AO_x + 2x\ e^- = A\ (\text{in solution } A_yB_{1-y}) + x\ O^{-2} \qquad (Ib)$$

$$A\ (pure) = A\ (\text{in solution } A_yB_{1-y}) \qquad (Ic)$$

The overall cell reaction is simply the transfer of A in the pure (reference) state to the solution phase. The Gibbs energy change of the reaction is:

$$\Delta G_{Ic} = \Delta G^\circ + RT\ln a_A \qquad (1.2)$$

when specifying the phase of the reference state the same as that of pure A at the measurement temperature.

The value of ΔG is obtained from the open circuit potential according to the following equation:

$$\Delta G = -nFE = -2x\ FE \tag{1.3}$$

Therefore the activity of A in solution A_yB_{1-y} is directly calculated from the measured open circuit potential by

$$a_A = \exp(-2x\ FE/RT) \tag{1.4}$$

Another view of this process is to consider the associated reaction occuring at both electrodes

$$x\ O^{-2} = \tfrac{1}{2}\ O_2\ (g) \tag{Id}$$

Since the a_A in the reference electrode (pure A) is higher than that in the working electrode, the partial pressure of O_2 that would be in equilibrium with each electrode is lower in the reference electrode. This chemical potential difference causes oxygen ions to transfer from the working electrode to the reference one.

The transport process, however, results in an electron accumulation at the low oxygen chemical potential electrode (left side), and electron depletion is produced at the electrolyte surface at the high oxygen chemical potential electrode (right side). This produces an electric potential gradient across the electrolyte. At the point of equilibrium, the chemical potential gradient of the oxygen ions is balanced by the electric potential gradient across the electrolyte so that O^{-2} electrochemical potential gradient is zero. This balance at equilibrium is mathematically represented by the following equation:

$$-nFE = \int_{\mu'_{O_2}}^{\mu''_{O_2}} t_{ion}\, d\mu_{O_2} \tag{1.5}$$

where t_{ion} is the ionic transference number defined as the fraction of ionic conductivity to the total electric conductivity. When $t_{ion} \sim 1$ the above relation is reduced to

$$-nFE = \mu'_{O_2} - \mu''_{O_2} \qquad (1.6)$$

where E is the measured open circuit emf, F is the Faraday constant, n is the number of electrons participating in the half cell reaction. Thus, by careful design of such electrochemical cells the measurement of the open circuit emf is related to the chemical potential difference for the transported species (O^{-2}). If the chemical potential is well known at one electrode (termed reference electrode), then the only unknown is the chemical potential of the transported species at the other electrode (termed working electrode). The difference between reactions Ia and Id is

$$A + x/2\ O_2 = AO_x$$

and the sum of Ib and Id is

$$AO_x = A\ (\text{in solution } A_yB_{1-y}) + x/2\ O_2$$

The overall cell reactions are identical and thus equation 1.4 is the same as equation 1.6.

The Gibbs energy of formation of compound AB was measured in a cell of the type:

$$A, AO_x//YSZ//AB, B, AO_x \qquad (II)$$

$$A + x/2\ O^{-2} = AO_x + 2e^- \qquad (IIa)$$

$$B + AO_x + 2e^- = AB + x/2\ O^{-2} \qquad (IIb)$$

$$A(a_A) + B(a_B) = AB(a_{AB}) \qquad (IIc)$$

Expressing the reactions in which all components in their standard states ($a_i = 1$) are reversibly changed from the reference state ($a_i = 1$) to the state at which the

measurement is made(a_i), the Gibbs energy associated with each change is expressed as follows:

$$A(a_A) = A(a_A = 1) \qquad \Delta G_{1.7} = (G^o_A - G_A) = RT \ln\left(\frac{1}{a_A}\right) \qquad (1.7)$$

$$B(a_B) = B(a_B = 1) \qquad \Delta G_{1.8} = (G^o_B - G_B) = RT \ln\left(\frac{1}{a_B}\right) \qquad (1.8)$$

$$AB(a_{AB} = 1) = AB(a_{AB}) \qquad \Delta G_{1.9} = (G_{AB} - G^o_{AB}) = RT \ln a_{AB} \qquad (1.9)$$

Along with the standard Gibbs energy of formation of compound AB:

$$A(a_A = 1) + B(a_B = 1) = AB(a_{AB} = 1) \qquad \Delta G_{1.10} = \Delta G^o_{1.10} \qquad (1.10)$$

Upon summation of reactions (1.7) through (1.10), the overall cell reaction Iic is obtained and the expression for the standard Gibbs energy of the reaction (1.10) is established as follows:

$$\Delta G_{1.6} = 0 = RT \ln\left(\frac{a_{AB}}{a_A a_B}\right) + \Delta G^o_{1.10} \qquad (1.11)$$

The value of $\Delta G^o_{1.10}$ is determined experimentally by measurement of the open circuit potential and is related to the activity values through the equation (1.11).

CHAPTER 2
EXPERIMENTAL STUDIES

Description of Apparatus and Measurement Techniques

The solid-state electrochemical cell enclosure assembly used in this study is depicted in Figure 2-1. The cell enclosure was a closed-one-end alumina tube 45.7cm in length and 5.08 cm outside diameter. It was secured onto a water-cooled brass cell head by means of a Viton O-ring. Four 0.318cm cajon through-bore fittings were located on the cell head while another 0.318cm through-bore fitting was located at the center of the cell head. Alumina sheaths were passed through these fittings. The central fitting passed an alumina sheath (single bore, 0.318 cm O.D.) through which an inconel wire was inserted to suspend the cell assembly within the enclosure. Inconel lead wires were passed through a double bore alumina sheath through one of the outer four fittings on the cell head to make connections to the reference and working electrodes of the cell. A thermocouple (Type S: Pt-10% Rh, Pt) was passed through another outer fitting. The remaining two bores on the brass cell head were provided for the argon purge gas inlet and outlet. The exposed ends of the alumina sheaths were sealed by means of epoxy resin. The thermocouple tip was placed in an alumina casing and sealed by means of high temperature alumina cement.

The temperature of measurement was typically in the range 773 to 1473 K. At high temperature, there was concern that volatilization losses would affect the working

electrode composition. For this reason two different cell constructions, designed to minimize electrode material evaporation, were used.

The cell design designated Type I and termed 'compression design' is a modification of the original design developed by Egan and coworkers [Del79, Alq83, Ega85], and is shown schematically in Figure 2-2. Alumina disks, 2.0 cm diameter and 0.6 cm thick with a countersunk hole (1.0 cm diameter and 0.3 cm in depth), were used as crucibles for the electrode material and were custom fabricated by Bolt Technical Ceramics (Conroe, Texas USA). The countersunk holes of the necessary diameter were created by ordering a special tool incorporating a diamond cutting edge on the outer surface of the cylindrical drill. The working electrode was comprised of a mixture of the metal alloy and the stable oxide, while the reference electrode contained a mixture of the pure metal and metal oxide powder. A yttria stabilized zirconia (YSZ, 8 to 10 % yttria in zirconia) disk, and 2.54 cm diameter and 0.16 cm thick, was used as the oxide solid electrolyte, supplied by Zircoa, Inc. (Solon, Ohio). The faces of the alumina crucibles and YSZ electrode were carefully polished using a carbide coated grinding conveyer belt to roughen the contact surfaces to provide good seal between the electrolyte and the crucibles. The alumina crucibles containing the electrode materials were placed on either side of the YSZ electrolyte. The cell was, in turn, pressed between stainless steel plates and the entire assembly was held together by four tantalum rods.

A tungsten foil 0.005 cm thick with a hole ~ 0.6 to 0.8 cm diameter was placed between the electrolyte and each of the crucibles. The diameter of the hole in the tungsten foil was slightly smaller than the 1.0 cm countersunk hole in the crucible. This was necessary because after filling up the crucibles with electrode material, an overlap of

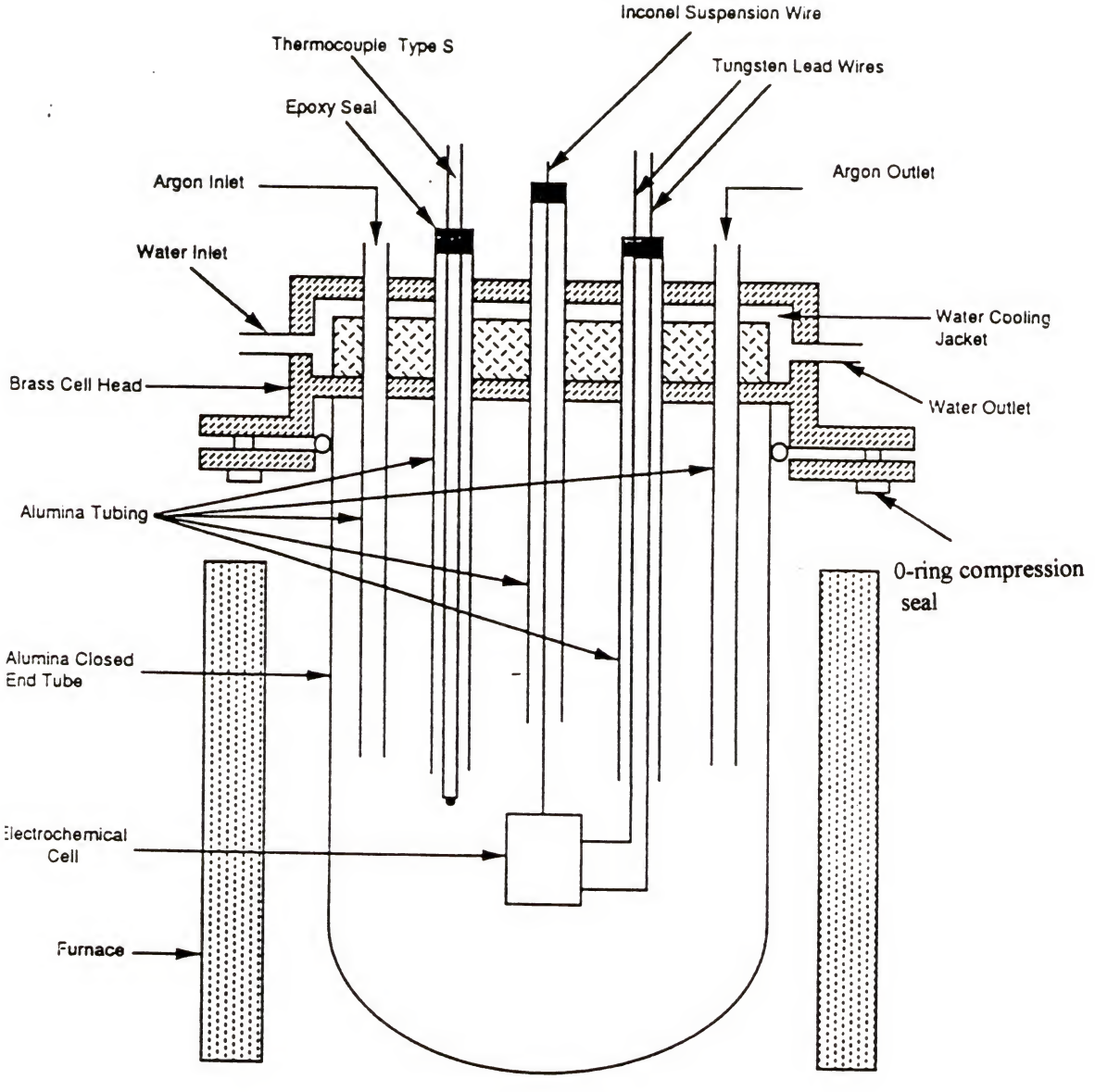

Figure 2-1. Schematic of the solid state electrochemical cell assembly.

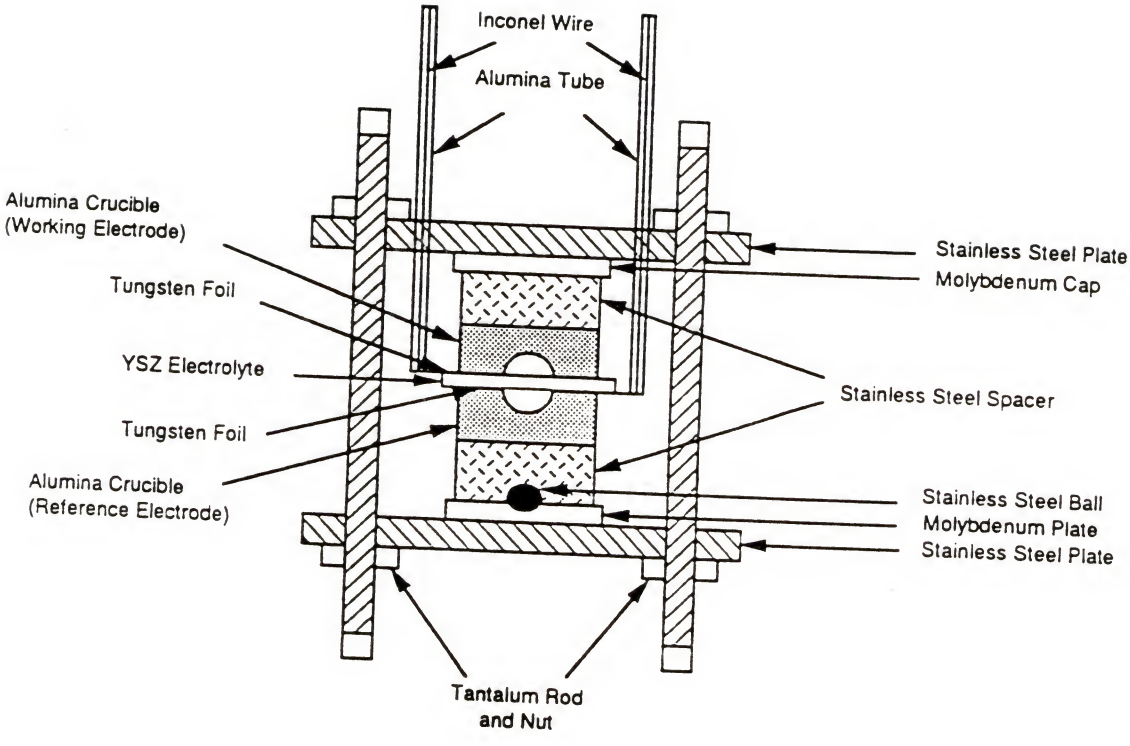

Figure 2-2. Schematic of the compression design for the electrochemical cell (type I).

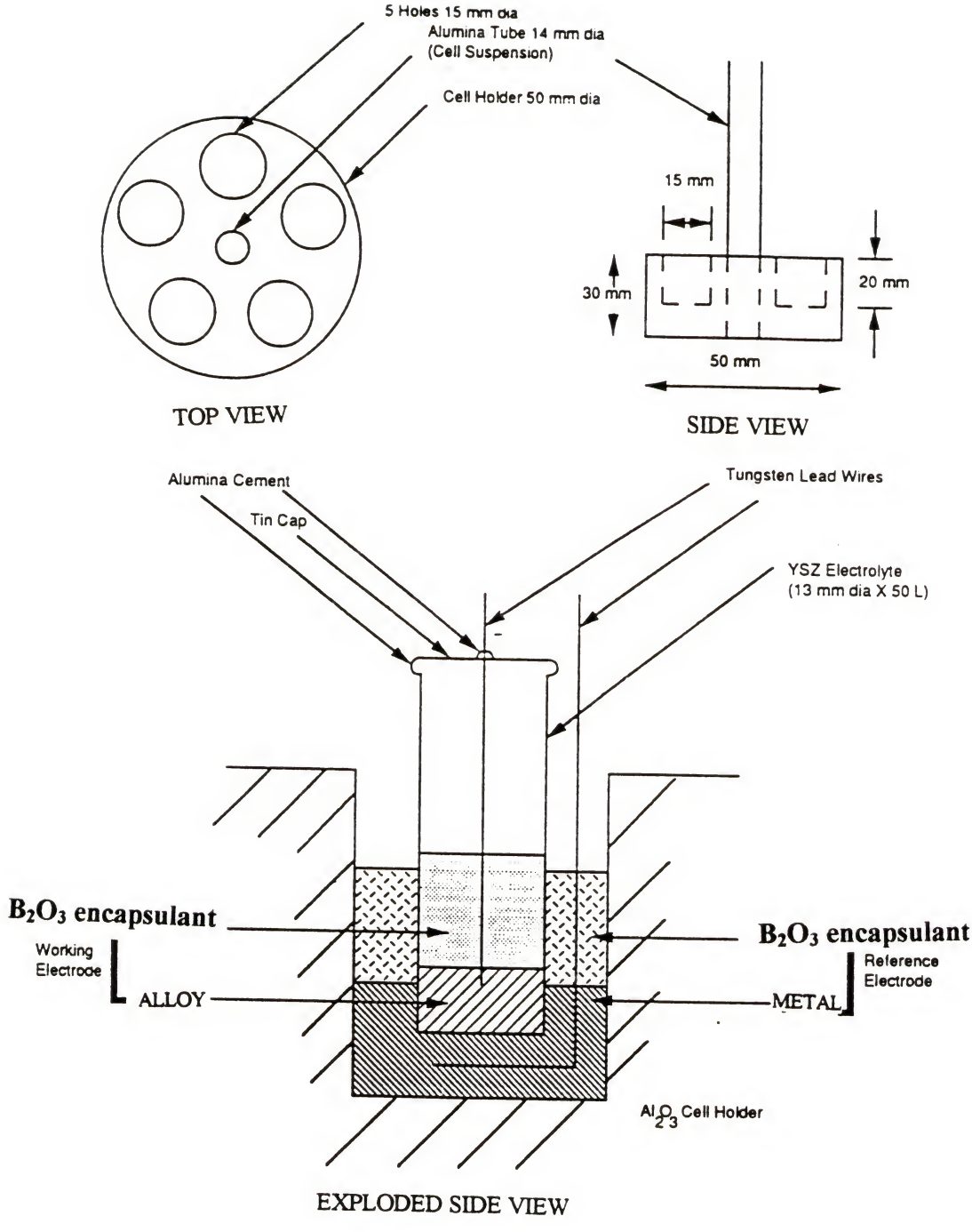

Figure 2-3. Schematic of the encapsulated design for the electrochemical cell (type II).

about 0.2 to 0.4 cm of tungsten metal was maintained for ensuring electrical contact with the electrodes. The rough surfaces of the crucibles and the electrolyte gave a good seal when the tungsten foil was placed in between the electrode and the electrolyte, and the tantalum rods were screwed on tight. The choice of tungsten foil over commonly used platinum was based upon the fact that platinum when used in such experiments was readily involved in the reaction with the vapor phase of the electrodes causing severe damage to the point of breakage. Furthermore, platinum being significantly more expensive than tungsten was not a good choice. A test cell was run with to verify the acceptable use of tungsten foils. It was observed that even though the tungsten was readily oxidized, the measured voltage difference across the electrodes changed by less than 0.5%. The reason being that the oxidation reactions in the two compartments had a natural tendency to cancel each other's effect. Tungsten foils of thickness of the order of 0.005 cm were optimum in their performance as electrical contacts, especially because of their greater capacity to deform compared to thicker foils which being brittle are subject to cracks under the effect of mechanical stress. Care was taken to ensure that the centers of the holes in the alumina crucibles and tungsten foils were aligned with each other while assembling the working and reference electrodes.

This cell design relied on the difference in thermal expansion between the Ta rods and stainless steel plugs to form a compression seal between the electrode crucible rim and the electrolyte disk. The cell was held aligned with the vertical axis of suspension and was imparted some degree of rotational freedom by means of a 0.1 cm diameter stainless steel ball seated at the base of the molybdenum plate. This was necessary because of the brittle

nature of the YSZ electrolyte. Any additional stress due to uneven mechanical tightening of the tantalum nuts could cause the electrolyte to break.

Inconel lead wires were well suited for spot weld contact with the tungsten foils and was used instead of tungsten. Tungsten wire posed a problem during spot welding, because of its high melting temperature (~ 3683 K) and was, thus, replaced by inconel. It was determined by electrical measurements of cell resistance that the spot weld contact and the lead wire IR drop did not seriously affect the voltage readings and that the variations were less than 1% when compared to the observed voltages during the experiment.

Cell Type II, also termed 'encapsulated design', was a cell arrangement in which a maximum of five alloys compositions could be studied simultaneously. As shown in Figure 2-3(a) and (b), the cell holder was designed with five cylindrical holes (15 mm diameter and 20 mm depth) along the periphery. These holes housed the YSZ electrolyte crucibles that were cylindrical, flat-one-end closed tubes (13 mm diameter and 50 mm length). The annular space between the YSZ crucible and alumina cell holder contained the reference electrode material comprised of the metal and the metal oxide. The working electrode, which consisted of the alloy of the desired composition and the most stable oxide, was placed inside the YSZ crucible. Tungsten wires were used as the leads for both electrode compartments. The open ends of the YSZ tubes were sealed by means of tin caps pasted onto the tubes using alumina cement.

Owing to the open design of such a cell arrangement the problem arose in not being able to contain the vapors of the more volatile component of the alloy under investigation, especially at high temperature. This was avoided by the incorporation of

B_2O_3 powder (typically 0.5 g) in both the electrode compartments. B_2O_3 melts at about 450°C and is a viscous liquid immiscible with the liquid metal electrode materials. It is believed that the liquid B_2O_3 fully encapsulates the electrode material and provides an effective mass transfer barrier to As or P escape from the melt. This approach to reducing volatilization losses has long been used in the bulk crystal growth of group III arsenides and phosphides. Several test cells were assembled to quantify the influence of B_2O_3 encapsulant on the experimental results. The following systematic cell was used:

$$A, AO_x//YSZ//A, AO_x, B_2O_3 \qquad \text{(III)}$$

The cells were run for both indium and gallium (A=In, Ga) at the typical temperature range 773 to 1123 K and open circuit emfs were recorded. The values were of the order of 1 to 4 mV (equivalent to a maximum value of 1.16 kJ/mol) amounting to less than 5% of the experimental measurements in such cells. With B_2O_3 in both the compartments, the measured voltage difference was less than 1 mV which corresponded to an error of less than 0.5%. The effect of B_2O_3 in both the compartments was determined to well offset each other so that the impact of B_2O_3 was presumed negligible.

The cell assembly was heated in a resistance furnace that consisted of two heating zones, the temperature of each zone being controlled by a microprocessor-based digital process controller (Micristar Model 828D, Control Systems, Research Inc.). The furnace had the capacity to reach a temperature of 1400°C and maintain temperature uniformity to within ± 0.5 K. The entire cell assembly was blanketed in a flowing gas stream of Ar. This purge stream was purified by passing the gas sequentially over hot Ti sponge (1123 K), a molecular sieve trap, and a liquid nitrogen cold trap.

The cell emf was measured with a Keithley Model 196 digital multimeter of high input impedance. A pressure/flow controller-Type 250B (MKS Instruments, Inc.) was used to monitor the gas pressure and purge gas flowrate. The pressure in the cell assembly could, however, be manually adjusted with the inlet and exit valves to the system. Any pressure in excess of the preset value was released through the automatic on/off pneumatic valves triggered by the Micristar process controller.

The experimental apparatus, as outlined in the previous section, is schematically shown in Figures 2-1 to 2-3. Electrodes of the cells were prepared from components in pure states. They were mixed together in the electrode crucibles and prepared to give a well-packed mixture in the electrode compartments. The electrode crucibles were then physically contacted with the YSZ electrolyte to achieve the desired cell. Prior to the cell operation it was necessary to leak check the assembly. This was achieved by a series of successive evacuation and purging steps and monitoring the pressure. Evacuation was performed by a high vacuum system to pressure levels in the range 10^{-3} to 10^{-4} Torr. An acceptable leak proof cell condition was determined when the cell assembly pressure stayed within the vacuum range and exhibited less than 0.0001 Torr increase in pressure over a duration of 120 s. High purity argon was used as the inert purge gas with the purge flow rate adjusted between 1 to 2 standard cm^3/s. The cell temperature was programmed to rise at the rate of 0.02 Ks^{-1} to the measurement temperature.

Measurements were initiated typically after 2 to 3 days when equilibrium was achieved at the first temperature setting. The cell was determined to be at equilibrium when the open circuit emf values were stable (within 0.1 mV over a period of two hours). Cell reversibility was verified by applying a small current to the cell in both directions and

verifying that the cell voltage returned to its original value. The cell was also observed to be reversible for small temperature increments and decrements (order ~ 5 K). At the conclusion of the experiment, the cell compartments were again checked for leaks by successive evacuation and purge steps and pressure monitoring. The electrodes were examined for evidence of oxidation and were analyzed by X-ray diffraction to confirm the absence of side-reactions.

Experimental Results in Binary Systems

As discussed in Chapter 1, the indium and gallium arsenides and antimonides are the systems of interest in this study. These materials are the building blocks of the semiconductor alloys used in the optoelectronics industry. The electrical and optical properties of these alloys depend on the stoichiometry of the alloys and since they are often grown with near equilibrium boundary conditions the alloy compositions can be estimated by equilibrium considerations. Activity measurements in both solid and liquid phases of these alloys have been performed in this study using solid state galvanic cells.

Ga-As System

Phase diagram data. The phase diagram for the Ga-As system has been fairly well studied by numerous authors [Sol74, Kos55, Hsi74, Hal63, Rub66, Rak70, Vig73, Per80, DeW86, Dut83, Ceo89, Yam88, Ans84], and has been shown to be characterized by the existence of the congruently melting compound GaAs. Because of high pressures, the phase diagram region close to pure As composition is not yet been accurately determined.

Most of the data are in fairly good agreement except for the results of Koster and Thoma [Kos55]. A summary of literature data is presented in the next chapter.

Calorimetric and enthalpy data. The enthalpies of formation and fusion as well as low temperature Cp value for GaAs have been reviewed by Sirota [Sir68], Martosudirjo and Pratt [Mar74], Piesbergen [Pie63], Holste [Hol72], Cox and Pool [Cox67], Dash et al. [Das74], Lichter and Sommelet [Lic69] and Richman and Hockings [Ric65] by calorimetric methods such as calorimetric precipitation, drop calorimetry, differential thermal analysis, thermometry and oxygen calorimetric bomb. The mixing enthalpy for the liquid has been determined by Yamaguchi et al. [Yam88] by drop calorimetry over a temperature range of 800 to 1550 K. The heat capacity data for GaAs compound [Cox67, Das74 and Lic69] show large discrepancies. Due to this reason, Chatillon et al. [Cha90] performed a least square fit to the heat capacity data of these authors to obtain an expression for optimized heat capacity data in the temperature range 150 to 1511 K. This expression was used in performing third law analysis of the measured Gibbs energy data for Ga-As system in this study.

Vapor pressure and Gibbs energy measurements. The equilibrium vapor pressure above solid GaAs and liquid solutions has been measured by several researchers. Above 1510 K, GaAs vaporizes incongruently with an excess of As. Although several polymers of As exist, the predominant species below the melting temperature are As_2 and As_4. Unless care is taken to maintain a particular stoichiometry, when the temperature is above the maximum congruent vaporization temperature, the preferential loss of As will lead to a two-phase Ga-rich melt-GaAs(s) equilibrium. Both partial pressure and total pressure measurements have been reported in the literature. The partial pressures of As_2 and As_4

have been measured [Pup74, Dro58, Gut61, Art67, DeM70, Fox74 and Hir85] using Knudsen cell mass spectrometry. Total arsenic pressure measurements have been performed by van den Boomgaard and Schol [Boo61], Folberth [Fol58], Lyons and Silvestri [Lyo61] using the dew point technique, by Rakov et al. [Rak70] using continuous weighing technique, by Vigdorovich et al. [Vig73], Richman [Ric63], Hegewals et al. [Heg88] using Bourdon gauge and by Khukhryanskii et al. [Khu74], and Panish [Pan74] using dynamic methods incorporating transport by H_2 gas flow or equilibrium with H_2 and AsH_3 gas flows. No experimental information is available on the standard Gibbs energy of formation of GaAs (s) at a temperature above 743 K. The Gibbs energy of formation of GaAs(s) was measured by Abbasov et al. [Abb66], Krestovnikov et al. [Kre71], and Sirota [Sir68] by electrochemical method in the temperature range 637 to 743 K. These emf measurements were performed at low temperature and were found inconsistent with the phase diagram data [Cha90]. Recently, Lee [Lee92] conducted emf measurements for Ga activity along the Ga-rich liquidus curve (two-phase equilibrium GaAs-liquid) in the temperature range 923 to 1373 K.

There exists significant discrepancy between the vapor pressure data of the numerous authors [Dro58, Gut61, Art67, DeM70, Fox74, Fox73, Rub66, Boo57, Fol58, Lyo61, Rak70, Ric63, Hsi74, Khu74a, Khu74b and Pan74]. A major problem has been the complications associated with the As vaporization and the subsequent formation of As_2 and As_4 species. The isolation of the gaseous species and their individual contribution to the total measurement in the mass spectrometric measurements and vapor pressure studies is not easily quantified. Depending upon the temperature, either As_2 or As_4 is the main constituent of the vapor phase [Art67, Ric63, Pup74, Dro58, DeM70, Pan74, Lyo61

and Rak70]. For the total pressure measurements or when only one species partial pressure is measured, the remaining species partial pressures are calculated from the equilibrium constant K_p for the dissociation reaction:

$$As_2(g) = \tfrac{1}{2} As_4(g) \qquad \left(K_p = \frac{P_{As_4}^{1/2}}{P_{As_2}} \right) \qquad (2.1)$$

One of the difficulties in comparing the data is the large uncertainity in the value of K_p. Chatillon et al. [Cha90] have recalculated the literature As vapor pressure data referred to As(s) and have presented an equation for P_{As_4} calculations based upon transformation equation involving K_p. Even after such corrections were applied to the vapor pressure data, significant disagreement still existed. This being the case, the motivation behind this study was to measure the standard Gibbs energy of formation of GaAs (s) using a solid state electrochemical cell. Cell type II was used to extend the temperature limit of measurement beyond that of the previous molten salt studies.

Standard Gibbs Energy of Formation of GaAs (s)

The cell that was used in the experiment is shown below along with the half cell reactions:

$$B_2O_3(l), Ga_2O_3(s), Ga\ (l, pure)//YSZ//GaAs\ (s), As(s), Ga_2O_3(s), B_2O_3(l) \quad (IV)$$

$$Ga\ (l, pure) + 3/2\ O^{-2} = 1/2\ Ga_2O_3 + 3e^- \qquad (2.2)$$

$$1/2\ Ga_2O_3 + As\ (s, pure) + 3e^- = GaAs\ (s) + 3/2\ O^{-2} \qquad (2.3)$$

$$Ga\ (l, pure) + As\ (s, pure) = GaAs\ (s) \qquad (2.4)$$

Applying Wagner's approximation [Wag57] to the chemical potential of the essentially stoichiometric compound GaAs the overall cell reaction is transformed to the following:

$$\text{Ga (l, pure)} = \text{Ga (ss)} \tag{2.5}$$

where ss denotes the solid solution Ga-As with composition fixed to lie along the solidus line towards the GaAs(s) + As(s) region. This is equivalent to measuring the chemical potential of Ga along the As-rich solidus of the compound GaAs. The standard Gibbs energy of formation of GaAs referred to Ga (l) and As (s) states is given by the following relation:

$$\Delta^{\circ}G_f(\text{GaAs}) = {}^{\circ}G_{\text{GaAs,s}} - {}^{\circ}G_{\text{Ga,l}} - {}^{\circ}G_{\text{As,rho}} = -3FE \tag{2.6}$$

where F is the Faraday constant (96,485 C/eq-mV) and E is the open circuit emf (mV).

The measured values of the open circuit potential at the various measurement temperatures are listed in Table 2-1. The emf values and the calculated $\Delta^{\circ}G_f(T)$ values have a near linear temperature dependence as shown in Figure 2-4. The $\Delta^{\circ}G_f(T)$ values are significantly lower (more negative) than the earlier reported emf measurements when extrapolated to this temperature range. One possible reason is the uncertainity in the oxidation state of Ga in the molten halide cells of the earlier work. Gallium has both a +1 and +3 oxidation state and the Gibbs energy difference between GaCl and $GaCl_3$ is relatively small. This would make the effective value of n less than 3 and thus make the value of $\Delta^{\circ}G_f(T)$ less negative.

Two methods were employed to check the consistency of the obtained results. In the first method, termed the second law method, the standard enthalpy of formation is related to the standard Gibbs energy of formation by the following equation:

$$\Delta^\circ H_f = - R\, d(-\Delta^\circ G_f/RT)/d(1/T) \qquad (2.7)$$

Thus, the slope of $-\Delta^\circ G_f/RT$ vs $1/T$ gives $-\Delta^\circ H_f/R$. For a linear temperature dependence of the Gibbs energy function the value of $-\Delta^\circ H_f$ is a constant. The slopes were measured graphically for each measurement temperature. The values of standard enthalpy of formation of GaAs by the second law method at different temperatures are shown in Table 2-2 and Figure 2-5. It is important to note that the second law analysis involves slope measurement, which is subject to considerable uncertainity. In the temperature range of the present work the average value for $\Delta^\circ H_f$ (T_{av} = 903 K) is -28.27 kcal/mol. The value obtained from the second law method after extrapolation of the $-\Delta^\circ G_f/RT$ vs $1/T$ curve to 298.15 K is $\Delta^\circ H_f(298.15\ K)^{II}$ = -25.83 kcal/mol.

The second consistency test, termed the third law method, includes high temperature C_p and standard entropies (hence the third law method). The standard enthalpy of formation $-\Delta^\circ H_f$ (298.15 K) is calculated using the following formalism:

$$-\Delta^\circ H_f(298.15\ K) = -\Delta^\circ G_f(298.15\ K) - \Delta_f\left\{^\circ H(T) - ^\circ H(298.15\ K)\right\} + T\Delta^\circ S_f(298.15\ K) + T\Delta_f\left\{^\circ S(T) - ^\circ S(298.15\ K)\right\} \qquad (2.8)$$

where Δ_f indicates thermal function difference of the formation reaction (eqn 2-4).

In the above treatment, pure component specific heats and the standard elemental entropies at 298.15 K were taken from the Janaf Thermochemical Tables [Jan85] and were consistent with those from Hultgren [Hul73]. The standard entropy of GaAs at

298.15K was taken from Piesbergen [Pie63] and Holste [Hol72]. The heat capacity data for GaAs (s) was taken from the optimized correlation by Chatillon et al. [Cha90].

It is interesting to see the temperature variation in the $-\Delta^{\circ}H_f(298.15\ K)$ values obtained from the third law analysis as shown in Figure 2-6 and Table 2-2. The values show systematic temperature dependence, suggestive of systematic errors. The error could be in either the $\Delta^{\circ}G_f$ (T) values or in the high temperature heat capacity difference data. However, the temperature dependence fluctuates and is acceptable within experimental errors.

The mean value of $\Delta^{\circ}H_f(298.15\ K)$ in this temperature range is -19.94 kcal/mol which agrees excellently with the measured value of -20.96 kcal/mol by Yamaguchi et al. [Yam94] using tin solution calorimetry and that of -19.69 kcal/mol measured by Martosudirjo and Pratt [Mar74] using precipitation calorimetry. It also compares well with the calculated value of -21.24 kcal/mol reported by Chatillon et al. [Cha90]. This is comparable to the experimental errors of $\pm$0.12 kcal/mol reported by Yamaguchi et al. [Yam94] and $\pm$0.11 kcal/mol reported by Martosudirjo and Pratt [Mar74]. It also compares well with the calculated value of -21.24 kcal/mol reported by Chatillon et al. [Cha90]. The value differs from the data of Thurmond [Thu65], Drowart and Goldfinger [Dro58], and Gutbier [Gut61]. The method used by Sirota [Sir58], Abbasov et al. [Abb66] and Krestovnikov [Kre71] reported emf measurements at temperatures below 743K, so the calculations of $-\Delta^{\circ}H_f(298.15\ K)$ were based upon extrapolations of their data. On the other hand, the data by Pupp et al. [Pup74] and Arthur [Art67] were too

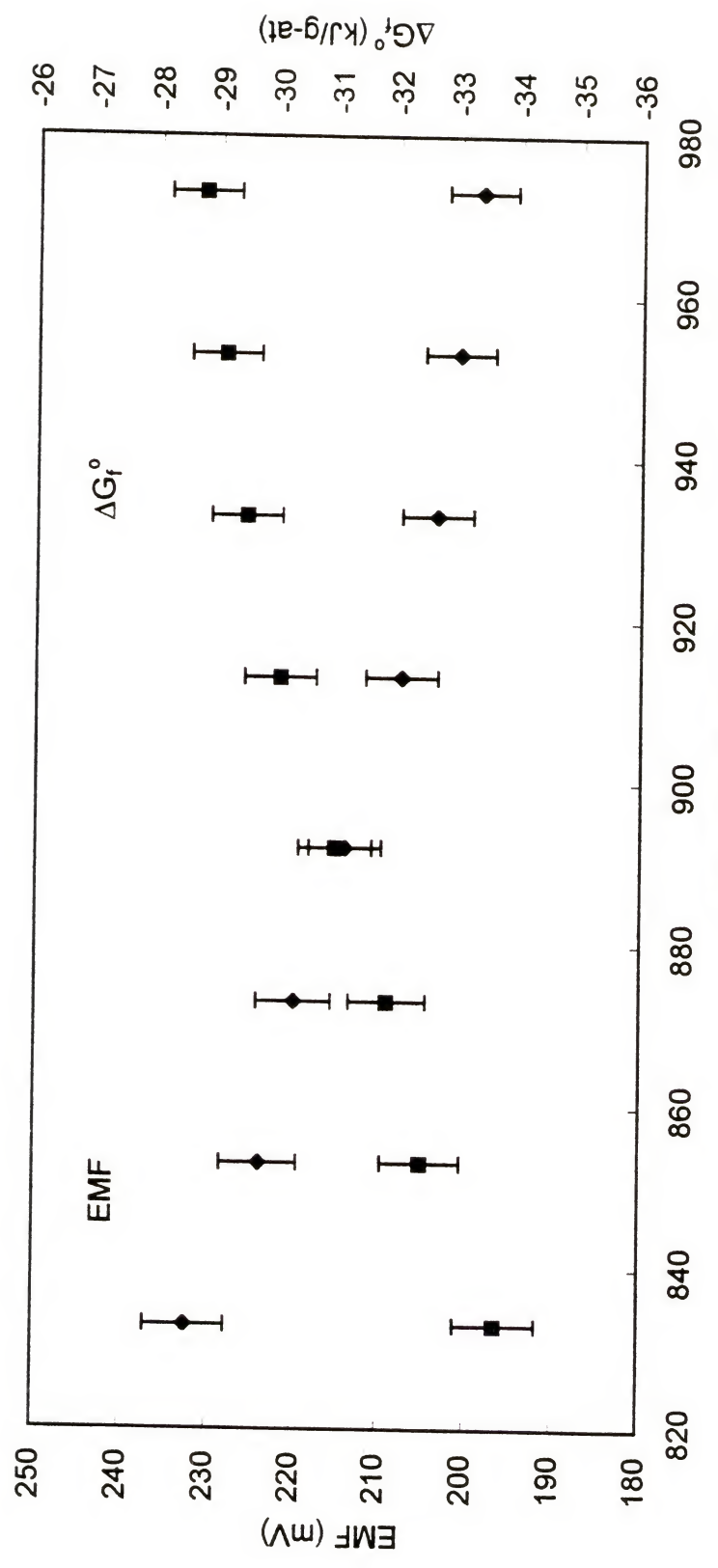

Figure 2-4. Temperature dependence of the open circuit emf and calculated standard Gibbs energy of formation of GaAs(s).

low. Thus, these data were discarded for comparison purposes. The reported values from literature have errors associated with errors in the values of specific heats, C_p, of pure components. The errors get easily propagated due to the temperature dependency of the C_p values. This is also seen in the calculated values in the present study. The temperature dependence seen in the present study also includes the errors associated with the C_p data. However, a possible reason for the temperature dependence is the increase in As loss as the temperature is increased.

In summary, the standard Gibbs energy of formation of GaAs (s) at temperatures above 743 K was measured by emf method and was checked for thermodynamic consistency using both second and third law analysis and comparing $-\Delta^{\circ}H_f(298.15\ K)$ values with the experimental measurements of Martosudirjo and Pratt [Mar74], and Yamaguchi et al. [Yam94]. The results from the third law analysis were in excellent agreement with the experimental data, however, the discrepancy between the measured and calculated values indicates random errors inherent to experimental measurement, and systematic errors inherent to the choice of Cp(T) data used in the calculations by numerous authors. Considering all uncertainities including those in the Gibbs energy measurements it is clear that the present calculations are in excellent agreement with literature values.

In-As System

Phase diagram data. Phase diagram data for In-As has been studied fairly extensively by several authors [Liu53, Hal63, Kar73, Per80, Kno85 and DeW86]. Most of the phase diagram data is available for In-rich segent of the phase diagram. Only the

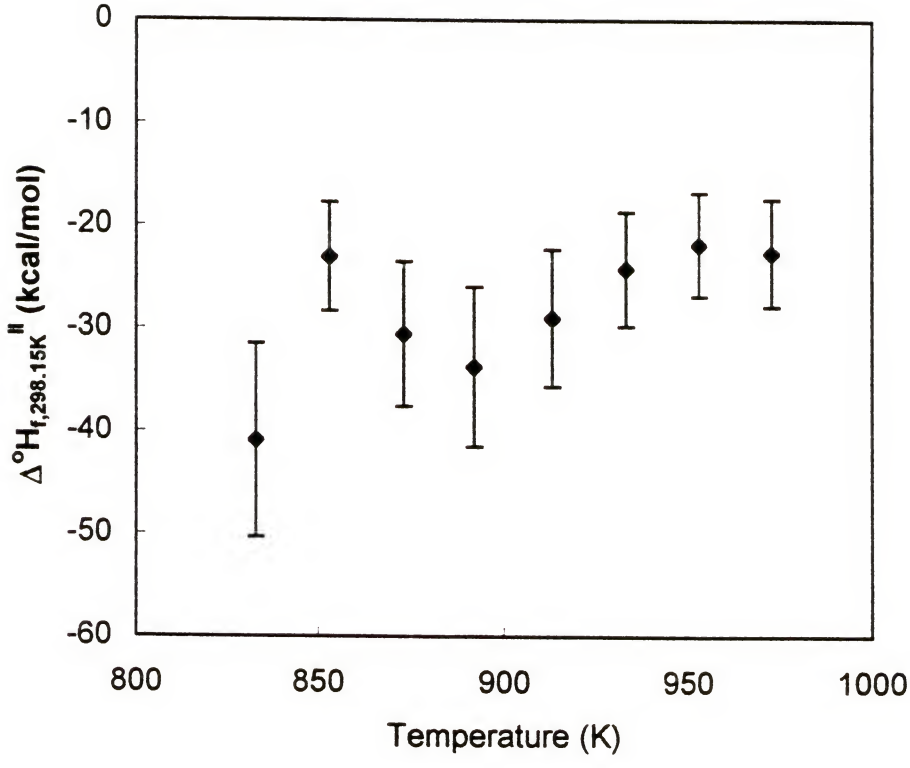

Figure 2-5. Calculated second law values of the enthalpy of formation of GaAs at 298.15K.

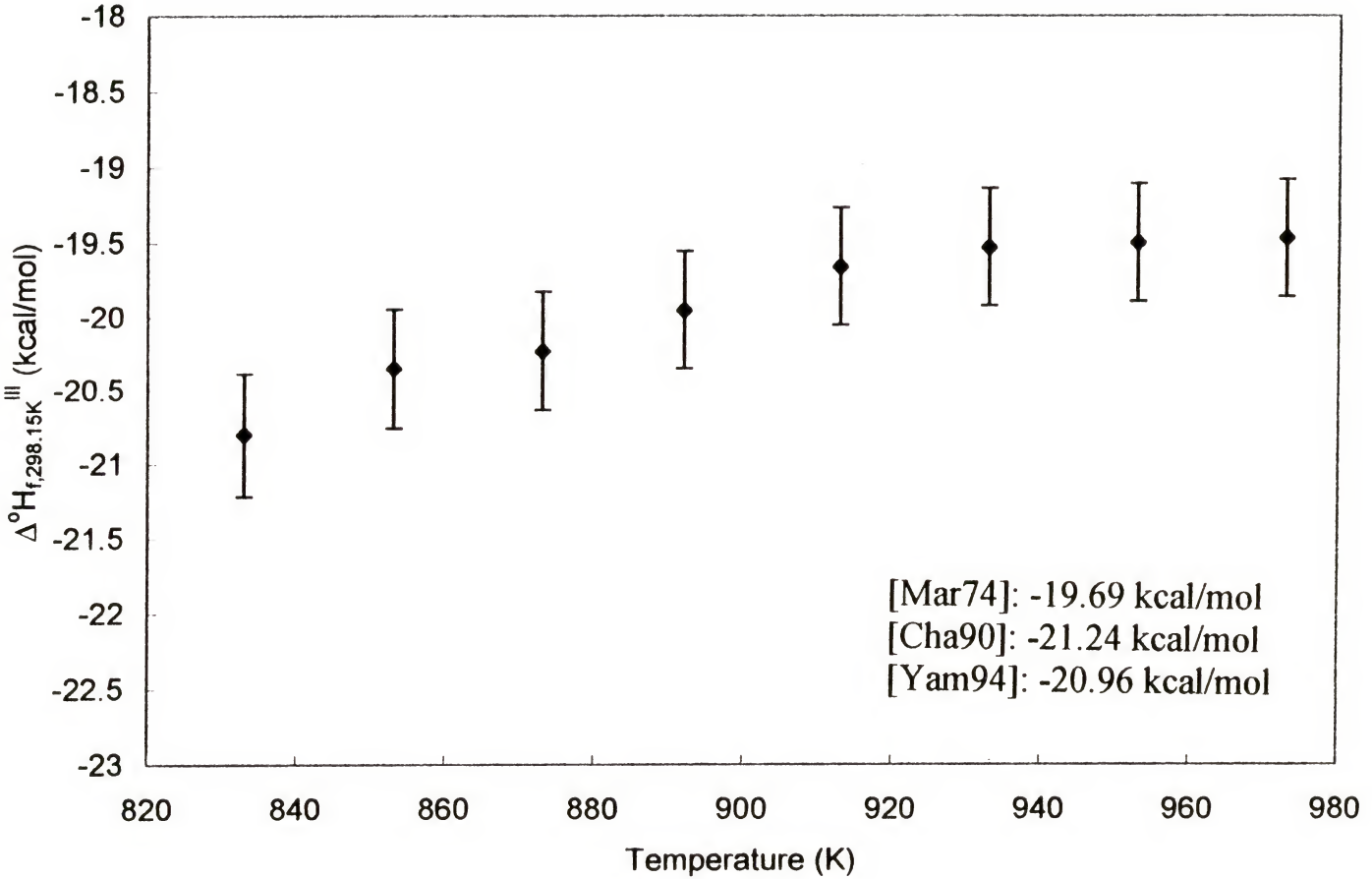

Figure 2-6. Calculated third law values of the enthalpy of formation of GaAs at 298.15K.

data by Liu and Peretti [Liu53] and Karataev et al. [Kar73] extend to the As rich-segment of the phase diagram ($x_{As} > 0.70$). The measurements of Hall [Hal63] and Perea and Fonstad [Per80] were made by heterogeneous equilibrium and weight loss technique. Liu and Peretti [Liu53] used differential thermal analysis (DTA) and X-ray analysis, while Knobloch and Thoma [Kno85] and DeWinter and Pollack [DeW86] used source dissolution method. Karataev et al. [Kar73] measured values by dew point and continuous weighing technique.

Calorimetric and enthalpy data. The enthalpy of formation of InAs has been determined by Yamaguchi et al. [Yam88] over a wide range of temperature 700 to 1500 K using drop calorimetry. Standard enthalpy of formation of InAs at 298 K was determined by Schottky and Bever [Sch58] using dissolution calorimetry and by Sharifov et al. [Sha63] using a calorimetric bomb. Enthalpy of fusion data is available from Cox and Pool [Cox67] and Yamaguchi et al. [Yam88] at their measured fusion temperatures of 1213 K and 1221 K respectively by drop calorimetry. Heat capacities have been determined in the temperature range 298 to 1200 K by drop calorimetry [Cox67, Lic69]. The measured heat capacity data was correlated by means of a least square fit using a polynomial expansion in terms of temperature in the range 160 to 1211 K [Cha90]. This correlation was used to perform a third law analysis on the measured Gibbs energy data in the present work. The pure compound standard entropy for InAs at 298.15 K was selected as 20.84 cal/mol, a value recalculated by Chatillon et al. [Cha90] from thermometric measurements of Piesbergen [Pie63], Dash et al. [Das74] and Holste [Hol72].

Vapor pressure and activity data. Partial pressures of As_2 and As_4 have been measured by Knudsen cell mass spectrometry [Pup74, Gut61, Gut59 and Gol59]. Total pressure measurements were made using static methods [Boo57, Fol58 and Kar73] such as dew point technique, and by dynamic method such as transport of As_2 and As_4 in a H_2 flow [Khu74, Khu77].

The vapor pressure data reported for In-As system show a wide distribution. Activities of In in the two phase region InAs-As was measured by electrochemical methods [Kre71, Abb64] upto a maximum temperature of 784 K. More recently Tmar et al. [Tma87] measured As_2 pressure along the liquidus curve in the In-rich segment of the phase diagram over a temperature range of 846 to 1086 K. Direct measurement of In activity has been made in the single liquid phase extending all the way to the equilibrium liquidus curve (liquid+InAs) using emf technique in the temperature range of 920 to 1260 K [Ito82].

In this study, the activity of indium was measured along the In-rich liquidus in the In-As system in the temperature range 833 K to 1153 K using a solid state galvanic cell. Furthermore, since no data is available on the standard Gibbs energy of formation of InAs (s) at temperatures above 784 K, such measurements were also targeted. An assessment of the phase diagram and thermodynamic data for this system was performed by Tmar et al. [Tma84]. In their preliminary assessment work, liquid solution model parameters were estimated from an optimization of other data, primarily phase diagram data and arsenic partial pressure measurements. As discussed in the previous section for Ga-As system, arsenic activities in the liquid phase calculated from arsenic vapor pressure measurements is subject to considerable uncertainity because arsenic sublimes to form polyatomic vapor

species (primarily As_2 and As_4) at atmospheric pressure which have a wide range of scatter for equilibrium dissociation constants. In general, the thermodynamics of liquid As is not well defined. The situation is aggravated by the significant scatter in the partial pressure measurements that are likely produced by parasitic evaporation and chemical side reactions.

Owing to such reasons, the liquid solution thermodynamic behavior has not been accurately ascertained. The more recent assessment [Cha90] used recently measured liquid phase activity of Itoh et al. [Ito82], enthalpy data of Glazov et al. [Gla75] and Yamaguchi et al. [Yam88], and As_2 vapor pressure measurements of Tmar et al. [Tma87]. Predictions have suggested moderate negative deviations from ideal solution behavior.

In these experiments, both pure As (s) and As (l) can be used as the standard reference states for the As_2 and As_4 vapor pressure data. Selected values for $\Delta^\circ H_f(298.15\ K)$, $\Delta^\circ S_{GaAs}(298.15\ K)$ and $C_p(T)$ are available from the recent assessment work by Tmar et al. {Tma85]. As in the case for Ga-As system, $C_p(T)$ and the value for $^\circ S_{GaAs}(298.15\ K)$ for In-As system were recalculated [Cha90] using experimental $C_p(T)$ data of Cox and Pool [Cox67], and Lichter and Sommelet [Lic69]. The authors [Cha90] also recalculated As vapor pressure data by using an empirical equation for P_{As_2} and transforming the data using an equation for dissociation constant K_p. These calculations were referred to pure As (s) in the standard state. However, even after such corrections were applied to the vapor pressure data, significant disagreement still existed. Furthermore, the emf measurements [Kre71, Sir67, Abb66] in literature were performed

Table 2-1. Experimental Gibbs energy of formation of GaAs (s).

Temperature (K)	EMF (mV)	$\Delta^\circ G_f$ (kJ/g-at)
833	232.5	-33.65
853	224.0	-32.42
873	220.0	-31.85
892	214.0	-30.97
913	207.5	-30.04
933	203.5	-29.46
953	201.0	-29.10
973	198.5	-28.74

Table 2-2. Enthalpy of formation of GaAs (s) by second law analysis and the values at 298.15K by the third law method.

Temperature (K)	$\Delta^\circ G_f$ (kJ/g-at)	$\Delta^\circ H_f(T)^{II}$ (kcal/mol)	$\Delta^\circ H_f(298.15\ K)^{III}$ (kcal/mol)
833	-33.65	-40.93	-20.80
853	-32.42	-23.05	-20.35
873	-31.85	-30.60	-20.23
892	-30.97	-33.78	-19.95
913	-30.04	-29.01	-19.66
933	-29.46	-24.24	-19.53
953	-29.10	-21.86	-19.50
973	-28.74	-22.65	-19.47

at low temperatures and were found inconsistent with the phase diagram data [Tma85, Cha90]. Keeping in mind the uncertainity in the available thermodynamic data, especially the Gibbs energy data, experiments in this study were designed to obtain liquid phase In activity and high temperature Gibbs energy of formation of InAs (s).

Activity of In Along the In-rich Liquidus

The experimental cell used for the activity measurements along the In-rich liquidus line is schematically shown below:

$$B_2O_3(l), In_2O_3(s), In\ (l, pure)//YSZ//In_xAs_{1-x}\ (l), InAs\ (s), In_2O_3(s), B_2O_3(l) \qquad (V)$$

$$In\ (l, pure) + 3/2\ O^{-2} = In_2O_3 + 3e^- \qquad (2.9)$$

$$In_2O_3 + 3e^- = In\ (in\ In_xAs_{1-x}\ (l)) + 3/2\ O^{-2} \qquad (2.10)$$

$$In\ (l, pure) = In\ (in\ In_xAs_{1-x}\ (l)) \qquad (2.11)$$

The In activity was calculated from the following expression:

$$a_{In} = \exp\left(\frac{-3FE}{RT}\right) \qquad (2.12)$$

where F = Faraday Constant, 96,485 C/eq-mV

and E = Open circuit emf, mV

The results for the In activities along the liquidus are shown in Table 2-3 and Figure 2-7. In this experiment the working electrode contained the two phase mixture of InAs solid and In-rich liquid alloy. As the temperature was increased, some of the solid InAs dissolved in the In-rich liquid, decreasing the In composition of the equilibrium liquid solution. According to the phase diagram data, the composition x_{In}, decreases in a nearly exponential manner with temperature for In-rich compositions. The measured emf values

are expected to exhibit an exponential dependence and such is observed in the results. The results are in good agreement with the liquid phase In activity measurements conducted by Itoh [Ito82] using an electrochemical technique. However, the present set of data represent a stronger negative deviation from ideality than that suggested by Itoh.

Standard Gibbs Energy of Formation of InAs (s)

The cell that was used in the experiment for the measurement of standard Gibbs energy of formation of InAs (s) alongwith the half cell reactions is shown below:

$$B_2O_3(l),\ In\ (l,\ pure),\ In_2O_3\ (s)//YSZ//InAs\ (s),\ As\ (s,\ pure),\ In_2O_3\ (s),\ B_2O_3\ (l), \qquad (VI)$$

$$In\ (l,\ pure) + 3/2\ O^{-2} = 1/2\ In_2O_3\ (s) + 3e^- \qquad (2.13)$$

$$1/2\ In_2O_3\ (s) + As\ (s,\ pure) + 3e^- = InAs\ (s) + 3/2\ O^{-2} \qquad (2.14)$$

$$In\ (l,\ pure) + As\ (s,\ pure) = InAs\ (s) \qquad (2.15)$$

The above equation is transformed into the following overall cell equation by applying Wagner's approximation to the chemical potential of the essentially stoichiometric compound InAs (s):

$$In\ (l,\ pure) = In\ (ss) \qquad (2.16)$$

where ss denotes the solid solution In-As with composition fixed to lie along line towards the InAs(s) + As(s) region. This is equivalent to measuring the chemical potential of In along the As-rich solidus of the compound InAs. The standard Gibbs energy of formation of InAs referred to In (l) and As (s) states is given by the following relation:

$$\Delta^\circ G_f(InAs) = {}^\circ G_{InAs,s} - {}^\circ G_{In,l} - {}^\circ G_{As,rho} = -3FE \qquad (2.17)$$

The emf values, and the calculated standard Gibbs energy of formation of InAs are tabulated in Table 2-4 and can be seen in Figure 2-8 to exhibit a linear temperature

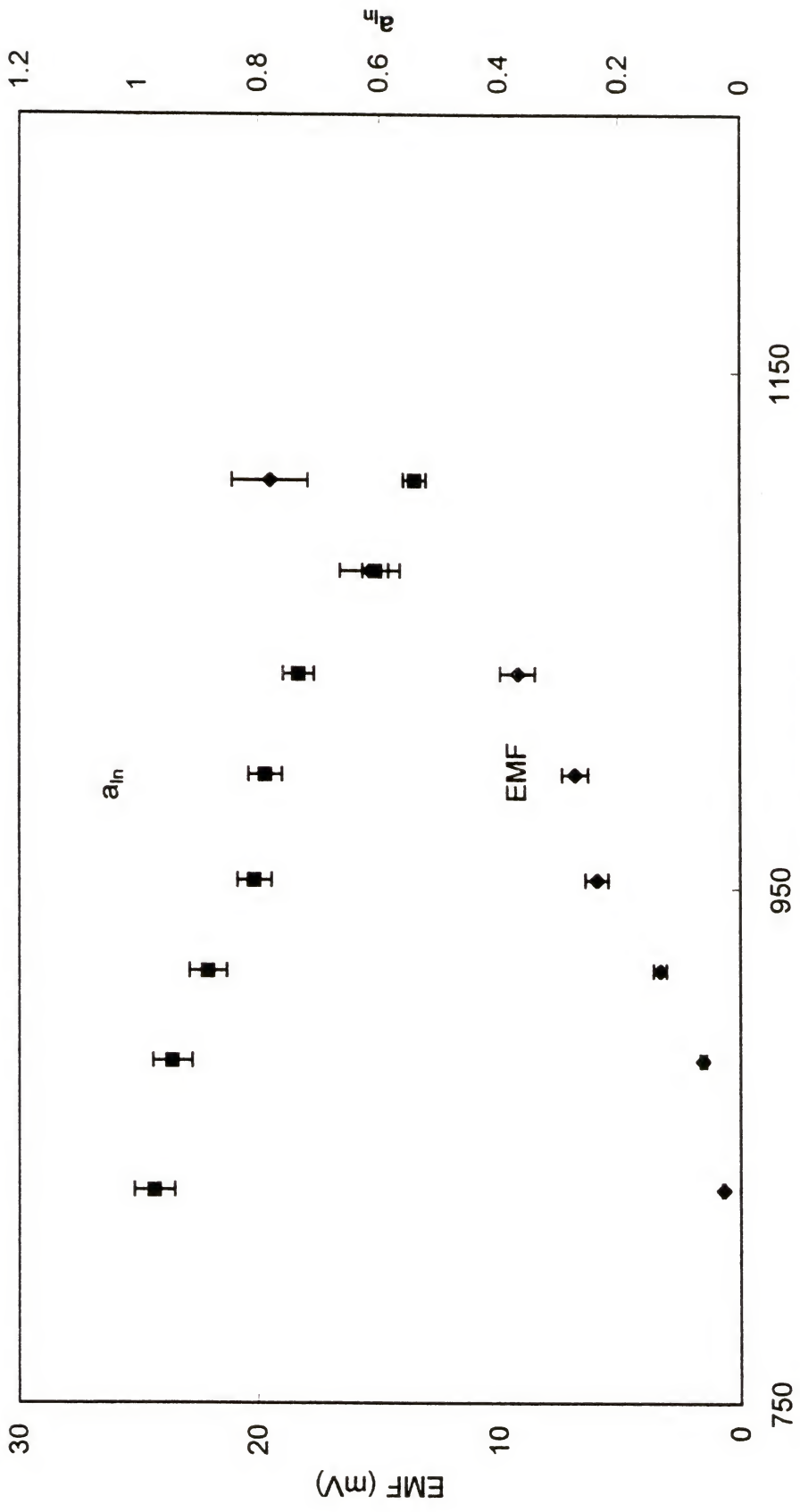

Figure 2-7. Measured emf and In activity along In-rich liquidus in the In-As system.

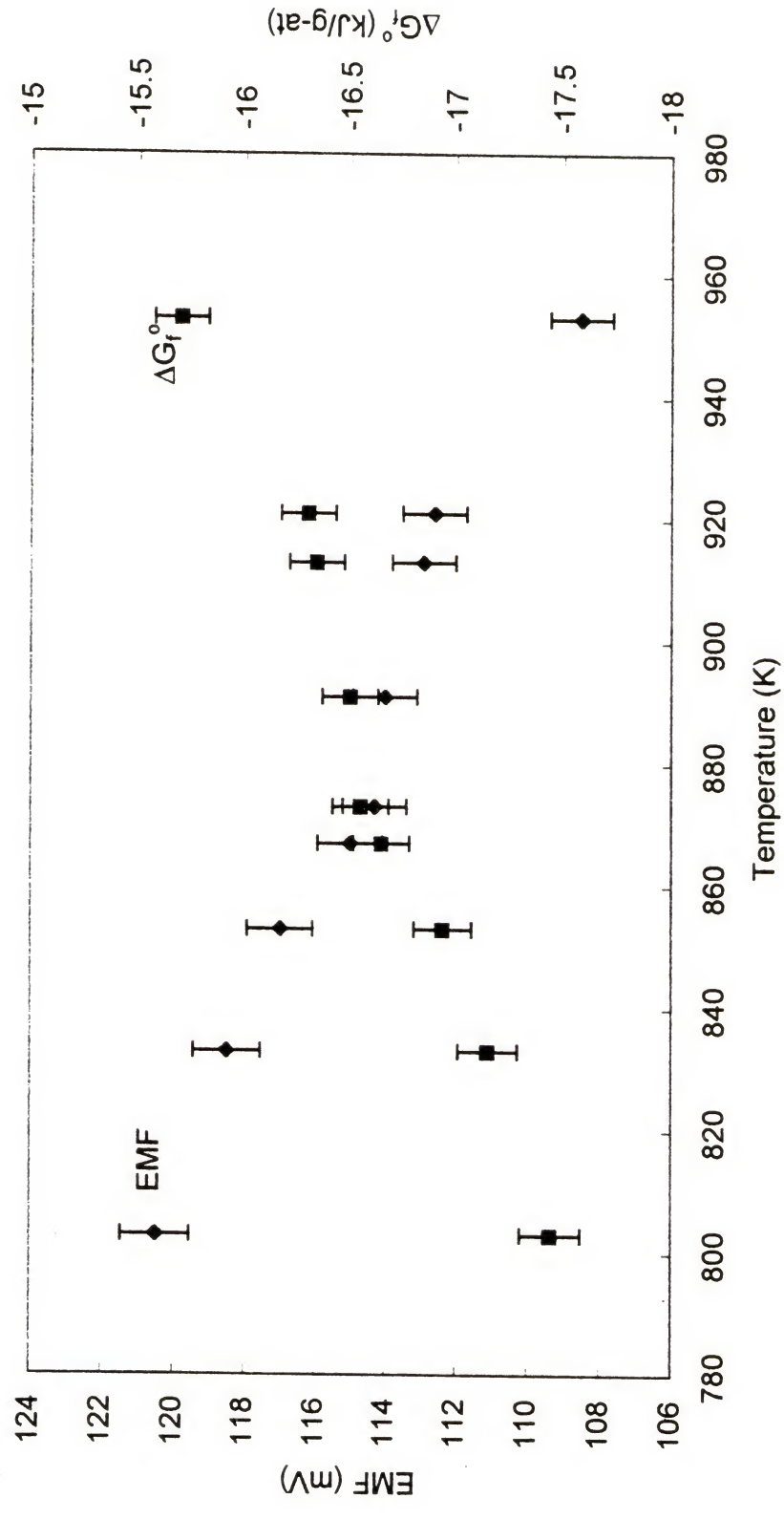

Figure 2-8. Temperature dependence of open circuit emf and standard Gibbs energy of formation of InAs(s).

dependence. The $\Delta^{\circ}G_f$ values compare well with the earlier emf measurements [Abb64 and Kre71] when extrapolated to the low temperature range. Some variation in the temperature dependence of the present data is indicative of possible As loss by volatilization (especially at higher temperatures) thereby resulting in lowering of the open circuit emf values. The values in the low temperature region have uncertainties related to difficulties in achieving equilibrium owing to slow diffusion and non-homogeneous two-phase solid mixture. Steady values were recorded at each temperature as being representative of the open circuit emf for the equilibrium cell at those temperatures.

As in the previous section for Ga-As system, both second and third law methods were employed to check the consistency of the Gibbs energy data for In-As system. Using the second law method, the standard enthalpy of formation was obtained by calculating the slope of $-\Delta^{\circ}G_f/RT$ vs $1/T$ curve which gave the value of $-\Delta^{\circ}H_f/R$ at the temperature of interest using the following expression:

$$\Delta^{\circ}H_f = -R\, d(-\Delta^{\circ}G_f/RT)/d(1/T) \qquad \text{(same as equation 2.7)}$$

The values of standard enthalpy of formation of InAs obtained from the second law analysis at different temperatures is shown in Table 2-5 and Figure 2-9. In the experimental range of temperature, the average value of $\Delta^{\circ}H_f(T_{av} = 878\ K)$ was -12.83 kcal/mol. The value obtained using the second law method after extrapolation of the $-\Delta^{\circ}G_f/RT$ vs $1/T$ curve to 298.15 K was $\Delta^{\circ}H_f(298.15\ K)^{II} = -11.92$ kcal/mol. Owing to extrapolation of experimental data and errors involved in slope measurement, the second law value is not as accurate as the value obtained from the third law analysis as described next.

Using pure component and solid compound C_p data and standard entropies, the standard enthalpy of formation $-\Delta^\circ H_f(298.15\ K)$ is determined by the third law method using the following formalism:

$$-\Delta^\circ H_f(298.15\ K) = -\Delta^\circ G_f(298.15\ K) - \Delta_f\left\{{}^\circ H(T) - {}^\circ H(298.15\ K)\right\} +$$
$$T\Delta^\circ S_f(298.15\ K) + T\Delta_f\left\{{}^\circ S(T) - {}^\circ S(298.15\ K)\right\} \qquad \text{(same as equation 2.8)}$$

where Δ_f indicates thermal function difference of the formation reaction.

It is interesting to see the temperature variation in the $\Delta^\circ H_f(298.15\ K)$ values obtained from the third law analysis as shown in Figure 2-10 and Table 2-5. The values show non-systematic temperature dependence, suggestive of random errors typical in the experiment. The temperature dependence varies and is acceptable within experimental errors. The mean value of $\Delta^\circ H_f(298.15\ K)$ in this temperature range is -14.53 kcal/mol. This compares excellently with the calorimetric measured values of -14.34 kcal/mol by Yamaguchi et al. [Yam94], -13.80 kcal/mol by Sharifov et al. [Sha63], and the calculated value of -14.05 kcal/mol reported by Chatillon et al. [Cha90]. This is also in agreement with the reported value of -14.80 kcal/mol by Schottky and Bever [Sch58]. The deviations in the calculated values of $\Delta^\circ H_f(298.15\ K)$ are of the order of $\pm$0.17 kcal/mol when compared to the mean value of -14.53 kcal/mol. This is comparable to the experimental errors of $\pm$0.24 kcal/mol reported by Yamaguchi et al. [Yam94] and $\pm$0.19 kcal/mol reported by Sharifov et al. [Sha63].

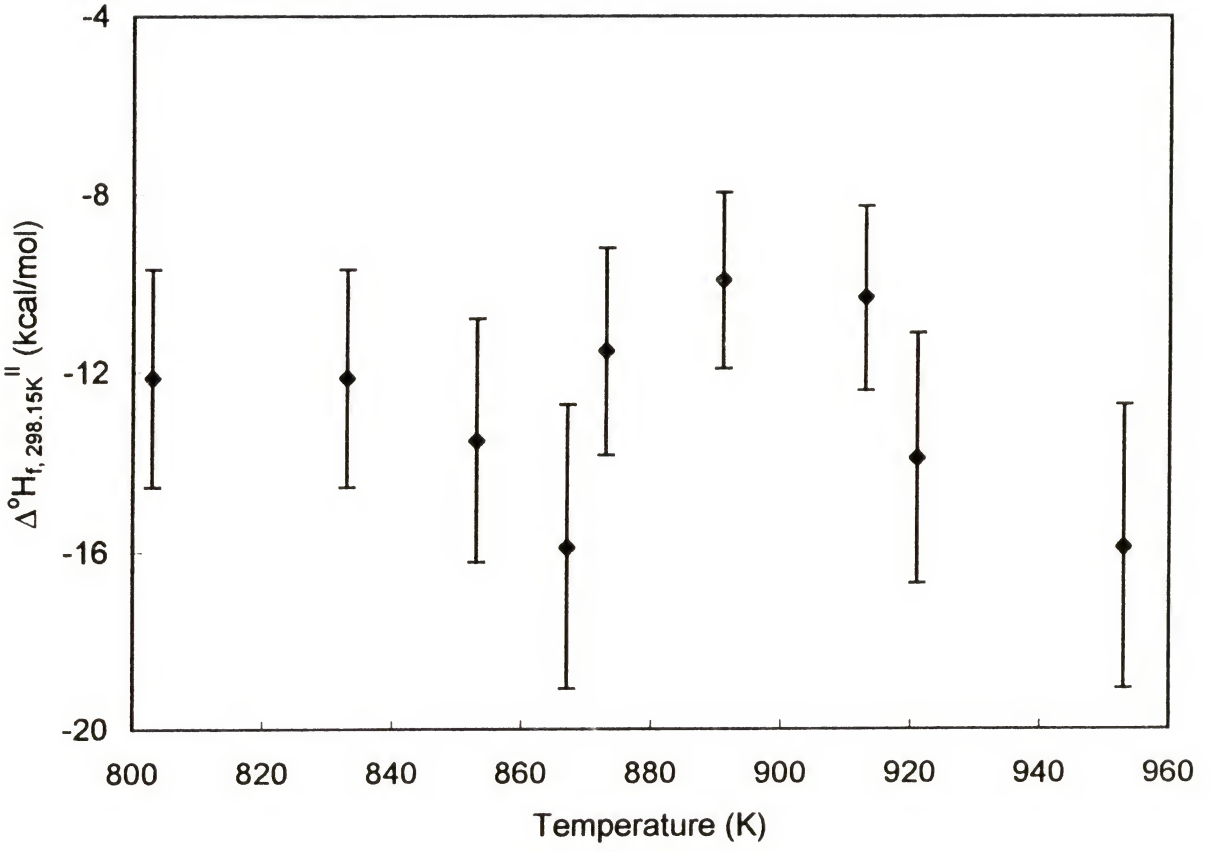

Figure 2-9. Calculated second law values of the enthalpy of formation of InAs at 298.15K.

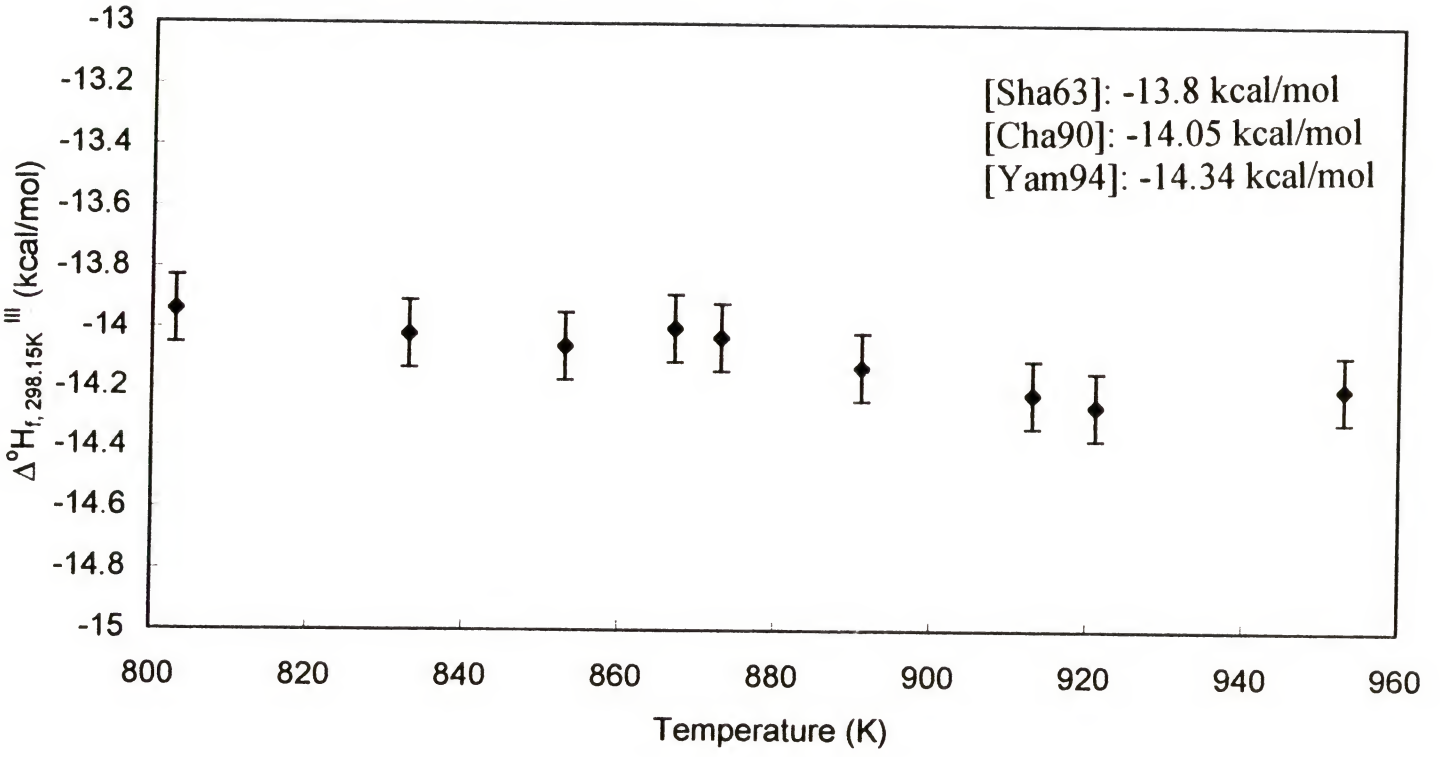

Figure 2-10. Calculated third law values of the enthalpy of formation of InAs at 298.15 K.

The experimental data exhibits tight distribution when compared to the deviations in the calculated values by Tmar and Chatillon [Tma87] and the measurements of Schottky and Bever [Sch58]. The value differs from the data of Pupp et al. [Pup74], Gutbier [Gut61] and Goldfinger and Jeunehomme [Gol59]. The emf method used by Abbasov et al. [Abb66] and Krestovnikov [Kre71] reported measurements at temperatures below 784 K, so the calculations of $-\Delta^{\circ}H_f(298.15\ K)$ were based upon extrapolations of their data. Thus, these data were discarded for comparison purposes. The reported values from literature have errors associated with errors in the values of specific heats of pure components, $C_p(T)$. The errors get easily propagated due to the temperature dependency of the $C_p(T)$ values. This is also seen in the calculated values in the present study. The temperature dependence seen in the present study also includes the errors associated with the $C_p(T)$ data. A possible cause exists in the temperature dependence of Gibbs energy data due to As losses due to volatilization.

In the above calculations, pure component specific heats and the standard elemental entropies at 298.15 K were taken from the Janaf Thermochemical Tables [Jan85] and were consistent with those from Hultgren [Hul73]. The standard entropy of InAs at 298.15 K was taken from Piesbergen [Pie63]. The results from analyses were in excellent agreement with the experimental data however; the discrepancy between the measured and calculated values indicates random errors inherent to experimental measurement, and systematic errors inherent to the choice of C_p data used in the calculations by numerous authors. Considering all uncertainities including those in the Gibbs energy measurements it is clear that the present calculations are in excellent agreement with literature values.

Sb-Te System

Recent investigations in the field of erasable optical recording technology have shown that materials which undergo a reversible phase transformation between the crystalline and glassy states upon irradiation are promising alternatives to magneto-optical materials. Many of these alternative recording media are based on chalcogenide alloys, most notably tellurium-containing alloys [Mar90]. In particular, the antimony-tellurium system is an attractive binary constituent for multicomponent optical storage media [Uij85, Poe85, Cha90 and Yam91]. Since the glassy state is obtained by quenching from the liquid state, insight into the thermodynamic properties and degree of ordering in the glassy state can be gained from study of the thermodynamic behavior of the equilibrium liquid state.

A thorough review of the thermodynamics of the Sb-Te system has been reported [Gho89]. The solid-liquid Sb-Te phase diagram is dominated by the fairly well characterized congruently melting compound Sb_2Te_3. The assessment results of Ghosh et al. [Gho89] also included two solid solutions in the Sb-rich segment of the phase diagram, though no experimental determinations of the solution thermodynamics for these two phases have been reported. The only thermodynamic property measurements for the liquid solution are two calorimetric determinations of the enthalpy of mixing throughout the entire composition range at a temperature near the melting point of Sb_2Te_3 [Mae72, Feu88]. These results showed an exothermic enthalpy change upon mixing with a minimum value reported at a composition close to the stoichiometry of the

Table 2-3. Summary of emf measurements for In activity along liquidus.

Temperature (K)	EMF (mV)	a_{In}	x^*_{In}	γ^*_{In}
833	0.70	0.971	0.970	1.003
883	1.53	0.941	0.945	0.996
918	3.30	0.882	0.927	0.952
953	5.90	0.806	0.908	0.888
994	6.80	0.788	0.876	0.899
1033	9.20	0.733	0.843	0.870
1073	15.40	0.607	0.803	0.756
1108	19.50	0.542	0.763	0.710
1128	21.0	0.523	0.736	0.711
1153	27.5	0.436	0.703	0.620

* Using Optimized Phase Diagram Data from [Tma84]

Table 2-4. Experimental Gibbs energy of formation of InAs (s).

Temperature (K)	EMF (mV)	$\Delta^{\circ}G_f$ (kJ/g-at)
803	120.5	-17.44
833	118.5	-17.15
853	117.0	-16.94
867	115.0	-16.65
873	114.3	-16.55
891	114.0	-16.50
913	112.9	-16.34
921	112.6	-16.30
953	108.5	-15.70

Table 2-5. Standard enthalpy of formation of InAs (s) by the second law analysis and values at 298.15K by the third law method.

Temperature (K)	$\Delta^\circ G_f$ (kJ/g-at)	$\Delta^\circ H_f(T)^{II}$ (kcal/mol)	$\Delta^\circ H_f(298.15\ K)^{III}$ (kcal/mol)
803	-17.44	-12.12	-13.94
833	-17.15	-12.12	-14.02
853	-16.94	-13.75	-14.06
867	-16.65	-15.90	-14.00
873	-16.55	-11.52	-14.03
891	-16.50	-9.94	-14.13
913	-16.34	-10.33	-14.22
921	-16.30	-13.91	-14.26
953	-15.70	-15.90	-14.20

compound Sb_2Te_3. In this study, the first experimental measurement of activity of the antimony in Sb-Te melts was performed.

Activity of Sb in Sb-Te Melts

The antimony activity was measured using a solid-state galvanic cell at a temperature near 911 K. The oxygen-ion conducting electrolyte yttria stabilized zirconia (YSZ) was selected in preference to a molten salt electrolyte because of the low boiling temperatures of the stable halides (e.g., 494 K for $SbCl_3$). With this selection of the electrolyte, the electrochemical cell used to measure the Sb activity is schematically represented as:

$$W/Sb,\ Sb_2Te_3//YSZ//\ Sb_xTe_{1-x},\ Sb_2O_3/W \qquad \text{(VII)}$$

The reference electrode consisted of pure liquid antimony in equilibrium with its stable oxide, Sb_2O_3. Assuming the solubility of oxygen in the Sb_xTe_{1-x} liquid phase is negligible, the activity of antimony, a_{Sb}, is related to the measured open circuit potential, E, by the following expression:

$$RT\ln a_{Sb} = RT\ln \frac{P_{O_2}^{I}}{P_{O_2}^{II}} = -3FE \qquad (2.13)$$

where T is the absolute temperature, R is the gas constant, F is the Faraday constant, and $P_{O_2}^{I,\ II}$ is the equilibrium oxygen partial pressure in the reference (I) or the working electrode (II).

The temperature of measurement was about 911 K; a temperature between the melting temperatures of pure Sb (904 K) or Sb_2Te_3 (891 K) and that of antimony sesquioxide (930 K). At this temperature, there was concern that volatilization losses

would affect the working electrode composition. For this reason both cell constructions depicted in Figures 2-2 and 2-3, designed to minimize electrode material evaporation, were used.

Measurements using the encapsulated cell assembly design was also used to conduct experiments on selected alloy compositions to confirm the findings of the compression cell assembly. The working electrode was comprised of a mixture of Sb_xTe_{1-x} and Sb_2O_3 Sb_2O_3 powder while the reference electrode contained a mixture of pure Sb and Sb_2O_3 powder. The annular space between the YSZ crucible and alumina cell holder contained the reference electrode material (Sb + Sb_2O_3), while the YSZ crucible contained the working electrode, which consisted of the alloy (Sb_xTe_{1-x}) of the desired composition and the most stable oxide (Sb_2O_3).

In these experiments B_2O_3 was not used. Careful design and assembly of these electrodes were able to yield stable emfs, however, the incorporation of B_2O_3 proved successful in reproducing these results in later experiments.

Nineteen alloys were studied throughout the entire composition range at a temperature near 911 K. The antimony activities were calculated from the measured emf and temperature with the use of equation (2.13) and are shown in Figure 2-11 as a function of composition. The results indicate that the solution is nearly ideal for Sb-rich compositions ($N_{Te} < 0.45$). For Te-rich compositions, however, moderate negative deviations from ideal solution behavior are evident.

Neglecting the small variation in activity in the measurement temperature range (908.6 to 915.7 K), the corresponding activity coefficient of tellurium in the melt was determined by integration of the Gibbs-Duhem relation using Darken's method [Dar53]:

$$\ln \gamma_{Te} = -\alpha_{Sb} N_{Te} N_{Sb} - \int_{N_{Te}=1}^{N_{Te}} \alpha_{Sb} dN_{Te} \qquad (2.14)$$

where $\alpha_{Sb} = \frac{\ln \gamma_{Sb}}{(1 - N_{Sb})^2}$ and N_i is the mole fraction of species, i. A summary of the experimental results and the calculated component activities, partial molar Gibbs energies Δg_i, and Gibbs energy of mixing (ΔG_{mix}) is given in Table 2-6. Smoothed values of ΔG_{mix} were combined with the calorimetric measurements of Feutelais et al. [Feu88] to yield the entropy of mixing, ΔS_{mix}, as displayed in Table 2-7 and Figure 2-12.

Discussion. There is considerable experimental evidence for the formation of short range order in Sb-Te melt. The enthalpy of mixing has been measured throughout the entire composition range in two different laboratories [Mae72, Feu88]. Both of the measurements show an exothermic enthalpy change with a minimum value near the composition of Sb_2Te_3. In addition, the electrical conductivity and viscosity data of Glazov et al. [Gla69] display an extremum near N_{Te}= 0.55. Furthermore, Abrikosov et al. [Abr59] pointed out that the thermoelectric power shows a sharp increase at the same composition. These results suggest that the melt structure has short range order, with the extent of ordering a maximum at a composition close to the stoichiometry of the highest melting compound, Sb_2Te_3.

The nearly ideal solution behavior for Sb-rich compositions is apparently a result of the measurement temperature (~ 911 K) being sufficiently greater than the liquidus

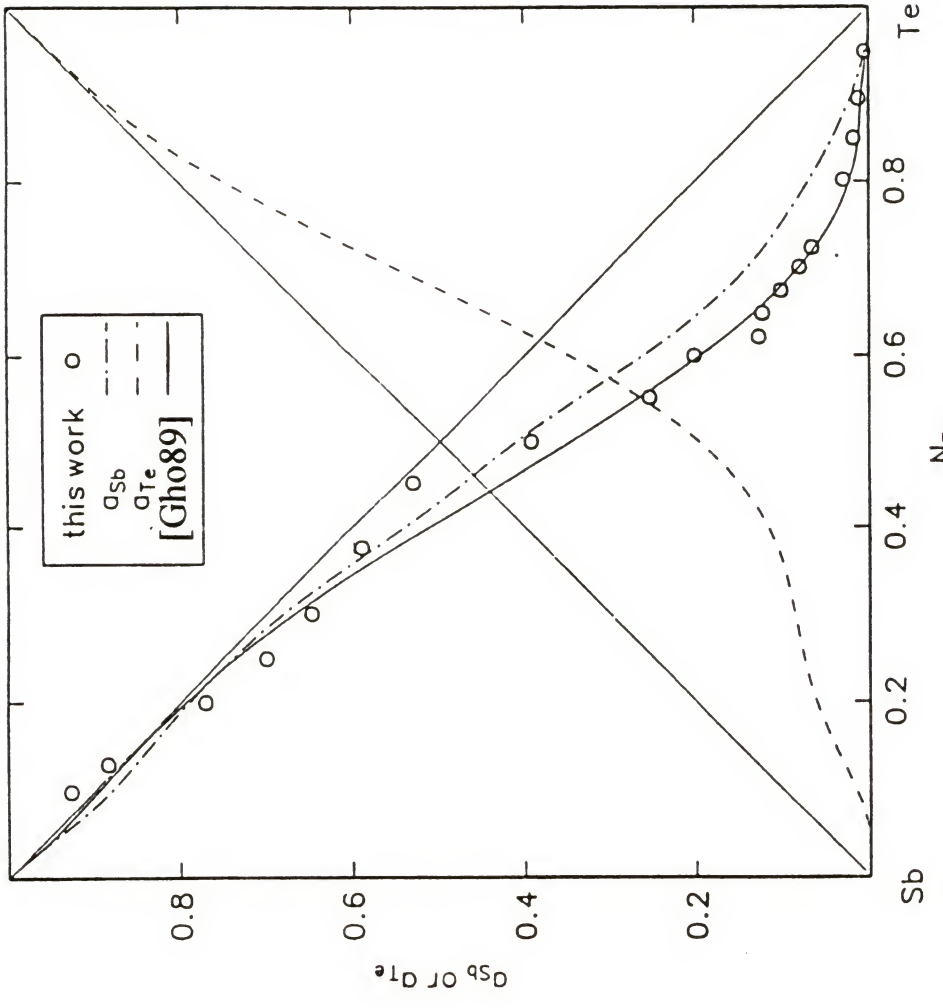

Figure 2-11. Activity of Sb in Sb-Te alloys.

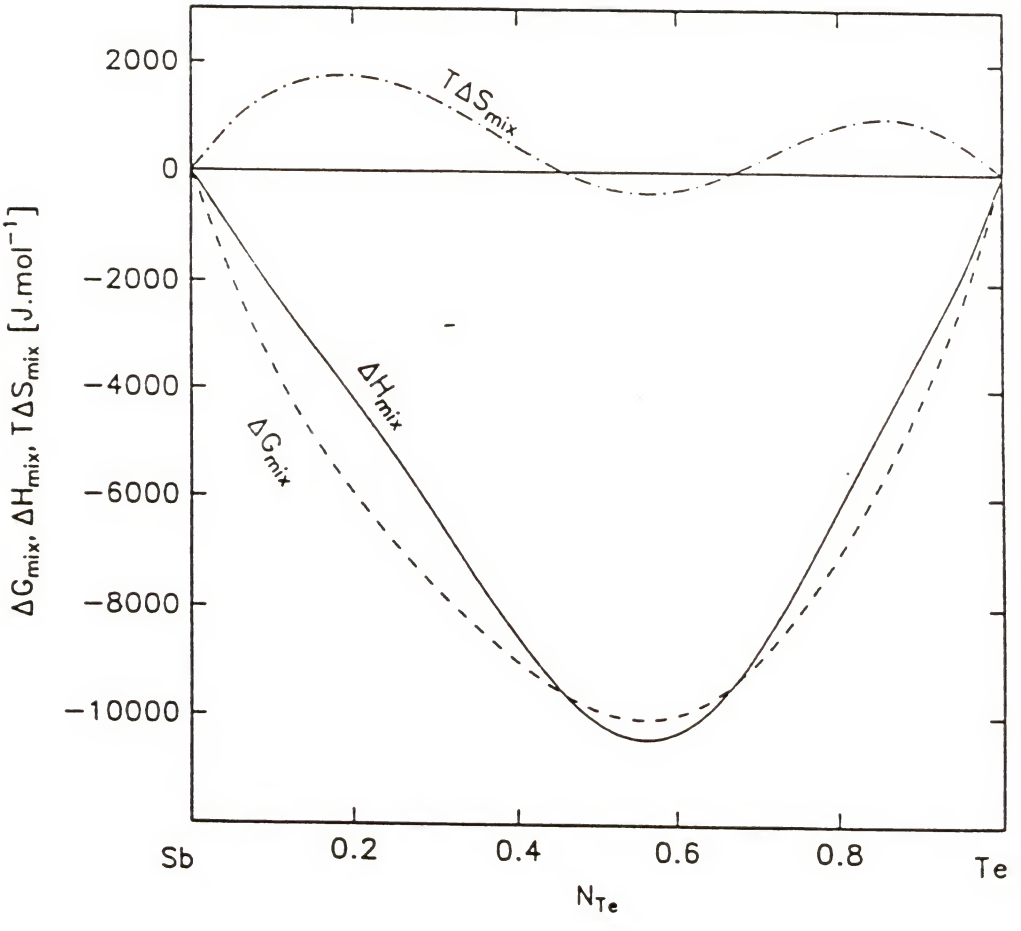

Figure 2-12. Calculated entropy of mixing values for Sb-Te alloys from calorimetric measurements and smoothed Gibbs energy of formation values.

temperature (minimum value near 813K at N_{Te} = 0.31 [Abr59, Bor86]) to dissociate the clusters. As the measurement temperature becomes closer to the liquidus value, the antimony activity shows negative deviations that are consistent with an increasing extent of unlike atom clustering. The Sb-Te system, however, does not show as high a tendency towards association as does the Sn-Te and Pb-Te systems [Kot88].

Figure 2-11 also shows the antimony activity proposed by Ghosh et al. [Gho89] as a result of their assessment study. In this work, a molten solution model with partial ionization developed by Hillert et al. [Hil85] was used to describe the melt behavior. Other researchers have used chemical theories in which molecular-like species are postulated to describe the apparent short range ordering between unlike atoms [Jor70, Cla82 and Som82]. The assessed antimony activity of Ghosh et al. [Gho89] shows excellent agreement with the measured values of this study for $0 < N_{Te} < 0.4$, while slightly less negative deviations were predicted for more Te-rich compositions. In this early assessment, these authors used the only available enthalpy of mixing data of Maekawa et al. [Mae72]. These data were measured at a higher temperature (935 K) than the more recent data of Feutelais et al. [Feu88] for which the temperature ranged from 909 to 918 K. Since the enthalpy of mixing is temperature dependent and more exothermic at lower temperatures, the solution behavior predicted from the assessment is expected to be slightly more ideal.

There are three reported measurements in the literature of the Gibbs energy of formation of the compound Sb_2Te_3 with a galvanic cell technique [Ger61, Sem69 and Mal86]. These results can be compared for consistency with the smoothed value of

Table 2-6. Summary of experimental results and calculated thermodynamic quantities for Sb-Te system.

Cell Type	N_{Sb}	T (K)	EMF (mV)	a_{Sb}	a_{Te}	Δg_{Sb} (kJ/mol)	Δg_{Te} (kJ/mol)	ΔG_{mix} (kJ/mol)
Encapsulated	0.051	915.6	139.4 ± 4	0.005	0.951	-40.36 ± 1.16	-0.38	-2.42
Encapsulated	0.105	915.6	115.7 ± 3	0.012	0.883	-33.50 ± 0.87	-0.95	-4.36
Encapsulated	0.150	914.2	105.7 ± 3	0.018	0.836	-30.60 ± 0.87	-1.36	-5.74
Encapsulated	0.198	915.6	92.1 ± 3	0.030	0.749	-26.66 ± 0.87	-2.20	-7.04
Encapsulated	0.276	915.6	71.3 ± 2.5	0.066	0.587	-20.65 ± 0.72	-4.06	-8.64
Encapsulated	0.298	908.6	66.0 ± 2.5	0.080	0.545	-19.10 ± 0.72	-4.59	-8.91
Encapsulated	0.325	914.2	60.3 ± 2.5	0.101	0.490	-17.44 ± 0.72	-5.42	-9.32
Encapsulated	0.351	914.2	55.3 ± 2	0.122	0.445	-16.00 ± 0.58	-6.15	-9.61
Encapsulated	0.378	913.9	54.4 ± 2	0.126	0.437	-15.75 ± 0.58	-6.29	-9.87
Encapsulated	0.400	911.8	42.0 ± 3	0.201	0.324	-12.16 ± 0.87	-8.54	-9.98
Compression	0.449	911.0	36.0 ± 1.8	0.253	0.274	-10.42 ± 0.52	-9.80	-10.08
Compression	0.500	909.6	24.5 ± 2	0.392	0.185	-7.09 ± 0.58	-12.77	-9.93
Compression	0.548	911.2	16.6 ± 0.8	0.531	0.132	-4.79 ± 0.23	-15.33	-9.56
Compression	0.624	910.6	13.9 ± 0.5	0.589	0.114	-4.01 ± 0.15	-16.44	-8.68
Compression	0.700	911.2	11.4 ± 0.5	0.647	0.095	-3.30 ± 0.15	-17.86	-7.67
Encapsulated	0.751	908.6	9.3 ± 0.8	0.700	0.077	-2.70 ± 0.23	-19.39	-6.85
Encapsulated	0.800	908.6	6.8 ± 0.8	0.771	0.055	-1.97 ± 0.23	-21.90	-5.96
Compression	0.870	909.6	3.2 ± 0.3	0.884	0.028	-0.93 ± 0.09	-27.09	-4.33
Encapsulated	0.901	908.6	2.0 ± 0.3	0.927	0.019	-0.57 ± 0.09	-29.48	-3.47

Table 2-7. Summary of smoothed thermodynamic mixing values for Sb-Te alloys at 911 K.

N_{Te}	ΔG_{mix} (J mol^{-1}) [this work]	ΔH_{mix} (J mol^{-1}) [Feu88]	$T\Delta S_{mix}$ (J mol^{-1}) T = 911 K
0.000	0	0	0
0.050	-1885	-1057	828
0.100	-3503	-2120	1328
0.150	-4839	-3157	1682
0.200	-5938	-4194	1744
0.250	-6864	-5264	1600
0.300	-7671	-6376	1295
0.350	-8387	-7498	889
0.400	-9015	-8563	452
0.450	-9532	-9473	59
0.500	-9894	-10124	-230
0.550	-10056	-10423	-367
0.600	-9975	-10306	-331
0.650	-9626	-9759	-133
0.700	-9004	-8822	182
0.750	-8129	-7589	540
0.800	-7030	-6188	842
0.850	-5734	-4747	987
0.900	-4224	-3332	892
0.950	-2399	-1862	537
1.000	0	0	0

Table 2-8. Values of the standard Gibbs energy of formation of $Sb_{0.4}Te_{0.6}$ at 540 K and 673 K (kJ/mole).

T_m (K)	[Mal86]	[Sem69]	[Ger61]	This Work
540	-13.63	-12.90	---	-12.28
673	-12.74	---	-12.34	-12.36

ΔG_{mix} of this study at the N_{Te} = 0.6 composition by considering the following thermodynamic sequence:

$$0.4\ Sb\ (T_m, s) \rightarrow 0.4\ Sb\ (911\ K, l) \qquad \Delta G_1 \quad (2.15)$$

$$0.6\ Te\ (T_m, s) \rightarrow 0.6\ Te\ (911\ K, l) \qquad \Delta G_2 \quad (2.16)$$

$$0.4\ Sb\ (911\ K, l) + 0.6\ Te\ (911\ K, l) \rightarrow Sb_{0.4}Te_{0.6}\ (911\ K, l) \qquad \Delta G_{mix} \quad (2.17)$$

$$Sb_{0.4}Te_{0.6}\ (911\ K, l) \rightarrow Sb_{0.4}Te_{0.6}\ (T_m, s) \qquad \Delta G_3 \quad (2.18)$$

The overall reaction in this sequence is simply the formation reaction at the galvanic cell measurement temperature, T_m. Values of $\Delta^\circ G_f(T_m)$ were calculated by combining the selected values of [Bar77] for ΔG_1, ΔG_2 and ΔG_3 with the value ΔG_{mix} = - 9.98 kJ/mole suggested by this study. The results of this calculation are compared to the galvanic cell measurements of $\Delta^\circ G_f$ at two selected temperatures in Table 2-6. This calculation indicates good agreement between the results of the solid and the liquid solution emf measurements. Using this sequence, the calculated value of $\Delta^\circ G_f(298.15\ K)$ for $Sb_{0.4}Te_{0.6}$ is - 12.05 kJ/mole.

Experimental Results in Ternary Systems

Data in ternary system Ga-In-As are scarce due to high vapor pressures associated with these alloys owing to the As component in the alloys. Furthermore, solid phase diffusivities are slow creating problems in the attainment of thermodynamic equilibrium. Some phase diagram data have been determined, primarily in the Ga-, In- rich composition ranges. Very scarce data however, exists on the thermodynamic properties of these alloys. Calorimetric measurements of enthalpies of formation and mixing were reported by Rugg

et al. [Rug95]. In this study, activity measurements have been performed in both liquid and solid solutions in the Ga-In-As system.

Activity of Ga in In-rich Ternary Liquid $Ga_xIn_yAs_{1-x-y}$ Solutions

The activity of gallium in the ternary liquid solution with indium and arsenic was determined at two overall In-rich compositions.

Most of the data exists in terms of phase diagram determinations [Van63, Hoc66, Woo58, Shi56] or calculations [Cre81, Lit91, Str69] in the pseudobinary phase region. It was essential to perform direct measurements for activity data in this system so that the validity of solution models used to describe this system could be judged. The experiments were designed under the constraints of high In compositions and low Ga and As contents. This was because at Ga-rich compositions the measurements were least accurate owing to the extremely low emf values generated; while at high arsenic compositions, the high arsenic vapor pressures caused experimental problems.

The following cell was used in the experiment:

$$Ga_2O_3,\ Ga(l,\ pure)//YSZ//Ga_xIn_yAs_{1-x-y}\ (l),\ Ga_2O_3 \qquad \text{(VIII)}$$

$$Ga\ (l,\ pure) + 3/2\ O^{-2} = Ga_2O_3 + 3e^- \qquad (2.19)$$

$$Ga_2O_3 + 3e^- = Ga\ (\text{in } Ga_xIn_yAs_{1-x-y}\ (l)) + 3/2\ O^{-2} \qquad (2.20)$$

$$Ga\ (l,\ pure) = Ga\ (\text{in } Ga_xIn_yAs_{1-x-y}\ (l)) \qquad (2.21)$$

The activity of gallium in the ternary alloy is given as:

$$a_{Ga} = \exp\left(\frac{-3FE}{RT}\right) \qquad (2.22)$$

The working electrode was designed by using measured amounts of InAs(s), GaAs(s) and pure In metal, along with some quantity of Ga_2O_3 powder. The amounts of the materials were chosen to yield two alloys of different compositions in the In-rich region of the ternary phase diagram. The amount of Ga_2O_3 in the electrodes was approximately 0.8g. The following are the compositions studied:

$In_{0.8465}Ga_{0.06788}As_{0.08563}$ (Cell I)

$In_{0.8253}\ Ga_{0.07561}\ As_{0.09911}$ (Cell II)

With the increase in cell temperature, the indium metal melts first (m.p. ~ 428 K). The solids InAs and GaAs start dissolving in the liquid indium melt to form an In-rich ternary liquid phase $Ga_xIn_yAs_{1-x-y}$ which is in equilibrium with the pseudobinary solid phase $Ga_XIn_{1-X}As$ where 'X' denotes mole fraction of GaAs in the pseudobinary solid phase. This was supported by the observation that emf vs time stayed constant (within +/- 0.05 mV for 2 hrs or more) at different temperature settings indicating achievement of cell equilibrium. As the temperature is increased, the In-rich ternary liquid phase $Ga_xIn_yAs_{1-x-y}$ gets leaner in the indium component while moving along the lines of constant In/As ratio on the liquidus surface of the ternary system. Once the terminal point is reached on the liquidus surface corresponding to the prepared alloy composition in the ternary phase diagram, the activity measurements correspond to the single ternary liquid phase $Ga_xIn_yAs_{1-x-y}$. The transition from the two-phase experimental measurement to that in the single phase ternary liquid phase gives the coordinates of the liquidus point.

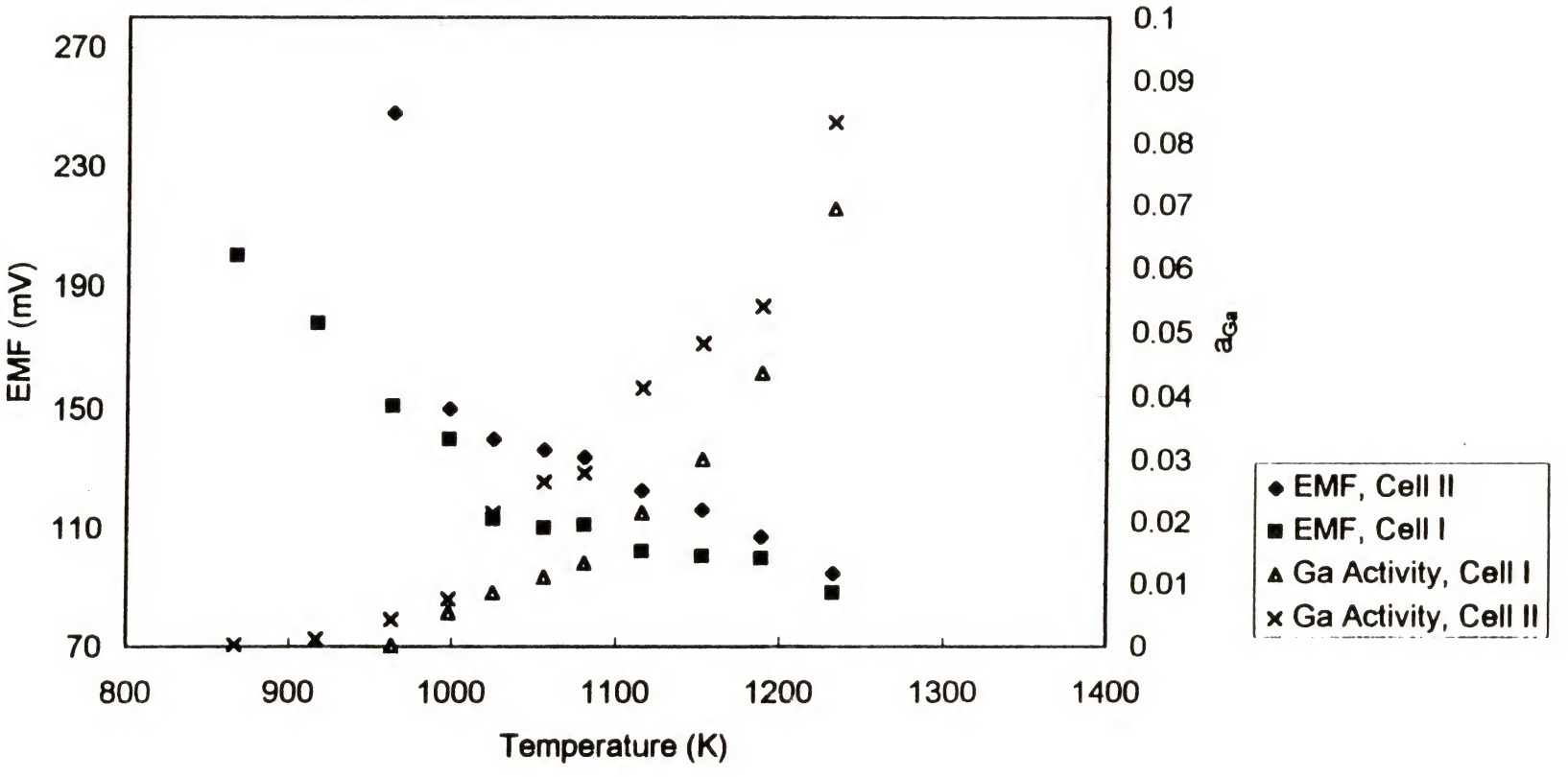

Figure 2-13. Activity of Ga in ternary liquid $Ga_xIn_yAs_{1-x-y}$ solutions along constant In/As ratios.

Table 2-9. Summary of emf measurements in the ternary system along lines of constant In/As ratio.

Temperature (K)	EMF (mV) Cell I*	EMF (mV) Cell II**	a_{Ga}^{I}	γ_{Ga}^{I}	a_{Ga}^{II}	γ_{Ga}^{II}
867	---	200.0	---	---	0.000325	---
917	---	178.0	---	---	0.001156	---
963	248.0	151.0	0.000127	---	0.00424	---
998	150.0	140.0	0.005334	0.079	0.00756	---
1025	140.0	113.0	0.00858	0.126	0.02150	0.280
1056	136.5	110.0	0.01107	0.163	0.02650	0.350
1081	134.0	111.0	0.01331	0.196	0.02796	0.370
1116	122.9	102.0	0.0215	0.317	0.04136	0.547
1153	116.0	100.4	0.03013	0.443	0.04825	0.638
1189	107.0	99.6	0.04356	0.642	0.05410	0.714
1233	94.5	88.0	0.06934	≈1.00	0.08330	≈1.00

* (Cell I) $x_{Ga} = 0.068$, $x_{In} = 0.847$
** (Cell II) $x_{Ga} = 0.076$, $x_{In} = 0.825$

The emf measurements for the two cells in the ternary Ga-In-As system are presented in Table 2-9 and shown in Figure 2-13. The emf versus temperature curves for the two cells show a nearly linear dependence. Both the cells, however, show a discontinuity in the emf versus temperature dependence at certain point in which the slope of the curve changes drastically indicating a transition from a solid-liquid two-phase region to a single liquid phase. The temperature at which this occurs is the liquidus temperature of the ternary alloy for that particular composition. The liquidus temperature obtained graphically for the alloy in Cell I ($x_{Ga} = 0.068$, $x_{In} = 0.847$) is 1020 K, and that for alloy in Cell II ($x_{Ga} = 0.076$, $x_{In} = 0.825$) is 1040 K. These values are in excellent agreement (within 10 K) extrapolated estimates at these compositions from experimental phase diagram data of [Van63, Hoc66, Woo58, and Shi56] and the calculations of [Str72]. The activity values as seen from Table 2-9 indicate negative deviations from ideal solution behavior in the ternary liquid phase $Ga_xIn_yAs_{1-x-y}$, the degree of non-ideality decreasing with increasing temperature.

Activity of GaAs (s) in the Pseudobinary Section GaAs-InAs

Very little information is available on the thermodynamics of the solid solution $Ga_xIn_{1-x}As$. There is a need to provide insight into the thermodynamic behavior of the compounds GaAs and InAs in the pseudobinary section GaAs-InAs of the ternary system, and to understand the interactions between the Ga and In atoms on the metallic sublattice. Such information makes it possible to examine the stability of the solid solution at different

temperatures and regions of the phase diagram, thereby, relating to the difficulty or ease of growing alloys from the melt by standard epitaxial growth techniques. The calculation of structural properties and phase diagram aids in evaluating these alloys for use in long wavelength infrared material (LWIR).

Electrochemical experiments were performed by Krestovnikov et al. [Kre73] allowing calculation of activities of GaAs and InAs in the solid solution, which they described as being ideal. Later studies on low temperature heat capacity and mass spectrometric vapor pressure measurements by Tmar et al. [Tma88] suggest immiscibility in the $Ga_xIn_{1-x}As$ system with a critical temperature of about 700 K. Experiments conducted by Ding et al. [Din86] provided direct evidence of the existance of a miscibility gap by high-resolution electron microscopy and electron and x-ray diffraction studies on annealed samples. In the present work a direct measurement of GaAs activity at one composition in the pseudobinary section as a function of temperature by electrochemical technique is reported.

The galvanic cell used in the experiment is shown below with the half cell reactions:

$$B_2O_3(l), Ga_2O_3(s), GaAs\ (s), As\ (s)//YSZ//Ga_xIn_{1-x}As, As\ (s), Ga_2O_3(s), B_2O_3(l) \quad \text{(IX)}$$

$$GaAs\ (s, pure) + 3/2\ O^{-2} = 1/2\ Ga_2O_3 + As\ (s, pure) + 3e^- \quad (2.23)$$

$$1/2\ Ga_2O_3 + As\ (s, pure) + 3e^- = GaAs\ (ss) + 3/2\ O^{-2} \quad (2.24)$$

$$GaAs\ (s, pure) = GaAs\ (ss) \quad (2.25)$$

where ss denotes GaAs in the solid solution $Ga_xIn_{1-x}As$.

Table 2-10. Summary of measured activities of GaAs in the pseudobinary $Ga_xIn_{1-x}As$ solid phase.

Temperature (K)	EMF (mV)	a_{GaAs}	$\Delta\overline{G}_{GaAs}$ (J/mol)	$\Delta\overline{H}_{GaAs}$ (J/mol)	γ_{GaAs}
873	3.5	0.961	-1013.3	20569	2.13
920	5.6	0.809	-1621.2	20569	1.79
928	6.1	0.802	-1765.9	20569	1.78
960	8.75	0.728	-2533.1	20569	1.61
968	12.47	0.638	-3610.1	20569	1.41
983	13.30	0.624	-3850.4	20569	1.38
1008	15.00	0.596	-4342.5	---	1.32
1023	13.5	0.632	-3474.0	-25885	1.47
1056	11.5	0.684	-3329.3	-25885	1.52
1088	9.5	0.738	-2750.3	-25885	1.64
1113	8.6	0.764	-2489.7	-25885	1.69

Experiments were conducted to verify the non-interference of B_2O_3 powder with the contents of the electrode material in both the compartments as discussed earlier. Once this was established a 'compression design' electrochemical cell was assembled. The working electrode was designed by depositing a 3 to 5μ thick film of $Ga_{0.451}In_{0.549}As$ on one surface of the solid electrolyte by either organometallic chemical vapor deposition (MOCVD) process or by vapor phase epitaxy (VPE) done at Epitaxx, Inc. The unwanted deposition on the edges of the YSZ disk were etched chemically and subsequently cleaned by rinsing in deionized water. Small quantities of Ga_2O_3, B_2O_3 and As powder were sprinkled uniformly on the deposited film. The preparation of the reference electrode was fairly simple. The constituent powders were mechanically mixed and placed in the reference electrode crucible. The quantity of B_2O_3 was approximately 0.6 to 0.8g. Electrical contact was made by means of tungsten foils sandwiched between the electrolyte and the electrode crucibles.

The open circuit emf of the galvanic cell is related to the standard chemical potential difference across the electrolyte or the partial Gibbs energy of GaAs in the solid solution. At equilibrium, the standard Gibbs energy of the reaction III is given as:

$$\Delta^{\circ}G_f = -3FE = RT\ln(a_{GaAs,s}) \qquad (2.19)$$

The activities obtained by these electrochemical measurements are presented in Figure 2-14 and Table 2-10 as a function of temperature.

Summary of data analysis. The activity of GaAs in the pseudobinary $Ga_xIn_{1-x}As$ solid phase is a decreasing function of temperature in the experimental range of 873 to 1113 K. Beyond this temperature range, however, the activity increases monotonically with temperature as shown in Figure 2-14. It appears that the pseudobinary section

GaAs-InAs exhibits a miscibility gap in the solid phase. The temperature at which the emf vs temperature curve shows a discontinuity in temperature dependence (transition from a monotonically increasing to monotonically decreasing function) is the coordinate of the miscibility gap at GaAs = 0.451 composition of the alloy $Ga_xIn_{1-x}As$. The activity data for temperatures above 1008 K for the alloy $Ga_{0.451}In_{0.549}As$ in the liquid single phase of the pseudobinary phase diagram, exhibit positive deviations from ideal solution behavior.

The present results are in disagreement with the previous emf activity measurements [Kre73] that reported ideal behavior for solutions rich in both GaAs and InAs. The results of this study, however, support the findings of Tmar et al. [Tma88] who identified $Ga_XIn_{1-X}As$ alloys as exhibiting a miscibility gap, the range being $0.27 < x_{GaAs} < 0.75$ at 950 K. They estimated the critical temperature from Knudson cell mass spectrometric studies of InAs activities to be about 880 K. This is significantly higher than the value of 700 K estimated from previous calculations [Tma87] from the pseudobinary phase diagram data and estimates of the interaction parameter assuming regular solution model and random distribution of Ga and In atoms in the metal sublattice. The present data suggests higher critical temperature, an estimate being between 950 to 1050 K. This is in good agreement with the critical temperature estimate by Ding et al. [Din86] as being in the range of 848 to 923 K. Shen et al [She95] performed an optimization of the ternary system in the pseudobinary GaAs-In-As phase diagram and calculated the miscibility gap in the solid phase region. Their calculation showed a critical temperature of 814.9 K.

The positive deviations from ideal solution behavior are suggestive of a disordered state and strong interaction between like atoms in the metal sublattice in accordance with the findings of [Tma87] suggesting positive excess entropy of mixing. The positive

deviations are in agreement with the calculations of Ban and Ettenberg [Ban73], though the measured values of this study suggest a higher degree of non-ideality.

In summary, the present work illustrates electrochemical measurements of GaAs activity in the pseudobinary solid region of the GaAs-InAs phase diagram confirming the existence of a miscibility gap and the presence of strong disorder in the solid phase. Earlier optimizations [Fos72, Pan72, Ant70, Cre81, Ona82a, Ona82b, Str69] and estimates from physical models [Str82, Str83, Str72] lead to values for the interaction parameter ranging from 3 to 14.650 kJ/mol. More experiments are required to obtain a complete understanding of thermodynamic behavior in the pseudobinary solid region and to determine precisely the range of immiscibility in the solid phase as well as the critical temperature. It is clear from the present work, however, that the interaction parameter has significant temperature dependence. Similar work conducted at different alloy compositions will yield more data points for the characterizing the solid phase in the pseudobinary cut and will aid in providing the necessary thermodynamic information for this section in the phase diagram.

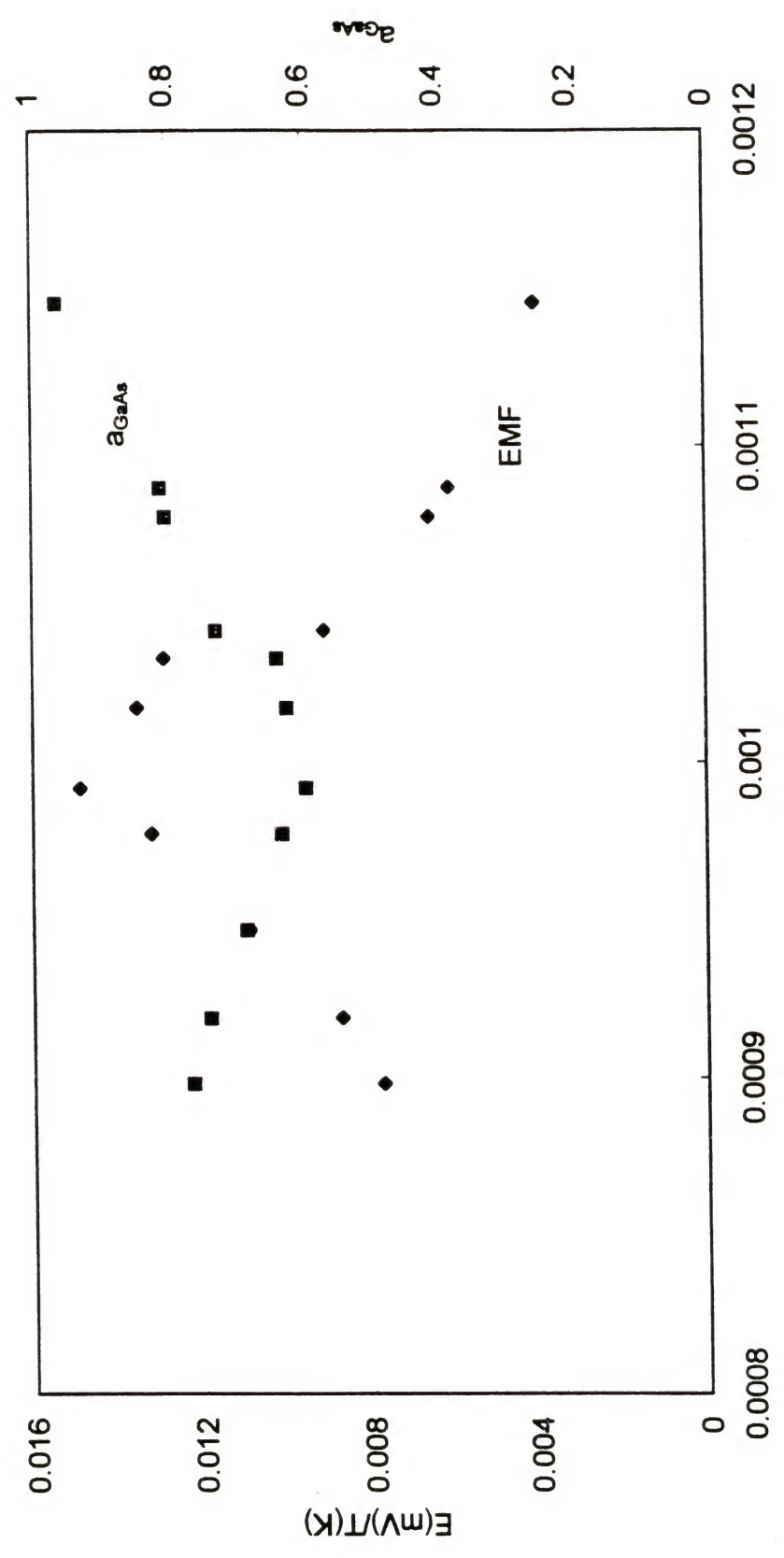

Figure 2-14. Activity of GaAs in the pseudobinary section GaAs-InAs.

CHAPTER 3
ASSESSMENT STUDIES

Assessment Procedure(Lukas Program)

An assessment is an optimization routine in which optimal values for the parameters of physical or chemical models describing the Gibbs energies of phases are estimated from the available thermodynamic properties of a system along with the phase equilibria data.

The values of the estimated parameters permit prediction and extrapolation for unknown properties of the system. Such model based predictions are of specific interest to systems in which thermodynamic property determinations are limited to certain regions of the phase diagram due to experimental difficulties (e.g., high vapor pressure of Group V elements) or to systems that are characterized by an excessively large number of experiments that contain inconsistent data. Experiments often require long equilibration times because of slow diffusion rates in the solid state. It is thus, economical and practical to utilize an appropriate thermodynamic model describing the thermochemical behavior of the system. The model parameters can be used to make predictions in unexplored regions of the phase domain, and in the case of ternary and higher order systems, perform calculations based upon the determined binary limits.

The first step in an assessment is to choose a suitable model for all phases, including the pure component, compound and the solution phases, that accurately describes the Gibbs energy of each phase. For solutions, this implies the formulation of a model for the excess Gibbs energy (ΔG^{ex}) of the mixture in terms of the temperature and concentration dependence. It is desirable to use as few terms as possible in the expression for ΔG^{ex} in order to avoid extrapolation difficulties. It is frequent that very different thermodynamic formulations result in very similar proposed phase diagrams [Wag58]. If experimental data can be reasonably well represented by several different thermodynamic models, a simpler model usually provides the clearest insight into the basic properties of the system and behaves better when extrapolating data. Thus, it is important to check the adopted thermodynamic model for physically unrealistic parameters.

Various types of solution models have been used for semiconductor solutions. In particular, the Redlich-Kister solution model has been found to adequately fit thermodynamic data for most of III-V semiconductor systems. Owing to it's widely accepted use for representation of thermodynamic properties of III-V semiconductor systems and ease of making reliable extrapolations, this model was chosen to represent the reported enthalpy, component activities and phase diagram data in this study. The expression is as follows:

$$\Delta G^{ex} = x_i x_j \sum \left(x_i - x_j\right)^{\nu} L_{ij}^{(\nu)} \qquad (3.1)$$

where the coefficients $L_{ij}^{(\nu)}$ are functions of temperature according to Lukas description [Luk77]:

$$L_{ij}^{(n)} = A_{ij}^{(n)} - B_{ij}^{(n)}T + C_{ij}^{(n)}T(1-\ln T) - D_{ij}^{(n)}T^2/2 - E_{ij}^{(n)}/2T - F_{ij}^{(n)}T^3/6 \qquad (3.2)$$

where the coefficients $A_{ij}^{(n)}$, $B_{ij}^{(n)}$ .... $F_{ij}^{(n)}$ are the model parameters fitted to the experimental data for the liquid phase in the optimization routine of the Lukas software. The coefficients $A_{ij}^{(n)}$ and $B_{ij}^{(n)}$ correspond to the temperature independent contributions to the excess enthalpy and entropy of mixing in the liquid phase. Whereas, the terms $C_{ij}^{(n)}$ ... $F_{ij}^{(n)}$ are the specific heat terms in the formation equation for the liquid phase from the elements in their standard states.

The even values of index n yield symmetric functions in composition and tend to flatten the parabolic nature of ΔG^{ex}. The odd values of n, on the other hand, tend to skew the parabolic function. Similar coefficients $a_{ij}^{(n)}$, $b_{ij}^{(n)}$ .... $f_{ij}^{(n)}$ are obtained during the optimization of model parameters for the solid compound phase. in which case the expression for the $L_{ij}^{(n)}$ coefficient for the solid phase is as follows:

$$L_{ij}^{(n)} = a_{ij}^{(n)} - b_{ij}^{(n)}T + c_{ij}^{(n)}T(1-\ln T) - d_{ij}^{(n)}T^2/2 - e_{ij}^{(n)}/2T - f_{ij}^{(n)}T^3/6 \qquad (3.3)$$

The parameters in this expression have the same connotation in the solid phase as do the parameters described above for the liquid phase. The solid III-V compound (e. g., GaAs) is regarded as a line compound, because of the typically narrow region of solid solution about its ideal stoichiometry of $x_V = 0.5$. The pure liquid phase was chosen as the reference state for the liquid solution. For the stoichiometric compound, the solid elements in their standard states were chosen as the references for the compound; the choice between pure solid and liquid reference states is entirely arbitrary.

Negligible mutual solubility between the pure solid Group III and V elements was assumed. Pure component SGTE (Scientific Group Thermodata Europe) lattice stabilities were employed to express the Gibbs energies of the elements in the stable phase relative to

the enthalpy of the "Standard Element Reference" {i.e, the enthalpies of the pure elements in their defined phases at 10^5 Pa and 298.15 K (denoted as G-H_{ser}) [Din89]}.

The Gauss method is adopted in the Lukas software for least square fitting the data. The strategy of the calculations was based upon the Newton-Raphson method. Marquardt's algorithm, which is a combination of Newton-Raphson method and the steepest descent method, was best suited to calculate complete phase diagrams and their sections. Flexibility is assigned in the optimization by the ability to choose different weighting factors for the source literature, and is taken as the reciprocal of the estimated accuracy of the measured values.

Two different versions of error equations were utilized, one being an explicit expression while the other an implicitely defined function. The choice of the error equation is governed by the type of data in hand, the expression chosen for the adjustable coefficients and partly by the stage of optimization. Especially in the early stages of optimizations, where the coefficients are far from the best values, the explicit version more probably directs the calculation to convergence than the implicit expression of the error equation.

The mean square of error was the criterion used to obtain the best fit, however, the lowest value did not necessarily imply the best thermodynamic description of the system. Examining the fit of each experimental data point to the values calculated from the optimization together with the mean square of error for the entire dataset was used as the criterion for a good fit.

Assessments of Binary Systems

Ga-As Assessment

Ga-As system has been investigated for it's thermodynamic properties and phase diagram by many investigators as discussed in section 2.2.1. The selected data set for phase diagram, enthalpy and Gibbs energy for Ga-As system are shown in Tables 3-1 through 3-3 together with the experimental method used, the range of measurements, and the estimated errors in the techniques employed.

Redlich-Kister polynomial was used to model the liquid phase, while a line compound description was used for the essentially stoichiometric compound $Ga_{0.5}As_{0.5}$. The pure liquid was chosen as the reference phase for the Ga-As system. However, for the stoichiometric compound, the solid elements in their standard states were chosen as the reference phases. Negligible solubility of Ga in As and of As in Ga was assumed, this assumption being consistent with other studies [Hal63 and Per80].

Four terms, two for the liquid phase and two for soild GaAs, $A_{ij}^{(n)}$, $B_{ij}^{(n)}$, $a_{ij}^{(n)}$ and $b_{ij}^{(n)}$, were sufficient to model the sytem. The terms $C_{ij}^{(n)}$ and $c_{ij}^{(n)}$ did not significantly improve the fit, and therefore were not included in the final optimization. This is consistent with the low values available for the experimental ΔC_p values for GaAs (l) and GaAs (s). The selected specific heat data and their references are listed in Table 3-2. The phase diagram is fairly well characterized for the system, however, the thermodynamic information in the $x_{As} > 0.5$ region and the high temperature region of the phase diagram is lacking.

Standard steps were followed to perform the optimization as outlined in the previous section. The salient features are:

1. The coefficients a_{31} and b_{31} were set to values determined by the temperature dependent expression for $\Delta^\circ G_f$ obtained from the present experiments.

2. Next, using only the Gibbs energy data of Lee et al. [Lee92] and this work the four coefficients A_{ij}, B_{ij}, a_{ij} and b_{ij} were optimized to obtain better start estimates of the parameter and also to ensure physical realism to the parameters.

3. Using these coefficients and only the Gibbs energy data, a reasonably good prediction was made for the phase diagram and the liquid phase enthalpy. However, the asymmetry reported in the experimental phase diagram data [Sol74, Kos55, Hsi77, Hal63, Rub66, Rak70, Vig73, Per80, DeW85] and the enthalpy of mixing data of Yamaguchi [Yam88] remained unfitted.

4. The asymmetry was introduced into the model by including another term A_{51} in the optimization. This parameter skews the parabolic nature of the liquid phase excess Gibbs energy function.

5. Using various combinations of only the enthalpy and Gibbs energy data, optimized coefficients were obtained and mean square error compared. Consistency was checked by the ability of the coefficients to predict the experimental phase. Inconsistent enthalpy and Gibbs energy data were then eliminated if an acceptable agreement was not achieved.

6. The coefficients were re-optimized using the combined thermochemical and phase diagram data. The coefficients yielding an optimal fit were retained.

7. Lastly, the optimization was repeated by including the coefficients C_{43} and C_{33} to check for significant C_p contribution. Since the fit to the data upon their inclusion was not

significant, consistent with the experimental C_p values, these parameters were excluded from the model description.

As many as 31 runs were performed for the assessment of the Ga-As system. The optimized coefficients for the Redlich-Kister model and lattice stability of GaAs are shown in Table 3-4. The comparision of experimental data with the optimized curves is shown in Figure 3-1 through Figure 3-3. The general agreement of the curves appears to be good.

When compared to Chatillon's assessment [Cha90], the calculated liquidus appears to have shifted to the As-rich side. This trend was also seen in Lee's experimental measurements [Lee92] on Ga activity along the liquidus. Chatillon's assessment [Cha90] predicts higher Ga activities especially at lower temperatures, while results of this work and Lee's measurements [Lee92] predict lower values for the gallium activity and stronger deviations from ideal solution behavior. In the low temperature regions, the phase diagram data by Sol et al. [Sol74], Hsieh [Hsi77] and Hall [Hal63] were inconsistent, mostly due to the experimental difficulties encountered in accurate observation of dissolution and precipitation of crystals in gallium rich melts during the heating and cooling cycles. Subcooling could also have been an issue during the cooling cycle resulting in untrue measurements. The As-rich eutectic data of Ceolin et al. [Ceo89] was determined more consistent than that reported by Koster and Thoma [Kos55].

The standard enthalpy of formation of GaAs (s) at 298.15 K agreed well with that determined calorimetrically by Martosudirjo and Pratt [Mar74]. The value suggested by Gutbier [Gut61] from mass spectrometry is too low (numerically). The enthalpy of fusion data by Lichter [Lic69] and Yamaguchi [Yam88] were retained in the selected data set. The liquid phase enthalpy of mixing data by Yamaguchi [Yam88] was well

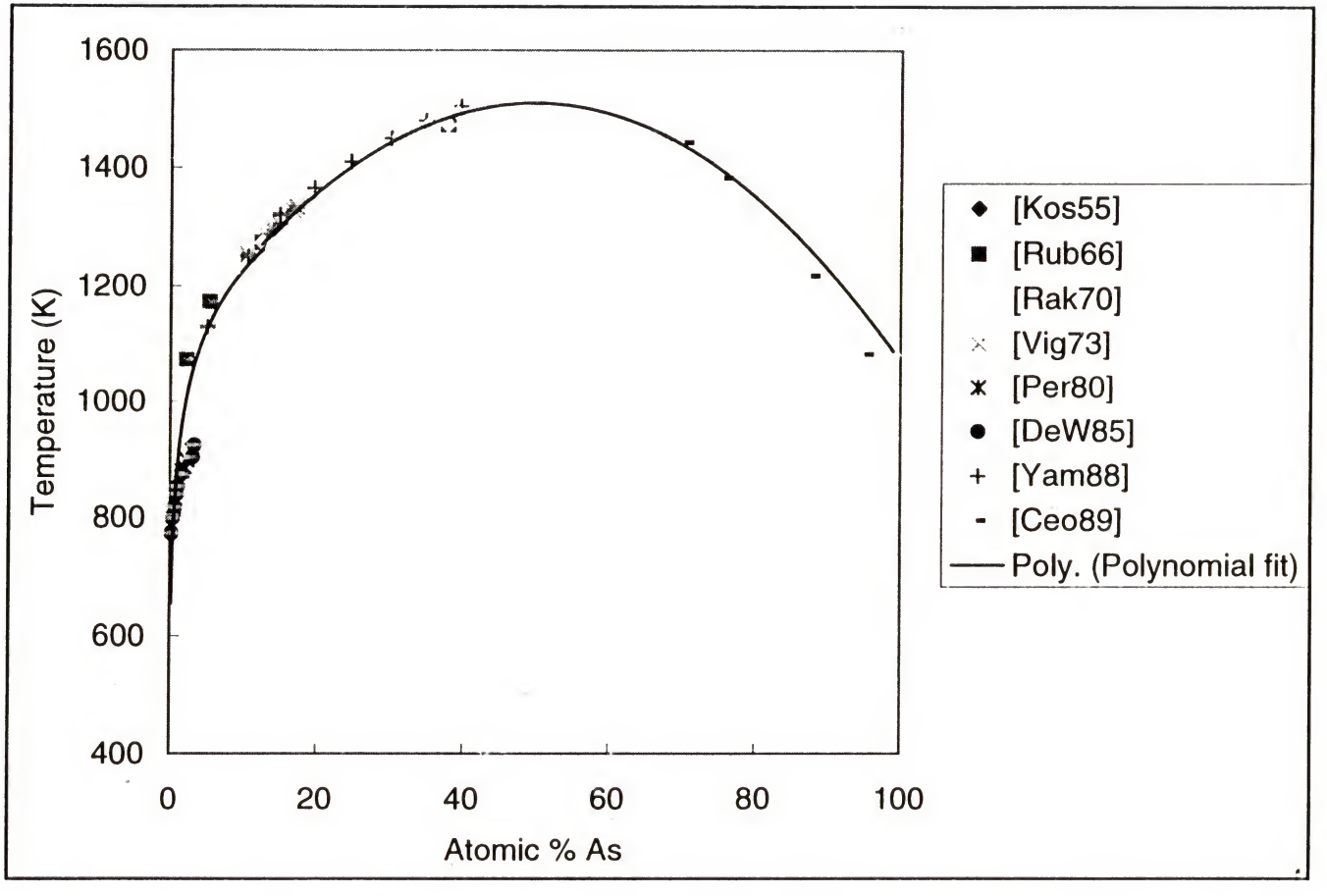

Figure 3-1. Optimized Ga-As phase diagram.

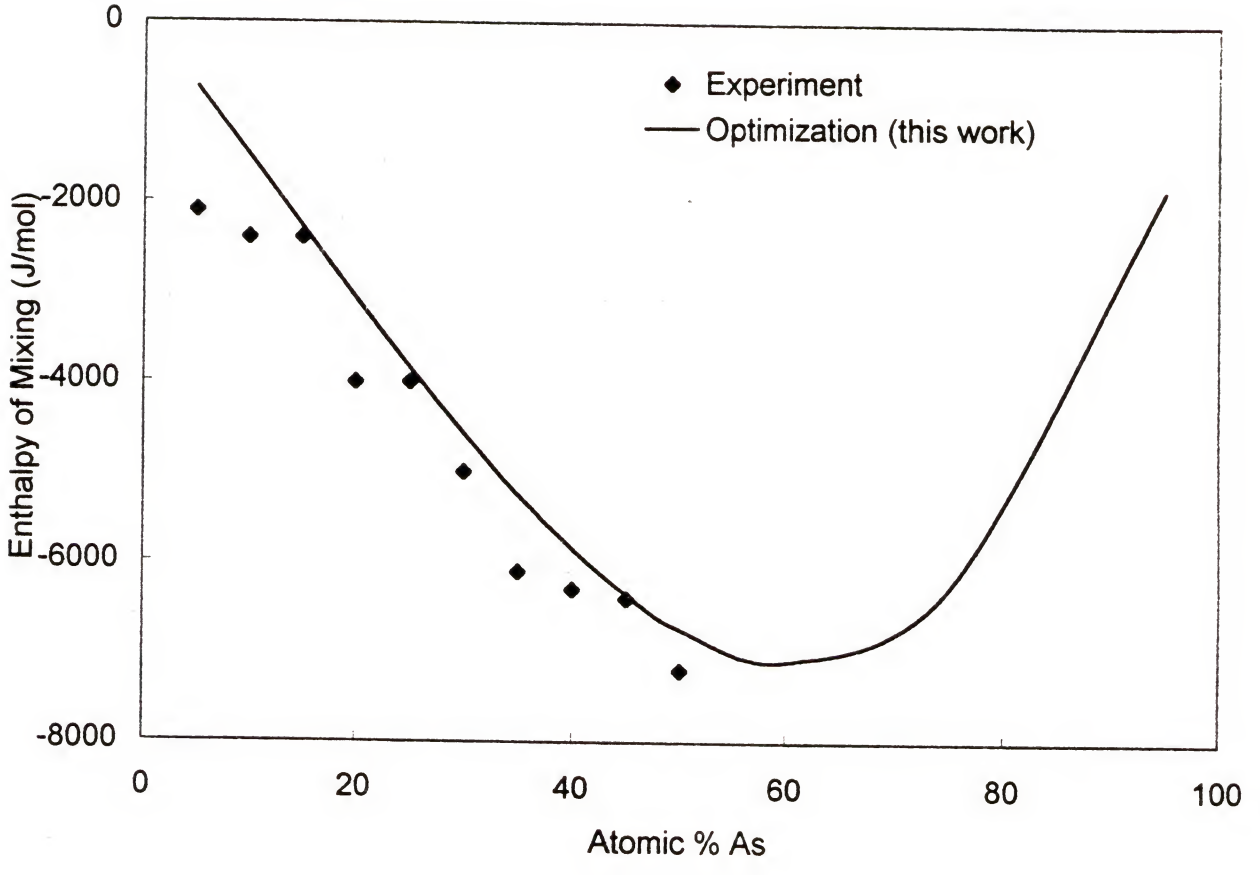

Figure 3-2. Optimized Ga-As liquid phase enthalpy.

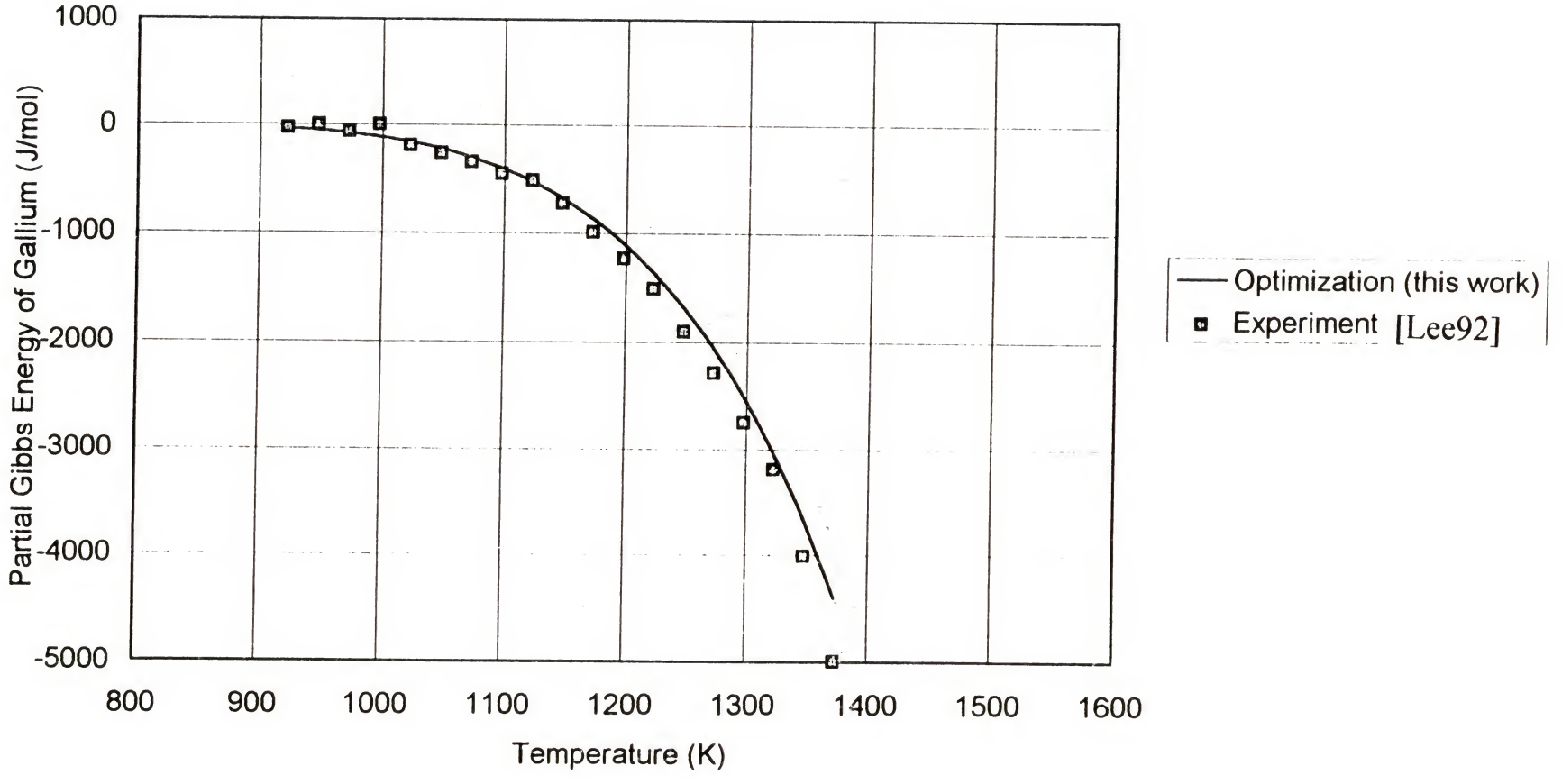

Figure 3-3. Optimized Ga activity along Ga-rich liquidus in the Ga-As system.

represented. However, the C_p (T) data of Lichter [Lic69] was found inconsistent with other data. It was concluded that there exists marked discrepancy in the reported C_p (T) data, and this was evidenced by a third law analysis discussed below. For this reason, the expression for optimized C_p (T) data from Chatillon's least square fit [Cha90] was adopted for third law calculations in this work.

The emf studies by Krestovnikov et al. [Kre71], Sirota [Sir68] and Abbasov et al. [Abb66] for the measurement of Gibbs energy of formation of GaAs were found inconsistent with the phase diagram data and rest of the thermochemical properties. The measurements for activity of gallium in the liquid phase by Wypartowicz and Fitzner [Wya88], Hall [Hal63] and Katayama et al. [Kat89] were rejected for the same reason.

To summarize, the calculated values of Gibbs energy values for Ga activity along the liquidus compare well with the experimental data of Lee et al. [Lee92] as is shown in Table 3-5 and Figure 3-3. The partial pressures associated with As_2 and As_4 vapor phases in the Ga -rich segment of the phase diagram are shown in Figure 3-4. The Gibbs energies of formation obtained from the optimization is also in good agreement with the experimental data of the present work as can be seen in Table 3-6.

In-As Assessment

Redlich-Kister polynomial was well suited to model the liquid phase, while a line compound description was used for the essentially stoichiometric compound $In_{0.5}As_{0.5}$. Either solid or liquid phase could be used as the reference for the system. As with the case of Ga-As system, pure liquid was chosen as the reference phase while solid elements in their standard states were chosen as the reference for the stoichiometric compound.

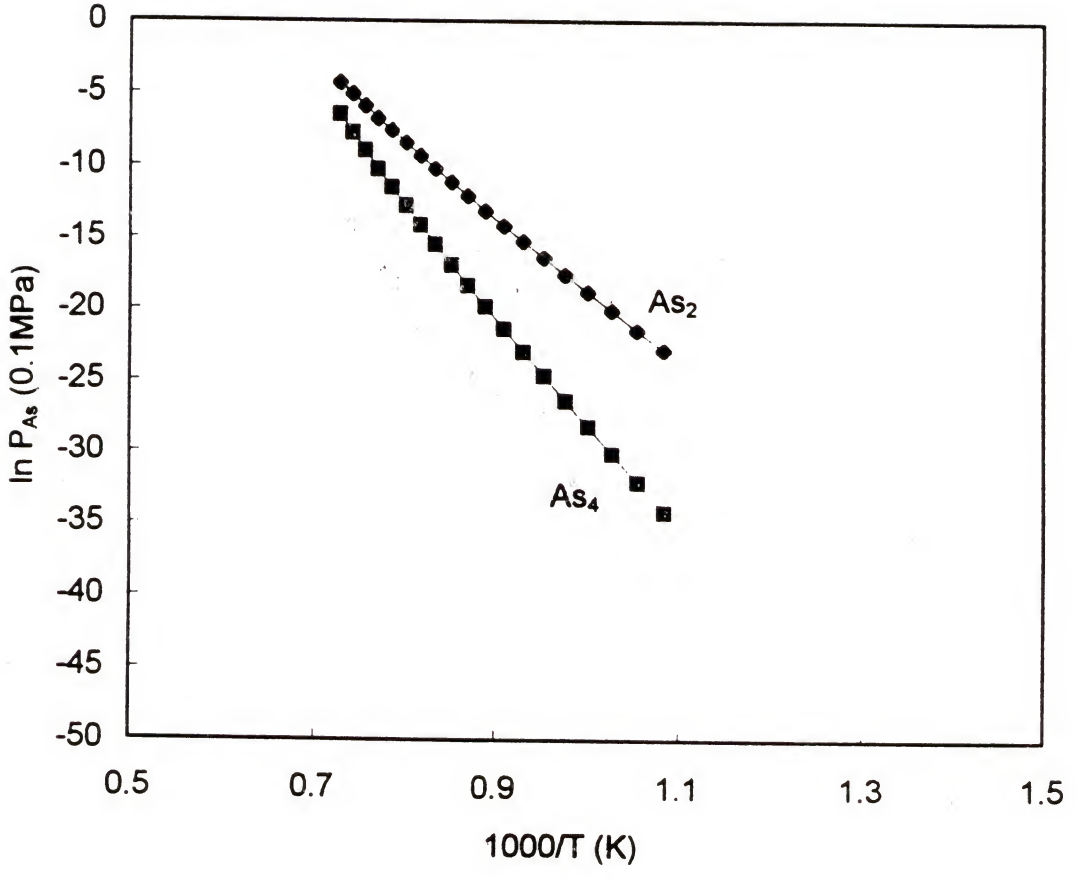

Figure 3-4. Vapor pressure of As in Ga-rich region of Ga-As phase diagram.

Table 3-1. Summary of selected experimental phase diagram data for Ga-As system.

Author [Reference]	Method of Measurement	Measurement Range T (K) x_{As}	Estimated Uncertainity +/- ΔT (K) +/- Δx_{As}
Koster [Kos55]	Differential Thermal Analysis	1273-1511 0.15-0.80	20 0.01
Rubenstein [Rub66]	Filtration Technique	723-1511 ---	20 0.05
Rakov et al. [Rak70]	Dew Point and Continuous Weighing	1447-1505 0.31-0.54	5 0.05
Vigdorowich [Vig73]	Bourdon Gauge and Vapor Density	1253-1353 0.10-0.22	20 0.05
Perea [Per80]	Heterogeneous Equilibrium and Weight Loss	853-943 ---	5 0.05
DeWinter [DeW85]	Visual Observation and Source Dissolution	623-923 ---	20 0.05
Yamaguchi [Yam88]	Drop Calorimetry	800-1500 ---	5 0.03
Ceolin et al. [Ceo89]	Neutron Diffraction	1083-1443 ---	15 0.02

Table 3-2. Summary of selected calorimetric and enthalpy data for Ga-As system.

Author [Reference]	Method of Measurement	Data Type	Temperature Range or Value	Estimated Uncertainity
Sirota [Sir68]	Oxygen Calorimetric Bomb	Enthalpy of Formation	-43848 (J/mol) 298 K	+/- 5000 J/mol
Lichter [Lic69]	Drop Calorimetry	Enthalpy of Fusion	52702 (J/mol) 1513 K	+/- 2500 J/mol
Lichter [Lic69]	Drop Calorimetry	Heat Capacity	421-1513 K	+/- 10 K
Martosudirjo [Mar74]	Calorimetric Precipitation	Enthalpy of Formation	-41148 J/mol 298 K	+/- 5000 J/mol
Yamaguchi [Yam88]	Drop Calorimetry	Enthalpy of Formation	800-1550 K	+/- 10 K

Table 3-3. Summary of selected vapor pressure and Gibbs energy data for Ga-As system.

Author [Reference]	Method of Measurement	Temperature Range (K)	Estimated Uncertainity +/- T (K) $\Delta P_{As_2}/P_{As_2}$
Drowart [Dro58]	Knudsen-cell Mass Spectrometry	1030-1136	10 30
Richman [Ric63]	Standard Bourdon Gauge	1323-1527	3 20
Pupp [Pup64]	Knudsen-cell Mass Spectrometry	1035-1239	10 20
Arthur [Art67]	Knudsen-cell Mass Spectrometry	890-1190	10 20
Rakov [Rak70]	Continuous Weighing	1448-1511	3 20
Foxon [Fox73]	Knudsen-cell Mass Spectrometry	850-1100	10 20
Khukhryanskii [Khu74]	Dynamic Method	973-1273	10 30
Panish [Pan74]	$H_2 + PH_3$ Flow Method	1255-1435	10 20
Lee [Lee92]	EMF	923-1373	5 ---
This Work	EMF	813-1013	5 5

Table 3-4. Optimized coefficients for Redlich-Kister model and lattice stability of GaAs.

	A_{ij} (J/mol)	B_{ij} (J/mol K)
Suffix (i,j)	j=1	j=2
i=4	-26966.58	4.06734
i=5	12947.10	10.11249

Table 3-5. Calculation of partial Gibbs energies of Ga and As along liquidus (in J/mol).

T (K)	x_{As}	μ_{Ga}	μ_{As}	μ_{Ga}^{+}	$\ln P^{*}_{As_2}$	$\ln P^{*}_{As_4}$	γ_{Ga}	γ_{As}	$RT\ln\gamma_{Ga}/x_{As}^{2}$
923	0.005	-39	-67652	-32	-22.9	-34.28	1.000	0.030	---
948	0.007	-57	-66203	---	-21.5	-32.24	1.000	0.031	---
973	0.010	-83	-64746	-67	-20.13	-30.22	1.000	0.033	---
998	0.013	-117	-63281	---	-18.82	-28.28	0.999	0.036	-49121.4
1023	0.018	-163	-61804	-198	-17.58	-26.45	0.999	0.038	-26263.8
1048	0.024	-224	-60312	-265	-16.40	-24.71	0.998	0.041	-30284.0
1073	0.031	-302	-58803	-349	-15.26	-23.02	0.997	0.044	-27890.7
1098	0.039	-401	-57274	-453	-14.17	-21.40	0.996	0.048	-24055.4
1123	0.048	-524	-55719	-512	-13.12	-19.84	0.993	0.053	-28466.2
1148	0.059	-677	-54135	-723	-12.12	-18.35	0.989	0.058	-30327.8
1173	0.071	-864	-52518	-988	-11.15	-16.90	0.985	0.064	-29238.9
1198	0.084	-1089	-50861	-1228	-10.21	-15.49	0.980	0.072	-28517.9
1223	0.099	-1359	-49160	-1511	-9.30	-14.13	0.971	0.080	-30530.8
1248	0.115	-1680	-47408	-1901	-8.42	-12.80	0.961	0.090	-31210.7
1273	0.132	-2060	-45598	-2286	-7.56	-11.50	0.949	0.102	-31796.4
1298	0.151	-2509	-43718	-2746	-6.73	-10.24	0.933	0.115	-32822.0
1323	0.171	-3038	-41758	-3189	-5.90	-8.97	0.915	0.131	-33415.1
1348	0.193	-3663	-39702	-4009	-5.10	-7.74	0.891	0.150	-34796.3
1373	0.216	-4406	-37528	-4996	-4.30	-6.50	0.870	0.173	-34072.6

$^{+}$ Denotes Ga activity from Lee [Lee92].

* Denotes calculated values using optimized $P^{o}_{As_2}$(0.1MPa) and K_p (T) data from Chatillon et al. [Cha90].

Table 3-6. Comparision of calculated Gibbs energy of formation of GaAs (s) referred to Ga (l) and As (s) with experimental data.

Temperature (K)	ΔG^{ex}, Optimized (J/mol)	ΔG^{ex}, Present Work (J/mol)
813	-33889.3	---
833	-33541.2	-33650
853	-33193.9	-32420
873	-32844.9	-31850
893	-32496.8	-30970
913	-32148.7	-30040
933	-31800.5	-29460
953	-31452.4	-29100
973	-31104.3	-28740
993	-30756.2	---
1013	-30408.0	---

Negligible solubility of In in As and of As in In was assumed, this assumption being consistent with phase diagram studies [Hal63 and Per80].

Four terms A_{ij},, B_{ij}, a_{ij} and b_{ij} were used to model the sytem. The terms C_{ij} and c_{ij} did not significantly improve the fit, and therefore were not included in the final optimization. This is consistent with the low values available for the experimental ΔC_p values for InAs (l) and InAs (s). The selected experimental data along with their methods of determination and estimated uncertainities for phase diagram, enthalpy and Gibbs energy for In-As system are listed in Table 3-7 through 3-9. The phase diagram is fairly well characterized for the system, however, the thermodynamic information in the $x_{As} > 0.5$ region and the high temperature region of the phase diagram is lacking. Owing to the availability of enthalpy of mixing values only for the $x_{As} < 0.5$ region, only one enthalpy term A_{41} was used for optimization.

Standard steps of optimization similar to the ones utilized on the Ga-As system were used for this system as well. First, the coefficient A_{41} was estimated by forcing a fit to the liquid phase enthalpy of mixing data of Yamaguchi et al. [Yam88]. Next, the coefficients a_{ij} and b_{ij} were estimated based upon the Gibbs energy of formation data of InAs as determined in the present study. The coefficients were then set to vary in a scheme of subsequent optimizations to least square fit the entire experimental dataset.

Each data point was checked for consistency with other data points by comparing the degree of fit to the model, as well as by the ability to back calculate other quantities. Optimizations were performed to calculate thermodynamic data from pure phase diagram data. In a similar set of reverse calculations, the consistency of the Gibbs energy, enthalpy and pure component data was checked by calculating the system phase diagram and

comparing with experimental data. This was helpful particularly because the phase diagram is the most well characterized information available on the system as opposed to the thermochemical properties. When such asssessments were completed and consistent data separated from inconsistent ones, model parameters were determined and are shown in Table 3-10.

The optimization compared fairly well with the recent assessment by Chatillon et al. [Cha90] however, at temperatures above 893 K there is a shift of the phase diagram towards the In-rich region as shown in Figure 3-5. This indicated that the calculated In activities were higher than those determined by pure phase diagram data or vapor pressure measurements of As. Vapor pressure measurements of As showed great discrepancy across the phase diagram, and thus were not reliable tools for performing accurate calulations. Gibbs energy data of formation of InAs and activity of In was used to perform predictions of the phase data. The Gibbs energy data skewed the phase diagram data towards In-rich region and flattened the curve at mid regions of the phase diagram. Lack of accurate thermodynamic data in the As-rich regions of the phase diagrams, made it difficult to provide a better fit to the As-rich segment of the system.

The data by Itoh et al. [Ito82] compared well with the activity data of the present study however, exhibiting a lower degree of non-ideality. Calorimetric measurements for enthalpies of fusion data by Cox and Pool [Cox67] and Lichter and Sommelet [Lic69] were used in the optimization. The liquid phase enthalpy data reported by Yamaguchi et al. [Yam88] was best represented by the calculated curve as shown in Figure 3-6. Invariant equilibria by Liu and Peretti [Liu53] compared well with the calculated curve.

The optimized curves agree well with experimental data as is evident through Figures 3-5 through 3-7.

Vapor pressure measurements for As_2 and/or As_4 species have been performed by Knudsen cell mass spectrometry [Pup74, Gut59 and Gol59]. Total arsenic pressure measurements have been performed by dew point techniques [Van57, Fol58, Kar73], Bourdon gauges [Vig73, Ric63] and gas flow methods [Khu74, Khu77]. In order to compare all the published results, it is necessary to transform the data by recalculating the partial pressures of As_2 and As_4 and the total pressures. Tmar et al. [Tma84] performed such calculations and compared the corrected experimental results with each other. They found significant discrepancy in the reported data. The results of Khukhryanskii et al. [Khu74] did not agree with our activity data and the calculated curve. This is consistent with the analysis of their data performed by Tmar et al. [Tma84] indicating that these measurements were erroneous because they treated As_2 as the main species while ignoring the arsenic component in As_4, AsH_3, AsH_2 and AsH species. The situation was aggravated because these variations were temperature dependent and uncertainity in the calculated enthalpies caused the activity of As to change seriously. Parasitic reevaporation, dissociative ionization of As_4 into As_2^+, the reversibility of evaporation and the calibration of the mass spectrometer are critical to the authenticity of the vapor pressure data reported. Tmar et al. [Tma84] corrected the values of Goldfinger and Jeunehomme [Gol59] by calculating the equilibrium dissociation constant of the reaction (2.1) and the calibration constant of their apparatus. This brought their values closer to the values by Pupp et al. [Pup74], though they were still lower and were thus discarded. High vapor pressure measurements of Van den Boomgaard and Schol

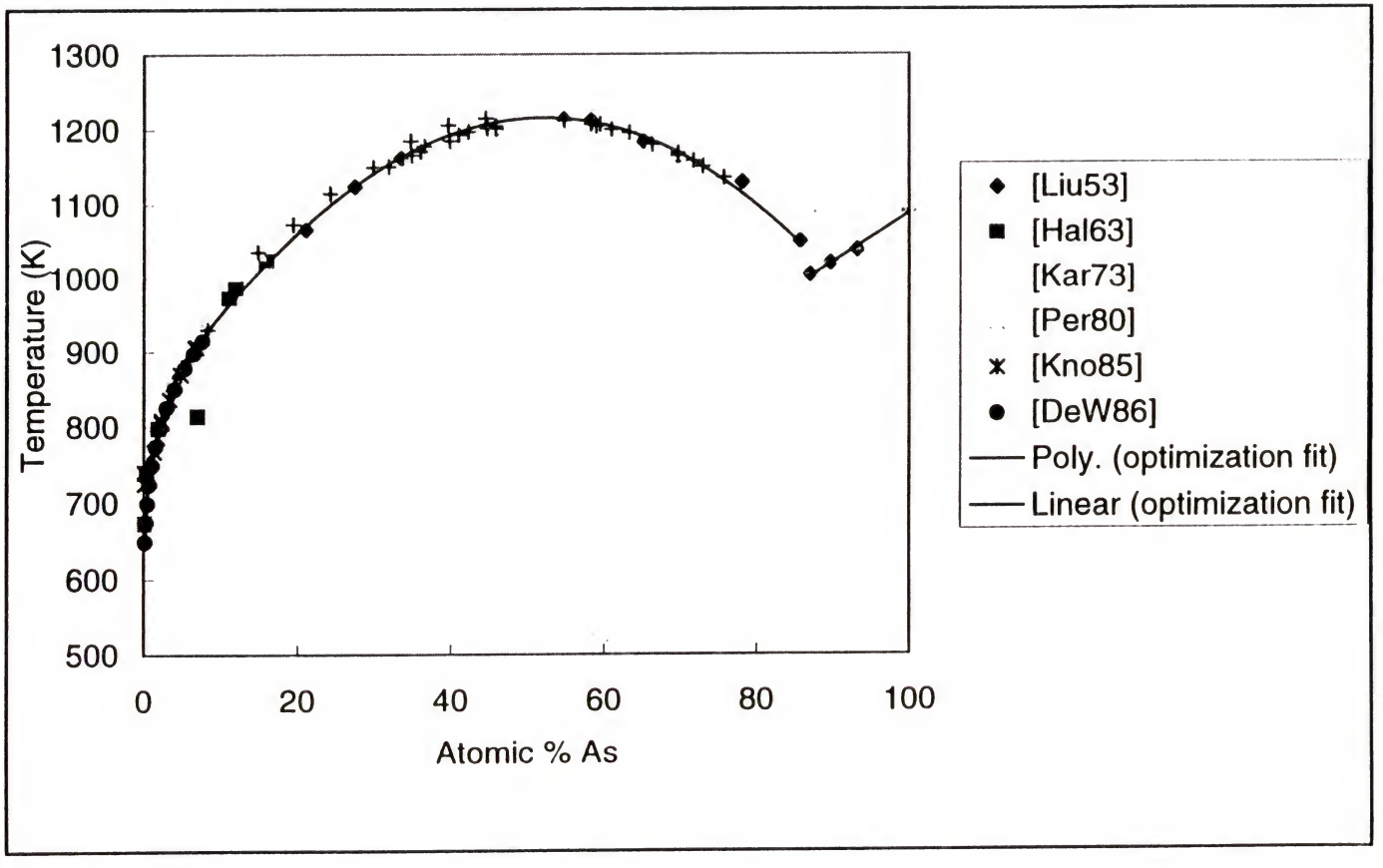

Figure 3-5. Optimized In-As phase diagram.

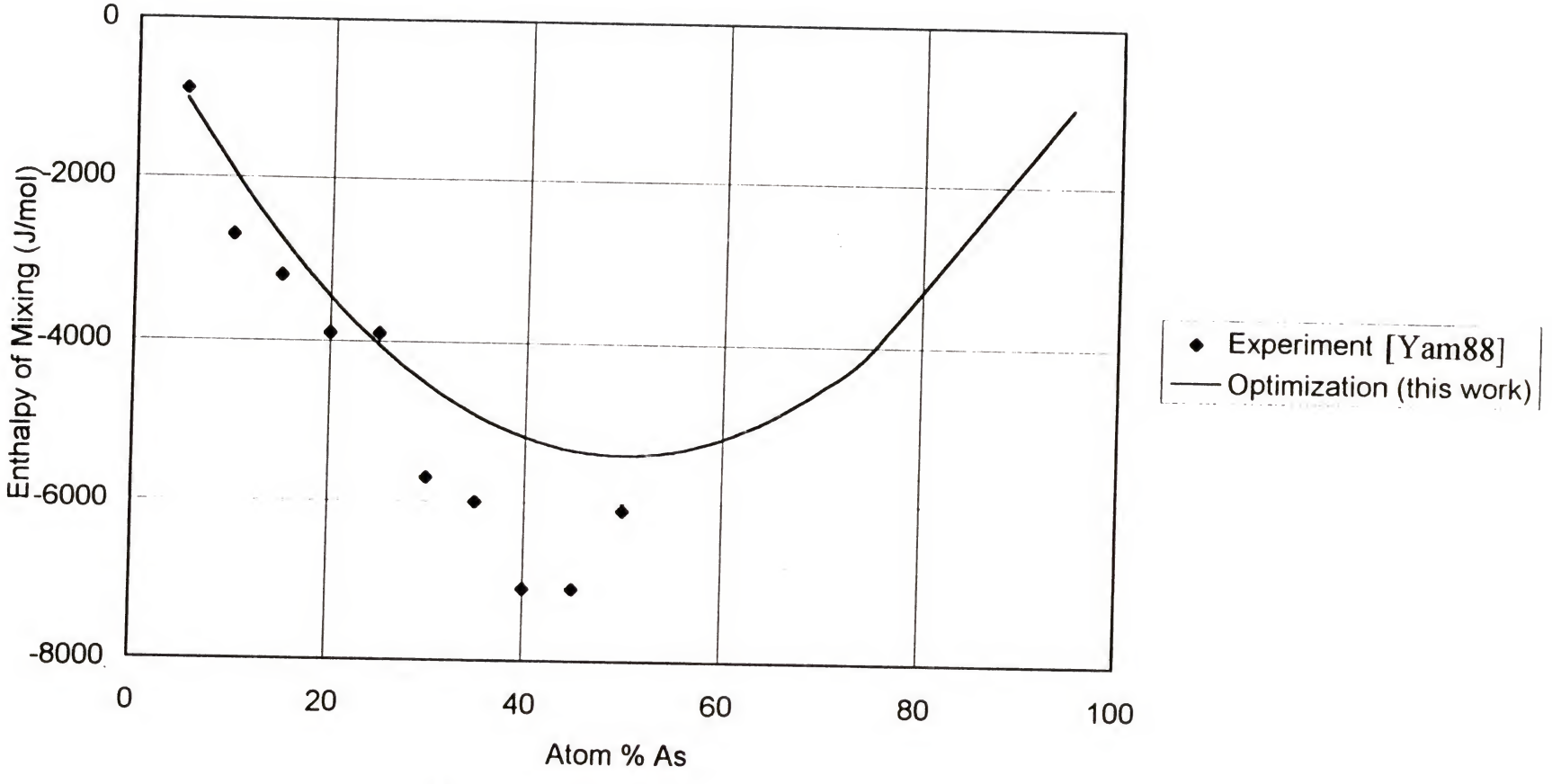

Figure 3-6. Optimized In-As liquid phase enthalpy.

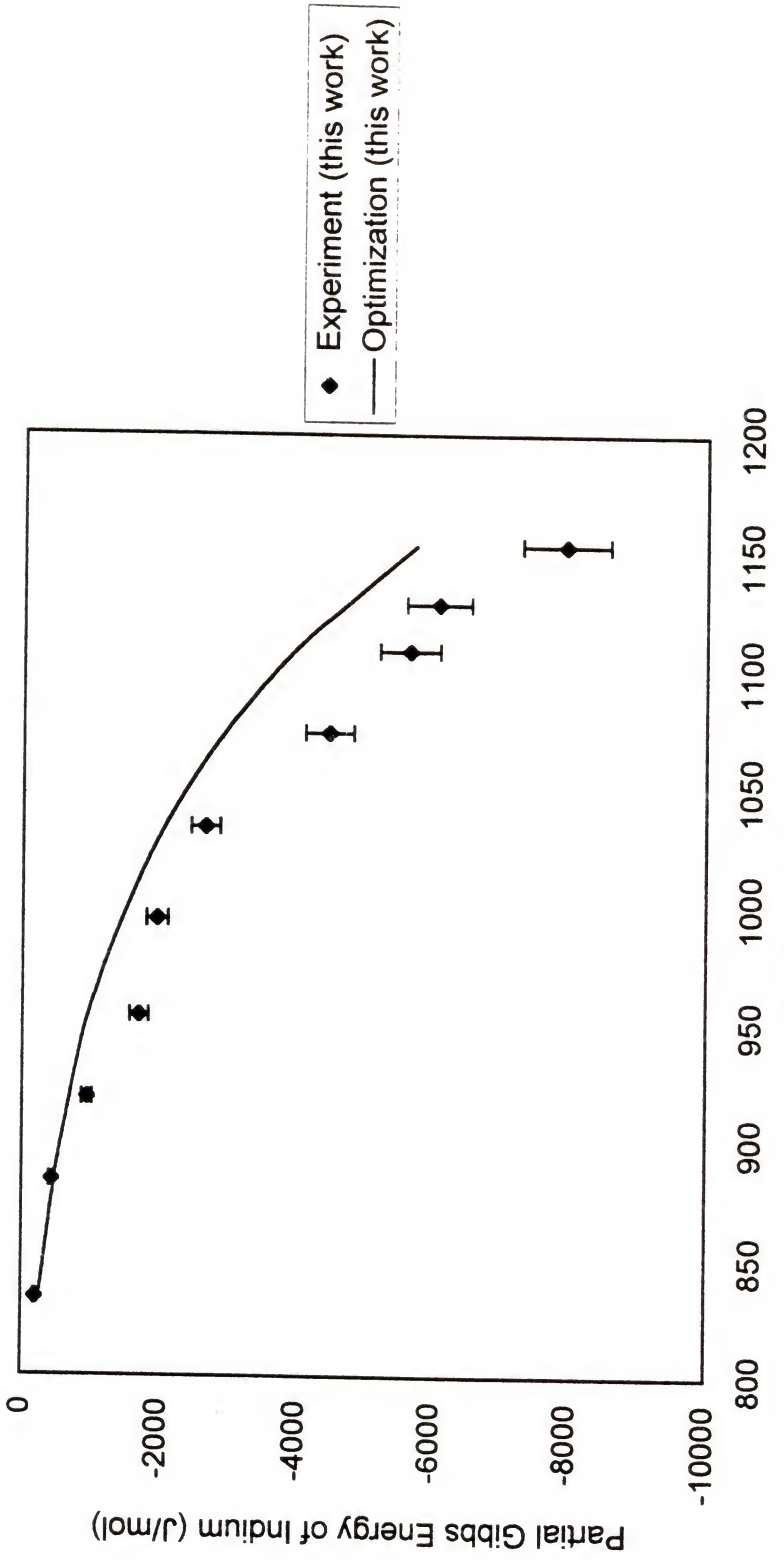

Figure 3-7. Optimized In activity along In-rich liquidus in the In-As system.

[Van57] and Karataev et al. [Kar73] especially on the In-rich side of the In-As system do not agree with the results of the present work and the data reported by Pupp et al. [Pup74]. This is probably due to the fact that InAs forms a layer at the surface of the indium melt creating a heat transfer barrier, thereby causing difficulties in accurate dew point temperature measurement. However, their data agreed well at high arsenic contents.

The emf data by Abbasov et al. [Abb64] and Krestovnikov et al. [Kre71] were retained during the earlier stages of optimization, but later were discarded because were found inconsistent with the low temperature data. The data by Krestovnikov et al. [Kre71] however, showed better agreement with the calculated curve and the measurements of the present study when extrapolated to the high temperature regions of the phase diagram of the In-As system. The discrepancy is probably due to poor stability of cells in their experiments due to poor diffusion or indium surface migration on the two phase mixtures (InAs +As).

The calculated values of Gibbs energy values for In activity along the liquidus compare well with the experimental data of this work and are summarized in Table 3-11 and Figure 3-7. The partial pressures associated with As_2 and As_4 vapor phases in the In-rich segment of the phase diagram are shown in Figure 3-8. The Gibbs energies of formation obtained from the optimization is also in good agreement with the experimental data of the present work as can be seen in Table 3-12.

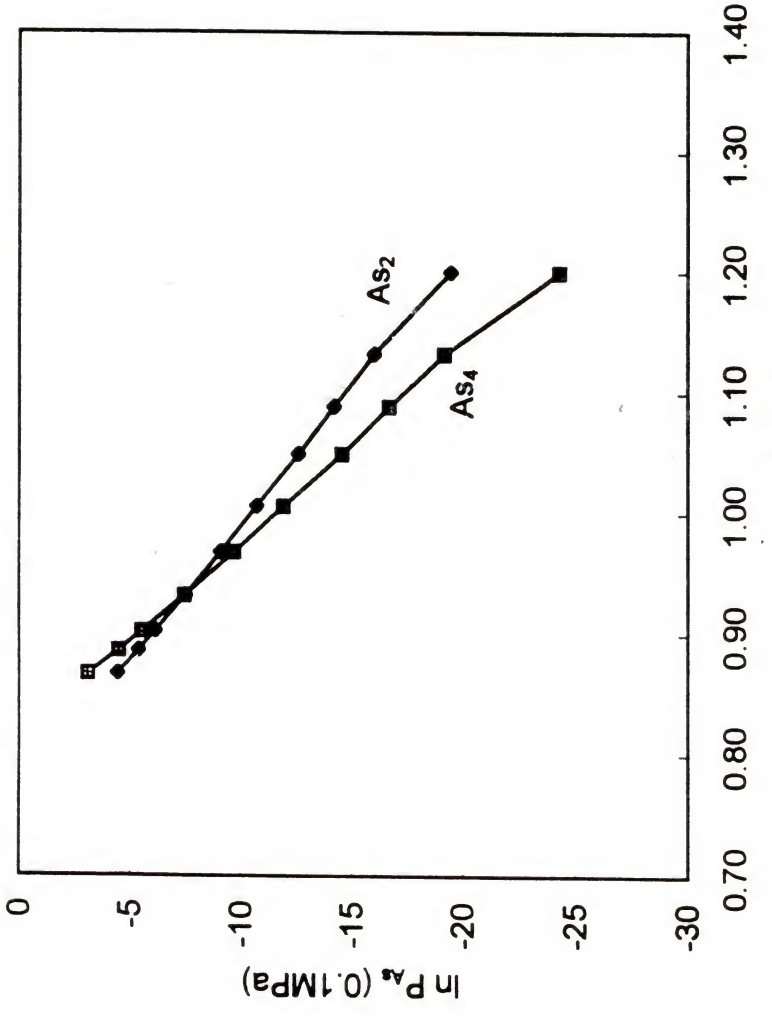

Figure 3-8. Vapor pressure of As in In-rich region of the In-As phase diagram.

Table 3-7. Summary of selected experimental phase diagram data for In-As system.

Author [Reference]	Method of Measurement	Measurement Range T (K) x_{As}	Estimated Uncertainity +/- ΔT (K) +/- Δx_{As}
Liu [Liu53]	Differential Thermal Analysis and X-ray Analysis	429-1215 0-1	10 0.03
Hall [Hal63]	Heterogeneous Equilibrium and Weight Loss	673-1024 0-0.16	10 0.02
Karataev [Kar73]	Dew Point and Continuous Weighing	1149-1220 0.35-0.74	10 0.02
Perea [Per80]	Heterogeneous Equilibrium and Weight Loss	849-929 0-0.08	10 0.02
Knobloch [Kno85]	Dissolution in LPE	724-906 0.007-0.07	5 0.01
DeWinter [DeW86]	Visual Observation and Source Dissolution	648-914 0.002-0.08	5 0.02

Table 3-8. Summary of selected calorimetric and enthalpy data for In-As system.

Author [Reference]	Method of Measurement	Data Type	Temperature Range or Value	Estimated Uncertainity
Schottky [Sch58]	Dissolution Calorimetry	Enthalpy of Formation	-30962 J/mol 298 K	+/- 3000 J/mol
Sharifov [Sha63]	Calorimetric Bomb	Enthalpy of Formation	-28870 J/mol 298 K	+/- 3000 J/mol
Cox [Cox67]	Drop Calorimetry	Enthalpy of Fusion	38511 J/mol 1213 K	+/- 3000 J/mol +/- 5K
Cox [Cox67]	Drop Calorimetry	Heat Capacity	298-1200 K	+/- 10 K
Lichter [Lic69]	Drop Calorimetry	Heat Capacity	298-1200 K	+/- 10 K
Glazov [Gla75]	Differential Thermal Analysis	Enthalpy of Fusion	39330 J/mol 1215 K	+/- 3000 J/mol +/- 5K
Yamaguchi [Yam88]	Drop Calorimetry	Enthalpy of Fusion	38300 J/mol 1221 K	+/- 3000 J/mol +/- 10 K
Yamaguchi [Yam88]	Drop Calorimetry	Enthalpy of Formation	700-1500 K	+/- 10 K

Table 3-9. Summary of selected vapor pressure and Gibbs energy data for In-As system.

Author [Reference]	Method of Measurement	Temperature Range (K)	Estimated Uncertainity +/- T (K) $\Delta P_{As2}/P_{As2}$
Van den [Van57]	Dew Point Method	1004-1215 K	10 20
Pupp [Pup74]	Knudsen-cell Mass Spectrometry	918-1084	10 50
Itoh [Ito82]	EMF Measurement	920-1260	5 5
Tmar [Tma87]	Knudsen-cell Mass Spectrometry	846-1086	5 10
This Work	EMF Measurement	833-1153	5 5

Table 3-10. Optimized coefficients for Redlich-Kister model and lattice stability of InAs.

	A_{ij} (J/mol)	B_{ij} (J/mol K)
Suffix (i,j)	j=1	j=2
i=4	-21600	0.0
i=5	0.0	0.0

$$^{\circ}G_{InAs,s} - 0.5^{\circ}G_{In,bct} - 0.5^{\circ}G_{As,rho} = -25113.3 + 7.780T$$

Table 3-11. Calculation of partial Gibbs energy of In along liquidus.

T (K)	x_{As}	μ_{In} (J/mol)	a_{In}	μ_{In}^{*} (J/mol)	a_{In}^{*}	μ_{As}^{**} (J/mol)	$\ln P_{As_2}^{**}$ (0.1MPa)	$\ln P_{As_4}^{**}$ (0.1MPa)	γ_{In}	γ_{As}	$RT\ln\gamma_{In}/x_{As}^{2}$
833	0.034	-202.7	0.971	-265	0.962	-38191.5	-19.47	-24.32	1.000	0.118	-38191.5
883	0.0549	-442.9	0.941	-482.2	0.936	-35416.9	-16.01	-19.20	0.996	0.146	-35416.9
918	0.0733	-955.4	0.882	-704.2	0.912	-33472.1	-14.20	-16.72	0.952	0.170	-33472.1
953	0.0921	-1708.1	0.806	-964.1	0.885	-31827.5	-12.60	-14.58	0.888	0.196	-31827.5
994	0.1240	-1968.6	0.788	-1463.4	0.838	-29171.3	-10.70	-11.93	0.900	0.236	-29171.3
1033	0.1570	-2663.4	0.733	-2073.5	0.786	-26775.4	-9.08	-9.70	0.870	0.282	-26775.4
1073	0.1970	-4458.3	0.607	-2937.5	0.720	-24098.4	-7.48	-7.46	0.756	0.341	-24098.4
1108	0.2370	-5645.3	0.542	-3943.6	0.652	-21600.1	-6.13	-5.54	0.710	0.404	-21600.1
1128	0.2645	-6079.5	0.523	-4714.4	0.605	-19938.0	-5.40	-4.50	0.711	0.450	-19938.0
1153	0.2970	-7961.3	0.436	-5728.5	0.550	-18073.3	-4.46	-3.13	0.620	0.511	-18073.3

* Denotes calculated values from the assessment by Tmar et al. [Tma84]

** Denotes calculated values (this study).

Table 3-12. Comparision of calculated Gibbs energy of formation of InAs (s) referred to In (l) and As (s) with experimental data.

Temperature (K)	ΔG^{ex}, Optimized (J/mol)	ΔG^{ex}, Present Work (J/mol)
803	-34880	-34880
833	-34184	-34300
853	-33720	-33880
867	-33395	-33300
873	-33256	-33100
891	-32838	-33000
913	-32328	-32680
921	-32142	-32600
953	-31400	-31400

In-Sb Assessment

Group III-antimonides are important constituents to the solid solutions used for long wavelength photodetector systems, owing to the direct nature of their bandgap structures and high electron mobilities. In particular, InSb has the lowest band gap energyand highest room temperature electron mobility of any other III-V compound semiconductor. To understand the electronic and structural characteristics of solid solutions comprising InSb, it is important to study the thermodynamic properties in the In-Sb binary in both the liquid and solid phase so as to predict multicomponent solution behavior, stability of solid solution and the nature of interactions within the alloy. The In-Sb system is, however, over-specified experimentally to the extent that it can be confusing and, at the same time erroneous to select data without checking for consistency. The purpose of this work is to systematically and critically analyze the data on In-Sb system in determining a consistent dataset that can explain the solution thermodynamics in the In-Sb system.

Phase diagram data. The phase diagram for the In-Sb system has been reported by several investigators [Pog49, Liu52, Hal63, Gor83] and a simple eutectic type of phase diagram was reported on either side of the compound [Pog49, Liu52]. The Sb-InSb eutectic occurs at a composition of $x_{Sb} = 0.68$ and a temperature of 767 K. The In-InSb eutectic is practically degenerate at $x_{Sb} = 0.007$ and a temperature of 427 K, approximately 1 K below the pure In melting temperature. InSb is the only III-V compound having a melting temperature, T_f, below that of a component element (i.e., Sb). Liu and Peretti [Liu52] investigated the In-Sb system by thermal, x-ray and metallographic methods of

analysis. The solid solubility of antimony in indium was less than $x_{Sb} \sim 0.0047$ as was the solid solubility of indium in antimony. The data of Pogodin et al. [Pog49] agrees quite well with the results of Liu and Peretti; their data are only slightly higher in temperature for Sb compositions $x_{Sb} = 0.40$. Hall [Hal63] performed liquidus measurements on the In-rich side of In-Sb binary. His liquidus measurements are significantly higher than those made by Pogodin and Liu and Peretti. Sharma et al. [Sha87], in their assessment work, have pointed out that the dissolution technique used by Hall was prone to error, especially at low solubilities of InSb in liquid In. However, the more recent work by Goryacheva [Gor83] is in good agreement with Liu and Pogodin's reported values. A summary of the phase diagram data is presented in Table 3-13.

Enthalpy data. Isothermal data for the enthalpy of mixing in the liquid phase have been reported by Yazawa et al. [Yaz68], Itagaki and Yazawa [Ita75, Ita77], Predel and Oehme [Pre76], Oehme and Predel [Oeh78], Wittig and Gehring [Wit67], and Vecher et al. [Vec74]. Rosa et al. [Ros80] and Oehme and Predel [Oeh78] measured the enthalpy of mixing at several temperatures in the temperature range 910 K to 1200 K. The literature values are in fair agreement with each other, however, the range for the maximum negative enthalpy of mixing, ΔH_m, is 2345 to 3725 J/mol in this temperature range. The enthalpy of mixing is not symmetric with respect to composition; the maximum exothermic ΔH_m being located in the range of $x_{Sb} = 0.40 - 0.45$.

Predel and Oehme [Pre76] performed a calorimetric investigation of the enthalpy of mixing of liquid In-Sb alloys over the entire concentration range. In their work, Rosa et al. [Ros80] determined the mixing enthalpies at a function of temperature with the aid of a high temperature calorimeter. The authors attributed the deviations from the regular

solution behavior to the existence of In_3Sb and InSb associates. Furthermore, their results indicate that the maximum ΔH_{mix} shifts to a lower magnitude at increased Sb content as the temperature is increased. Wittig and Gehring [Wit67] obtained mixing enthalpies at 973 K. Vecher et al. [Vec74] measured the enthalpy of mixing at 910 K by quantitative differential thermal analysis while Yazawa et al. [Yaz68] reported ΔH_{mix} values using the same technique. The enthalpy of fusion has been determined by a number of investigators [Ita77, Mec71, Nac58, Sch58, Lic69, Hul73, Ric65, Gar77, Bla70] and a summary is presented in Table 3-15. The results of Sirota and Yushkevich [Sir67], Nikol'skaya [Nik59], Abbasov and Mamedov [Abb70], and Terpilowski and Trzebiatowski [Ter60] for the standard enthalpy of formation are shown in Table 3-16. Also tabulated are the experimental techniques adopted by the several investigators [Sch58, Gad61, Nik59, Sch61, Jen67a, Jen67b, Kle55, Abb70, Lun63, Sir67, Ter60].

Gibbs energy data. There are five reported experimental determinations of component activities in liquid In-Sb solutions. Terpilowski [Ter59] and Terpilowski and Trzebiatowski [Ter60] measured the In activity in an electrochemical cell using a double bromide salt and found negative deviations throughout the entire concentration range in the temperature range 643 to 763 K. Hoshino et al. [Hos65], using a double iodide salt concentration cell, measured the In activity at 900 K in the liquid phase. Their measurements compared well with the results of Terpilowski. Both of the measurements assumed that the In ion that was transported in the fused salt electrolytes was monovalent. This prompted Chatterji and Smith [Cha73] to investigate the In activity in a galvanic cell using a solid electrolyte in which the oxidation state of In was trivalent. Four compositions were studied in the In-rich portion of the phase field.

Anderson et al. [And84] have pointed out the uncertainties involved in Chatterji et al.'s experiment and, after performing a third-law analysis, indicated their data to be inconsistent with other thermodynamic data. Anderson et al. set up two solid state electrochemical cells and measured the In activity at 973 K. Their work shows less negative deviation when compared to other investigators.

Four emf studies of the standard Gibbs energy of formation of InSb(s) are available in literature [Nik59, Abb70, Sir67 and Ter60] as summarized in Table 3.16.

Analysis of data on In-Sb system. As can be seen from Table 3-18, six parameters were required to adequately describe the In-Sb liquid phase by the Redlich-Kister polynomial. Three parameters were determined to be sufficient to model the solid InSb phase as a stoichiometric line compound.

The calculated phase diagram is shown in Figure 3-9 along with the experimental data from the literature including those omitted from the selected data set. The reported phase diagram data for In-Sb are fairly consistent and were thus used as the basis to check the consistency of the other thermodynamic quantities. Moderate, if not severe, discrepancy exists in the component activity and enthalpy of mixing data. The idea was to begin with less parameters for the liquid phase and as soon as the optimization indicated a decreasing (converging) mean square of error, increase the number of floating parameters. The procedure was as follows:

(1). The specific heat, C_p (12.97040 J/mol K) was estimated from the data of Lichter and Sommelet [Lic69], and Hultgren et al. [Hul73].

Table 3-13. Summary of In-Sb phase diagram data.

Reference	Method	T_m (K)	Ranges T (K) x_{Sb}	Accuracy ΔT (K) Δx_{Sb}
[Pog49]	---	---	476 - 879 0.01 - 0.91 0.001-0.003	5
[Liu52]	Thermal, X-ray Metallography	798	556 - 904 0.006-1 0.001-0.003	3-5
[Hal63]	Source Dissolution Technique	---	438 - 538 0.001 - 0.003	5 0.001
[Gor83]	---	---	731 - 797 0.25 - 0.45 0.001-0.003	5

Table 3-14. Summary of the enthalpy of fusion of In-Sb.

Reference	Method	ΔH_f (InSb) (kJ/g atom)
[Ita75]	Quantitative Thermal Analysis	24.35 ± 0.50
[Ita77]	Quantitative Differential Thermal Analysis	25.5 ± 1.0
[Nac58]	Drop Calorimetry	23.47 ± 0.80
[Sch58]	Calorimetry	25.52
[Lic69]	Drop Calorimetry	23.88 ± 0.40
[Hul73]	Evaluated	24.04 ± 0.80
[Ric65]	Differential Thermal Analysis	18.8 ± 6
[Gar77]	Quantitative Differential Thermal Analysis	24.27 ± 1.5
[Bla70]	Drop Calorimetry	24.69 ± 0.4

Table 3-15. Summary of the standard enthalpy of formation of InSb.

Reference	Method	T (K)	ΔH_f (InSb) (kJ/g atom)
[Gad61]	Bomb Calorimetry	298	16.28 ± 0.17
[Nik59]	EMF	298	15.36 ± 0.04
[Sch61]	Drop Calorimetry	298	14.23 ± 1.3
[Jen67a]	Solution Calorimetry	278	14.90 ± 0.21
[Jen67a]	Solution Calorimetry	273	15.27
[Jen67b]	Solution Calorimetry	298	15.31
[Kle55]	Tin Solution Calorimetry	723	18.07 ± 0.08
[Sch58]	Tin Solution Calorimetry	273	14.52 ± 0.46
[Abb70]	EMF	298	17.15 ± 0.84
[Lun63]	Tin Solution Calorimetry	273	15.32 ± 0.42
[Lun63]	Tin Solution Calorimetry	750	17.71 ± 0.42
[Sir67]	EMF	703	17.20
[Ter60]	EMF	703	18.83 ± 0.88

Table 3-16. Summary of Gibbs energy of formation of InSb for the reaction: $In_{(l)} + Sb_{(s)} = InSb_{(s)}$.

Reference	Method	ΔG_f @ 643 K (kJ/mol)	ΔG_f @ 763 K (kJ/mol)
[And84]	Derived	18.80	15.73
[Ter59]	Derived	20.87	18.19
[Hos65]	Derived	18.43	15.30
[Abb70]	EMF	17.78	14.73
[Nik59]	EMF	18.34	15.56
[Sir67]	EMF	18.47	15.50
[Ter60]	EMF	19.20	15.76

Table 3-17. Summary of selected dataset for In-Sb system.

Data Type	References
Phase Diagram	[Pog49, Liu52, Gor83]
Enthalpy	[Wit67, Lic69, Bla70, Hul73, Ita77, Oeh78, Ros80]
Gibbs Energy	[Hos65, Cha73, And84]

Table 3-18. Optimized coefficients for Redlich-Kister model and lattice stability of InSb.

n	$A_{In\text{-}Sb}$ (J/mol)	$B_{In\text{-}Sb}$ (J/mol K)	$C_{In\text{-}Sb}$ (J/mol K)
0	-25631.2	-89.47429	13.45816
1	-2115.4	1.31907	---
2	2908.9	---	---

Table 3-19. Invariant equilibria in the In-Sb system.

Reaction	Eutectic Composition At % Sb	Eutectic Temperature (K)	Reference
L = In(s) + InSb(s)	0.66	427.8	[Liu52]
	---	428	[Pog49]
	0.47	427.4	This study
L = $InSb_{(s)}$ + $Sb_{(s)}$	68.3	767 ± 3	[Liu52]
	70.4	779 ± 2	[Pog49]
	68.8	767.35	This study

Table 3-20. Summary of Ga-Sb phase diagram data.

Reference	Method	T_m (K)	Ranges T (K) x_{Sb}	Accuracy ΔT (K) Δx_{Sb}
[DeW86]	Source Dissolution Technique	---	648 - 923 0.003 - 0.2	3 - 5 0.001-0.003
[Mag68]	Differential Thermal Analysis	982.2 ± 0.3	823 - 982 0.08 - 1	3 - 5 0.001-0.003
[Gre55]	Thermal, X-ray Metallography	978.9 ± 1.0	820 - 980 0.06 - 1	3 - 5 0.001-0.003
[Kos55]	Thermal Analysis	976	850 - 980 0.05 - 1	5 0.003
[Hal63]	Source Dissolution Technique	---	520 - 960 0 - 0.30	5 0.001-0.003
[Cha77]	Source Dissolution Technique	---	670 - 820 0.006 - 0.07	3 - 5 0.001
[Gla58]	---	---	920 - 960 0.4 - 0.6	5 - 10 0.001-0.003
[Ded78]	---	---	725 - 870 0.015 - 0.10	3 - 5 0.001-0.003

Table 3-21. Summary of the enthalpy of fusion of GaSb.

Reference	Method	ΔH_f (GaSb) (kJ/g atom)
[Sch58]	d.t.a.	25.1 ± 2
[Mec71]	d.t.a.	32.4 ± 1.3
[Gar77]	d.t.a.	29.1 ± 1.7
[Gam75]	d.t.a.	27.6 ± 1.7
[Lun63]	Drop Calorimetry	31.0
[Cox67]	Drop Calorimetry	33.5 ± 3.2
[Lic69]	Drop Calorimetry	32.55 ± 0.4
[Bla70]	Drop Calorimetry	30.54 ± 1.3
[Gam75]	Drop Calorimetry	30.10 ± 1.3
[Hul73]	(Evaluated)	33.12 ± 0.6

Table 3-22. Summary of the standard enthalpy of formation of GaSb.

Reference	Method	T (K)	ΔH_f (GaSb) (kJ/g atom)
[Sch58]	Calorimetry	298	20.79 ± 0.9
[Sch59a]	Calorimetry	298	20.79 ± 0.9
[Abb64]	EMF	298	19.66 ± 2.1
[Lun63]	Calorimetry	633 - 833	23.43 ± 2.1

Table 3-23. Summary of Gibbs energy of formation of GaSb for the reaction: $Ga_{(l)} + Sb_{(s)} = GaSb_{(s)}$.

Reference	Method	T (K)	ΔH_f (GaSb) (kJ/g atom)
[Sch58]	Calorimetry	298	19.08 ± 1.5
[Abb64]	EMF	298	18.83 ± 1.3
[Sir67]	EMF	298	20.54
[Sha87]	Assessment	298	19.35*

(* denotes recalculated value using SGTE transformation)

Table 3-24. Summary of selected dataset for Ga-Sb system.

Data Type	References
Phase Diagram	[Gre55, Mag68, Cha77, DeW86]
Enthalpy	[Lic69, Hul73, Gam75]
Gibbs Energy	[Ger65, Ber74, And83, And75, Kat87]

Table 3-25. Optimized coefficients for Redlich-Kister model and lattice stability of GaSb(s).

n	$A_{Ga\text{-}Sb}$ (J/mol)	$B_{Ga\text{-}Sb}$ (J/mol K)	$C_{Ga\text{-}Sb}$ (J/mol K)
0	-13953.8	-61.45546	9.62320
1	1722.9	1.92588	---
2	2128.3	---	---

Table 3-26. Invariant equilibria in Ga-Sb system.

Reaction	Eutectic Composition At. % Sb	Eutectic Temperature (K)	Reference
$L = Ga_{(s)} + GaSb_{(s)}$	---	302.5	[Kos55]
	---	302.8	[Gre55]
$L = GaSb_{(s)} + Sb_{(s)}$	87	856	[Kos55]
	88.7	862.8 ± 0.5	[Gre55]
	---	861.5 ± 0.3	[Mag68]
	88.5	862.7	This study

(2). Using experimental enthalpy and Gibbs energy data, optimized coefficients were used to predict the phase diagram. Inconsistent thermodynamicdata were discarded.
(3). The combined thermochemical and phase diagram data set was taken together and the coefficients allowed to float. The coefficients obtained hereafter were tested for variation with experimental data. The best set of coefficients was selected which provided the optimal fit to the combined data set.

The optimized phase diagram (Figure 3-9) fits the experimental data of Liu and Peretti, Pogodin et al., and Goryacheva quite well. The data by Pogodin et al. was consistently higher than those by other authors and the optimized values, but were still retained as the deviations were within the experimental error limits. Hall's data, on the contrary, showed marked deviation with respect to the other data values at indium-rich compositions in the phase diagram. Eliminating Hall's data resulted in a significant improvement in the phase diagram fit and mean square error value. The calculated melting temperature of InSb (T_m = 800 K) and the two eutectic temperatures (427.1 K, 767.5 K) are in good agreement with the reported values as shown in Table 3-19.

The enthalpy of mixing experimental data compares quite well with the optimized plots. As can be seen from Figure 3-10, the ΔH_m curve is assymmetric in composition. The degree of assymmetry is fairly moderate and is taken into consideration in the calculation by the use of parameters in the phase description of the In-Sb liquid phase. There is a strong temperature dependence in the liquid phase enthalpy as indicated by Oehme and Predel [Oeh78]. This temperature dependence is reproduced well by the coefficients of the liquid phase as is clearly evident in Figure 3-10. The data by Vecher et al. [Vec74] are significantly higher in value when compared to Itagaki [Ita75, Ita77]

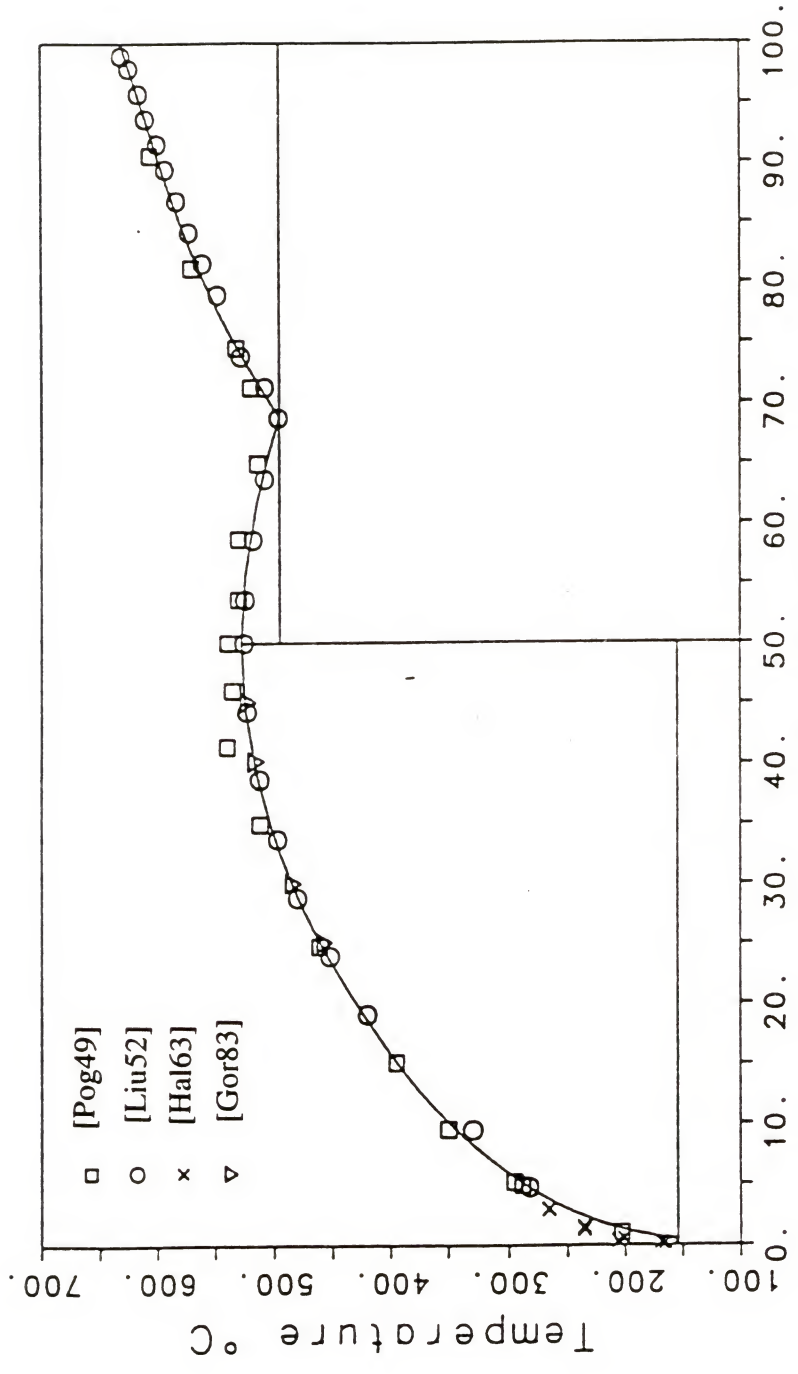

Figure 3-9. Optimized In-Sb phase diagram.

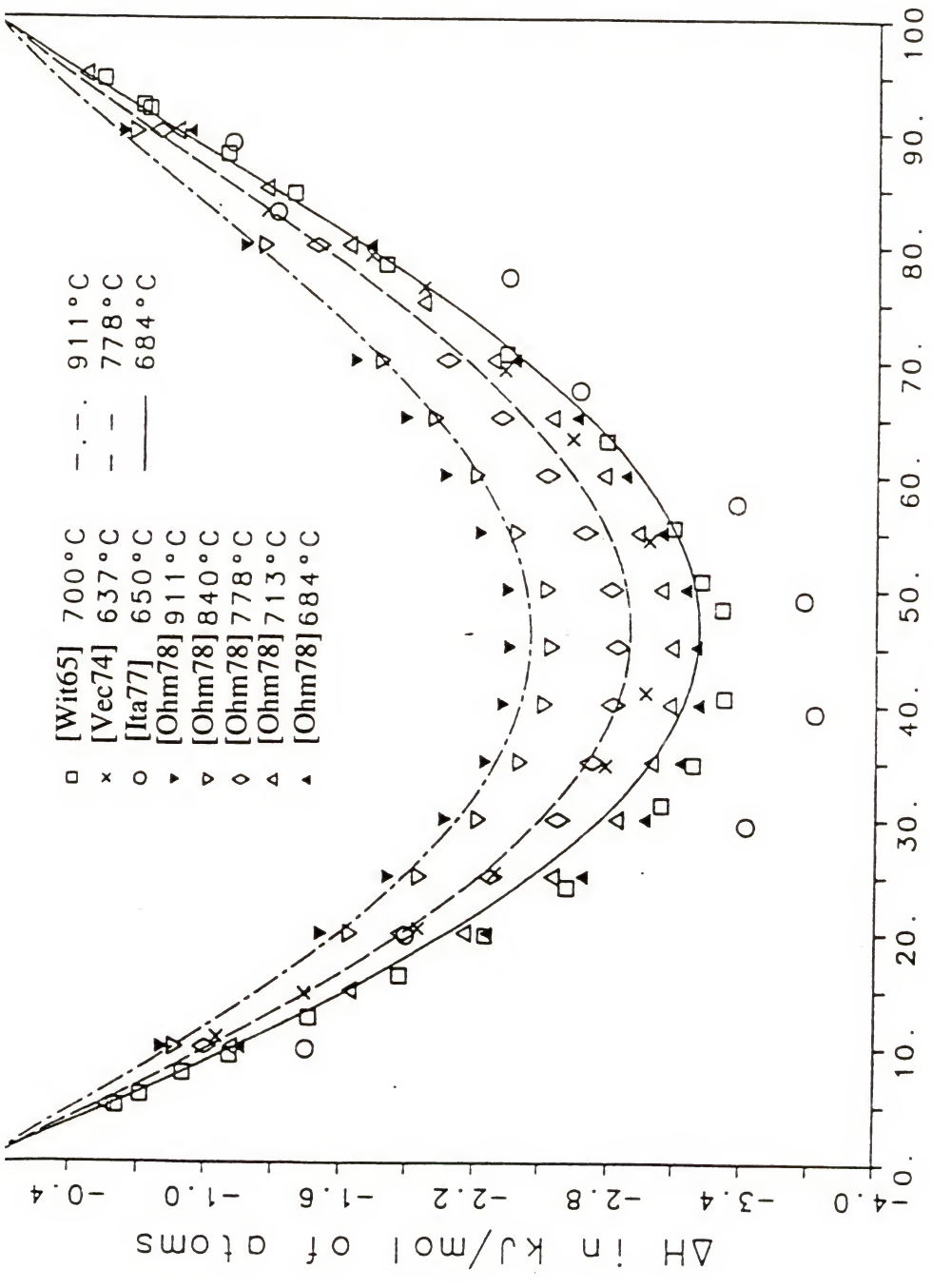

Figure 3-10. Optimized In-Sb liquid phase enthalpy of mixing.

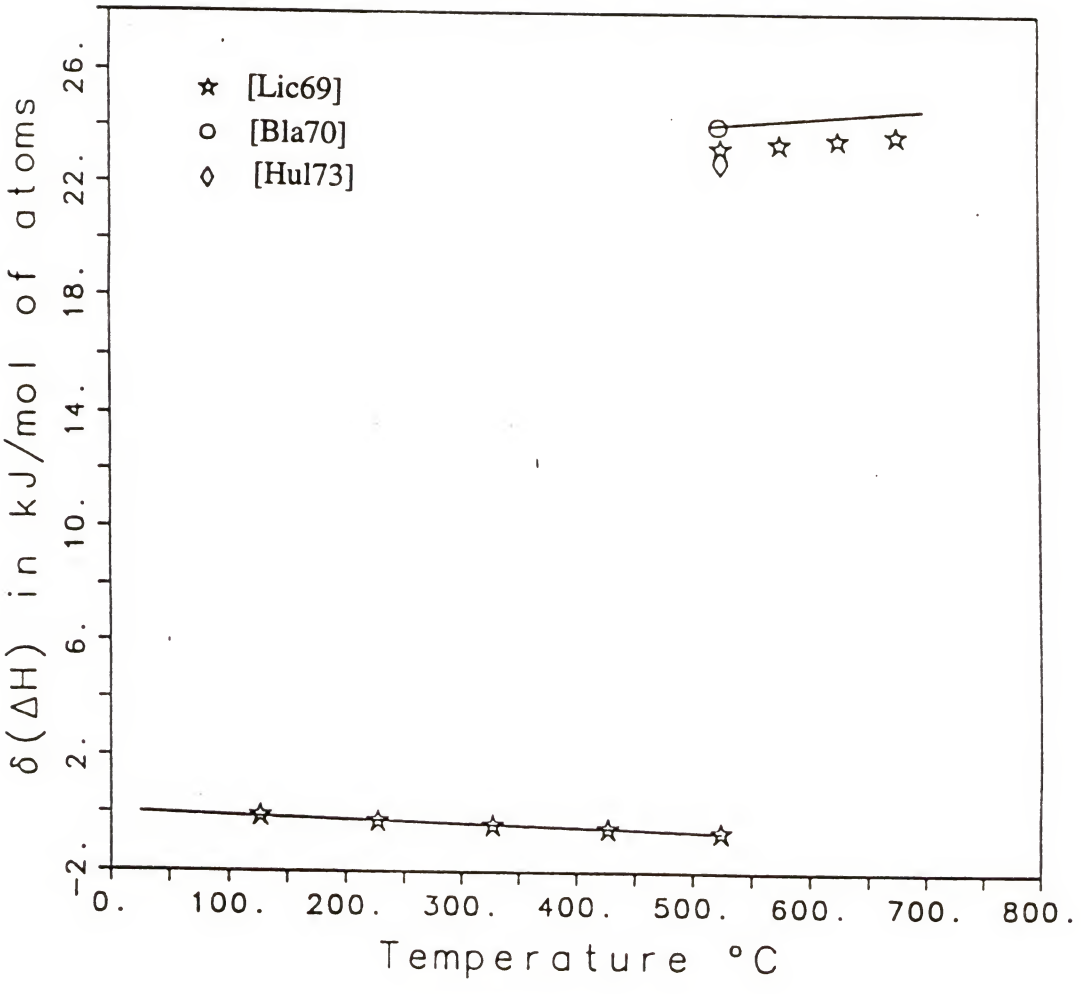

Figure 3-11. Optimized enthalpy changes for the reaction: In(s,l) + Sb(s,l) = InSb(s,l).

and Predel's data [Pre76]. Their data was thus not selected for the optimization. Wittig's data [Wit67] at 973 K was found to be consistent. The data reported by Itagaki for 923 K temperature were determined to be low, but were still retained as their inclusion did not affect the mean square error significantly. Furthermore, their data were found to be consistent with the phase diagram data. The fit of the calculated curves to the excess heat content data of Lichter and Sommelet is excellent, as shown in Figure 3-11. The $\delta(\Delta H)$ of the solid and liquid phase data in the plot was accomplished by subtracting out the heat content contributions from the pure elements. The component C_p data required in the calculation was taken from Hultgren [Hul73] . The relations used were:

(a) Below In Melting Point

$$\delta(\Delta H) = H_m - 0.5H_{In} - 0.5H_{Sb} \tag{3.5}$$

(b) Above In Melting Point and Below InSb Melting Point

$$H_{In} = (H_{In} - \Delta H_{melting,In})_{Hultgren} \tag{3.6}$$

$\delta(\Delta H)$, as above

(c) Above InSb Melting Point

$$\delta(\Delta H) = H_m(T) - H_m(T_m) - (T - T_m)\,({}^{liqIn}C_p / 2 + {}^{liqSb}C_p / 2) \tag{3.7}$$

The enthalpy of fusion of InSb is determined to be 25.32 ± 0.9 kJ/g atom and it compares well with the values listed in Table 3-14. Similarly, the Gibbs energy of formation of $InSb_{(s)}$ from $In_{(s)}$ and $Sb_{(s)}$ at 643 K and 763 K are calculated as -20.56 and -18.15 kJ/mol respectively. For the reaction involving In(l) and Sb(s) the respective values are -18.93 and -15.60 kJ/mol respectively and agree well with reported values in Table 3-15.

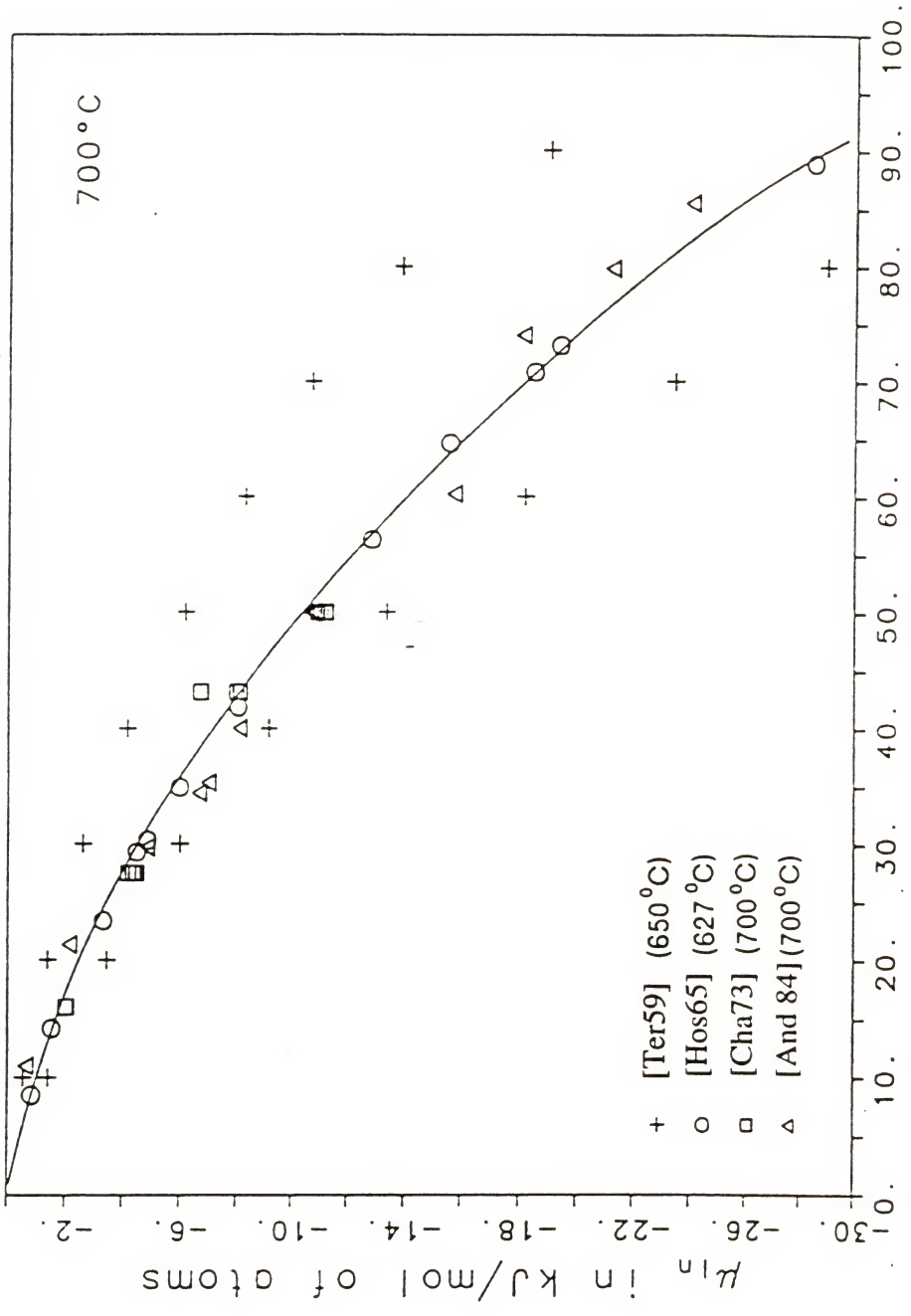

Figure 3-12. Optimized liquid phase In activity in the In-Sb system.

Figure 3-12 shows the calculated partial Gibbs energy, m_{In}, as a function of composition at 973 K as compared to the data of Anderson et al. [And84] and Chatterji and Smith [Cha73]. The calculated curve agrees well with these data and also gives an excellent fit to the data of Hoshino et al. [Hos65], though their reported values are at 900 K. The data by Terpilowski [Ter59] showed significant discrepancy.

Ga-Sb Assessment

Similar to the In-Sb system, the Ga-Sb sytem has been well characterized in terms of phase diagram information. The enthalpy of mixing and Gibbs energy data for the Ga-Sb system show some disagreement in the available literature values, partly because of the differences in experimental methods used and, partly because of the experimental problems encountered in measurements of these properties. Thus, the motivation towards performing an assessment of the Ga-Sb system is to determine a complete and a consistent data set which can be used to make accurate predictions for multicomponent systems containing the binary Ga-Sb system.

Phase diagram data. The phase diagram for the Ga-Sb system has been reported by several investigators [Hal63, DeW86, Mag68, Gre55, Kos55, Cha77, Gla58, Deg78] and have indicated a simple eutectic type of phase domain for the system [Mag68, Gre55, Kos55] with negligible solubility of either element in the other. A brief summary of the methods employed by the various investigators for the liquidus measurements is given in Table 3-20. Also shown in Table 3-20 are the temperature and composition ranges investigated by these authors and the reported (or estimated) accuracies in their respective measurements. The Sb-GaSb eutectic occurs at a composition of $x_{Sb} = 0.88$ and a

temperature of 863 K, while the Ga-GaSb eutectic is nearly degenerate. The melting temperature values as measured by various investigators [Sha87, Mag68, Gre55, Kos55, And83] range form 975 to 998 K; and the generally accepted value is 985 K [Hul73]. Greenfield et al. have reported the data of Maglione and Potier to be about 5 K below their data, while the data of Hall is as much as 5-10 K higher than their data. However, as was also mentioned for the case of In-Sb system, Sharma et al. suspect the data by Hall stating that the source dissolution technique used by Hall, was prone to error at low Sb compositions. Likewise, Hall's data is too high when compared with the liquidus measurements of Chang and Pearson [Cha77] and Dedegkaev et al. [Ded78]. Glazov and Petrov [Gla58] made measurements in the range $0.4 < x_{Sb} < 0.6$. Their values are significantly lower than the other reported values. Koster and Thoma report values which are consistently lower than other measurements throughout the composition range of their investigation.

Enthalpy data. The exothermic enthalpy of mixing in the liquid phase has been reported by Yazawa et al. [Yaz68], Predel and Stein [Pre71] and Gambino and Bros [Gam75] at a temperature near 1000 K. The data by Predel and Stein and Gambino and Bros agree quite well, however, the data by Yazawa et al. show significant deviations from the previous studies. Predel and Stein reported the maximum exothermic enthalpy of mixing at $x_{Sb} = 0.5$. Yazawa et al. used an adiabatic calorimeter to obtain mixing enthalpies and fitted the data to a fourth degree polynomial expansion in terms of Sb content.

The enthalpy of fusion has been reported by several investigators [Mec71, Sch58, Lic69, Hul73, Gar77, Bla70, Lun63, Gam75 and Cox67] and is tabulated in Table 3-21.

Schottky and Bever [Sch58] and Lundin et al. [Lun63] determined the enthalpy of formation of GaSb. These values are listed in Table 3-22.

Gibbs energy data. The Ga activity in the liquid phase has been measured by electrochemical techniques at around 1000 K [And83, Pon75, Dan70, And75, Ger65, Kat87]. The activity data of Pong [Pon75], Gerasimenko et al. [Ger65], and Danilin et al. [Dan70] show relatively large negative deviations from ideality. On the other hand, Hsi-Hsiung et al. [Hsi66] and Bergman et al. [Ber74] derived the activities from vapor pressure measurements. Bergman et al. directly determined the activity of Ga by means of a Knudsen cell coupled to a mass spectrometer. Their data as well as the values determined by Anderson [And75], Katayama et al. [Kat87] and Anderson et al. [And83] show moderate negative deviation from ideality and are in close agreement. In their work, however, Katayama et al. reported moderate deviation of the data by Anderson et al. from their measured values in the high and low composition ranges, i.e., $x_{Sb} = 0.2$ and $x_{Sb} = 0.8$.

The discrepancy in the degree of negative deviation of the Ga activity from ideality for a few authors [Hsi66, Ber74] compared to the others [And83, Pon75, Dan70, And75, Ger65, Kat87] might be attributed to the uncertainty in the Ga valency for the chloride molten-salt galvanic cells used. The possible existence of GaCl and $GaCl_2$ in addition to GaCl3 would result in an effective charge of less than the value of 3 assumed.

Anderson et al. [And83] found the Non-Random Two Liquid (NRTL) equation to best represent the activities reported in their work while also performing a consistency test on the other activity data. A summary of the Gibbs energy of formation of GaSb is presented in Table 3-23.

Analysis of data on Ga-Sb system. The selected data set for Ga-Sb is given in Table 3-24. Six parameters were required to adequately describe the liquid phase by the same Redlich-Kister formalism and are shown in Table 3-25, while four parameters were sufficient for the description of the solid GaSb phase as a stoichiometric line compound

The calculated phase diagram is shown in Figure 3-13 and appears to be in excellent agreement with experimental determinations of the liquidus. However, there exists marked differences in the melting temperature of GaSb amongst the various investigators [Sha87, Mag68, Gre55, Kos55, And83]. Similar to the In-Sb system, the Ga-Sb system exhibits a fairly consistent phase diagram data set and thus was used as a basis for a consistency check of the other thermodynamic data of the system. A similar process scheme was adopted for the Ga-Sb system as for the In-Sb system mentioned in the previous section and the same convergence criteria used. An initial estimate of 9.623 J/mol K was employed utilizing the specific heat data of Lichter and Sommelet [Lic69] for liquid GaSb and that of the liquid elements from Hultgren et al. [Hul73].

As is evident from Figure 3-13, the optimized phase diagram fits the data of Greenfield et al., Maglione and Potier, Cheng and Pearson and DeWinter et al. quite well. The data by Koster and Thoma and Glazov and Petrov are at least 5-10 K lower than the rest of the liquidus data. As in the case of In-Sb system, the data by Hall showed significant deviation in the gallium-rich region of the phase diagram, and for a similar reason was eliminated from the selected dataset. Table 3-26 indicates good agreement between the calculated melting temperature of GaSb (T_m = 984.8 K) or the eutectic temperature (862.7 K) with the reported values.

The liquid phase enthalpy of mixing data [Pre71, Gam75] compare well with the optimized data as shown in Figure 3-14. The parameters give an acceptable assymmetry and temperature dependence to the liquid phase enthalpy to compare well with the experimental measurements of Predel and Stein [Pre71] and Gambino and Bros [Gam75].

The data of Yazawa et al. [Yaz68] show discrepancy with the other two authors. Their data provide an incorrect temperature dependency of the mixing enthalpy and were considered to be inconsistent.

A similar set of calculations was performed for determining the excess heat content data of the solid and liquid phases as was done for the case of In-Sb system; an excellent fit is obtained as shown in Figure 3-15.

The enthalpy of fusion of GaSb is calculated to be 34.5 ± 0.8 kJ/g atom which compares well with literature values in Table 3-21. Furthermore, the Gibbs energy of formation of GaSb from $Ga_{(s)}$ and $Sb_{(s)}$ at 298 K is determined to be -15.49 kJ/g atom. SGTE transformation yields a value of -15.58 kJ/g atom for the pure components, Ga(l) and Sb(s), which agrees fairly well with the data in Table 3-22.

Figure 3-16 shows good agreement of the partial molar Gibbs energy (m_{Ga}) data with the reported values [And83, And75, Ger65, Kat87]. However, the data of Danilin and Yatsenki [Dan70] do not match well with the optimized curve and were determined to be inconsistent based on their ability to generate the phase diagram and fit the liquid phase enthalpy. As mentioned previously, their data exhibited significantly negative deviations from ideality.

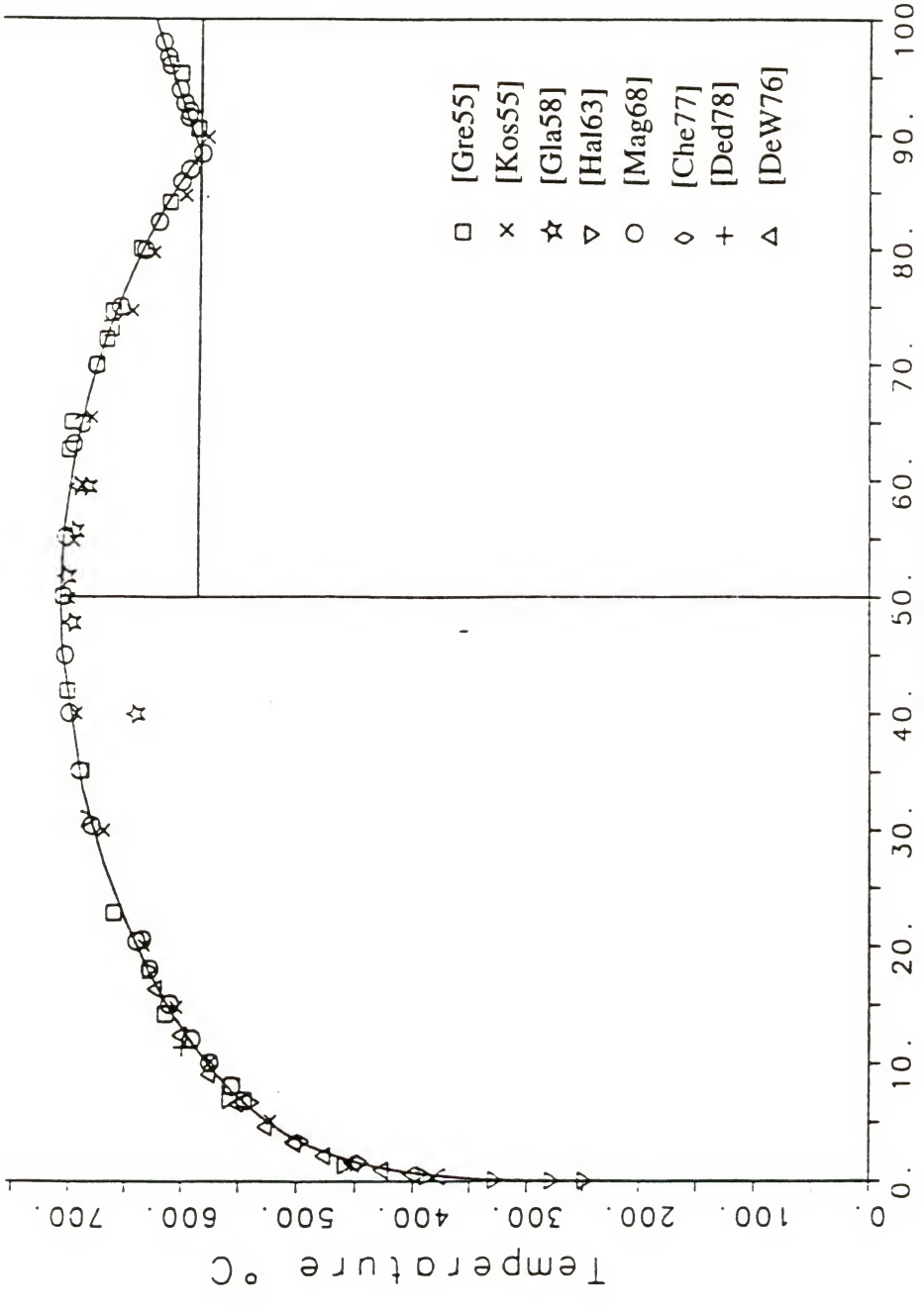

Figure 3-13. Optimized Ga-Sb phase diagram.

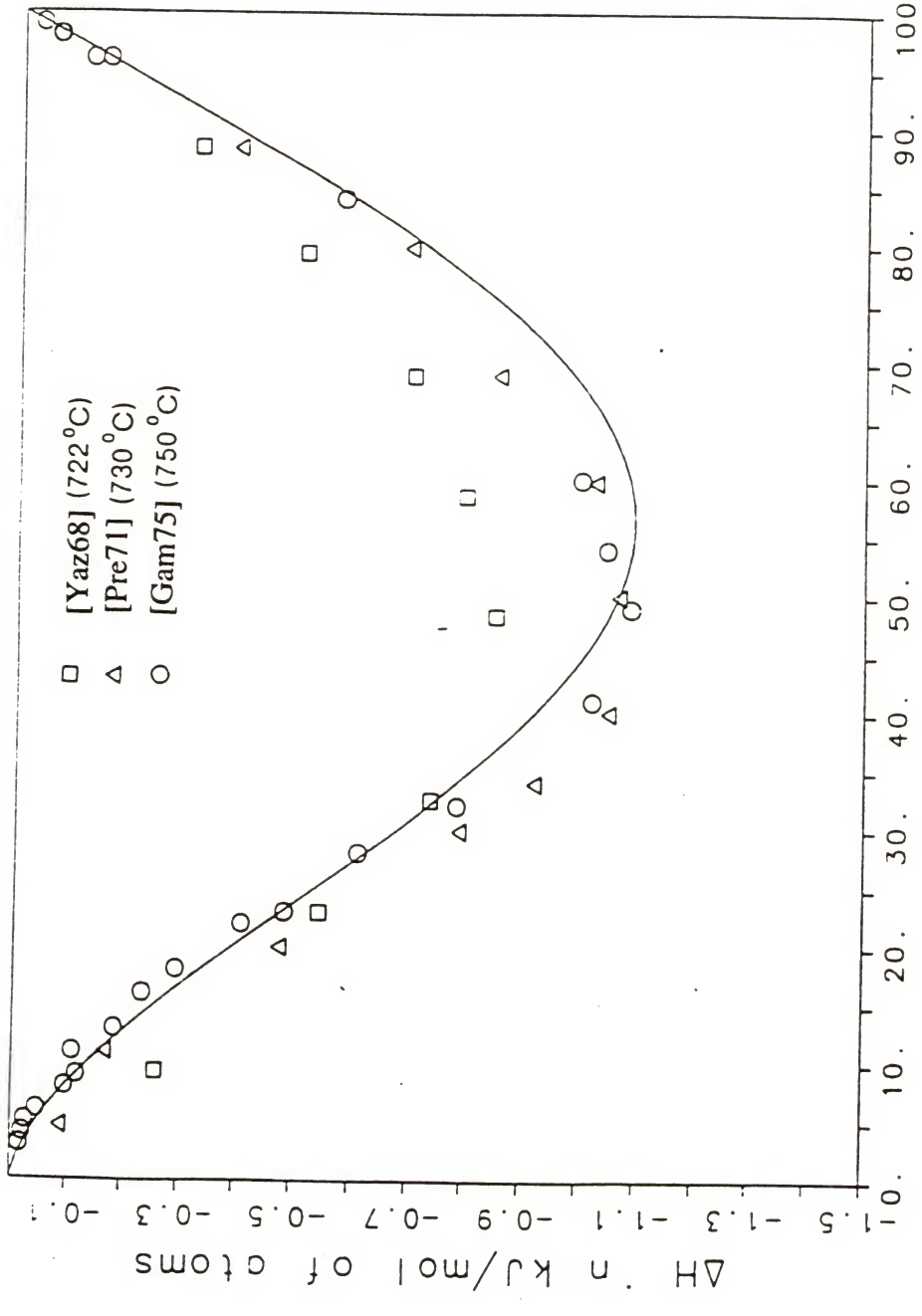

Figure 3-14. Optimized Ga-Sb liquid phase enthalpy of mixing.

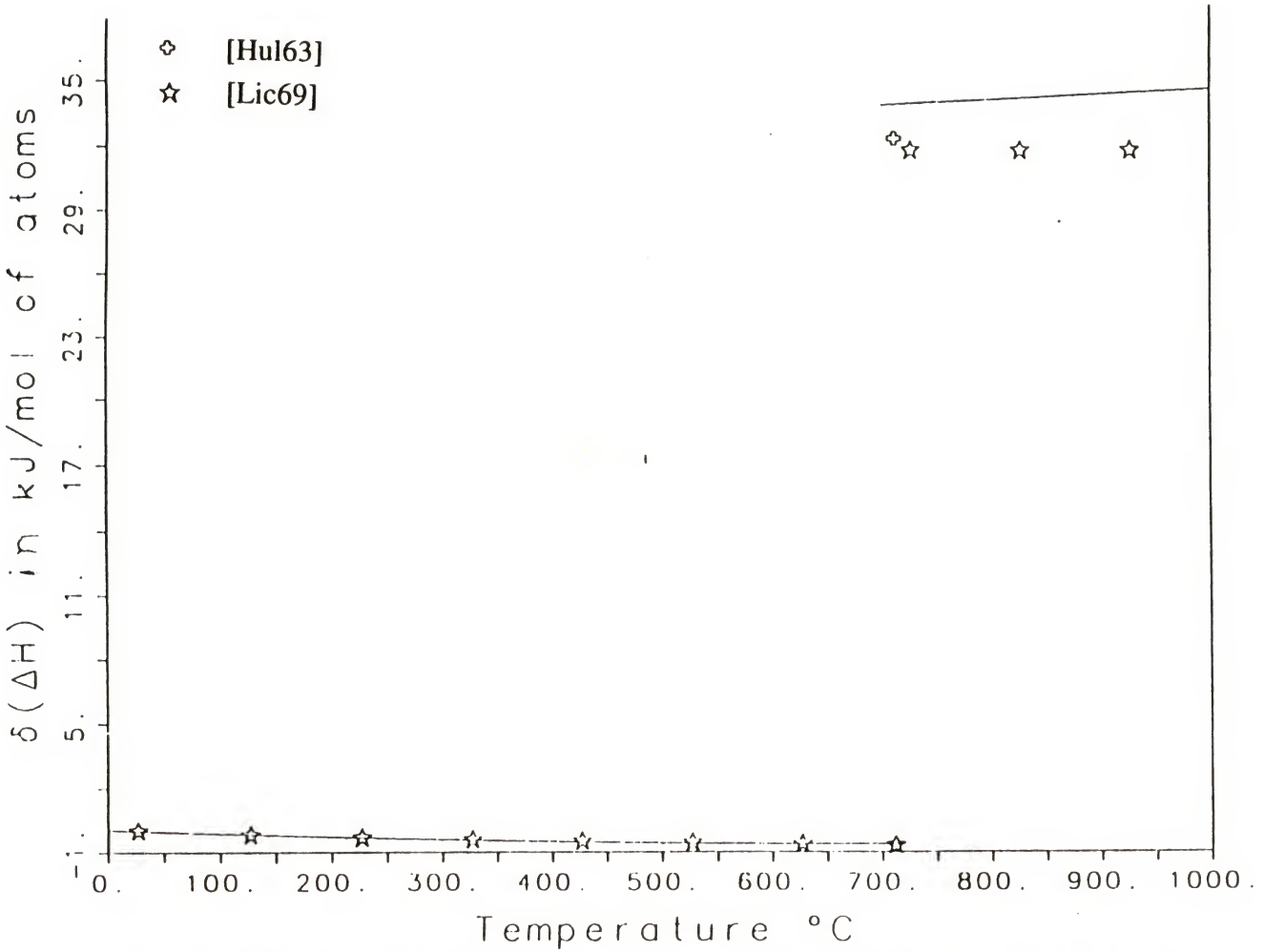

Figure 3-15. Optimized enthalpy changes for the reaction: Ga(s,l) + Sb(s,l) = GaSb(s,l).

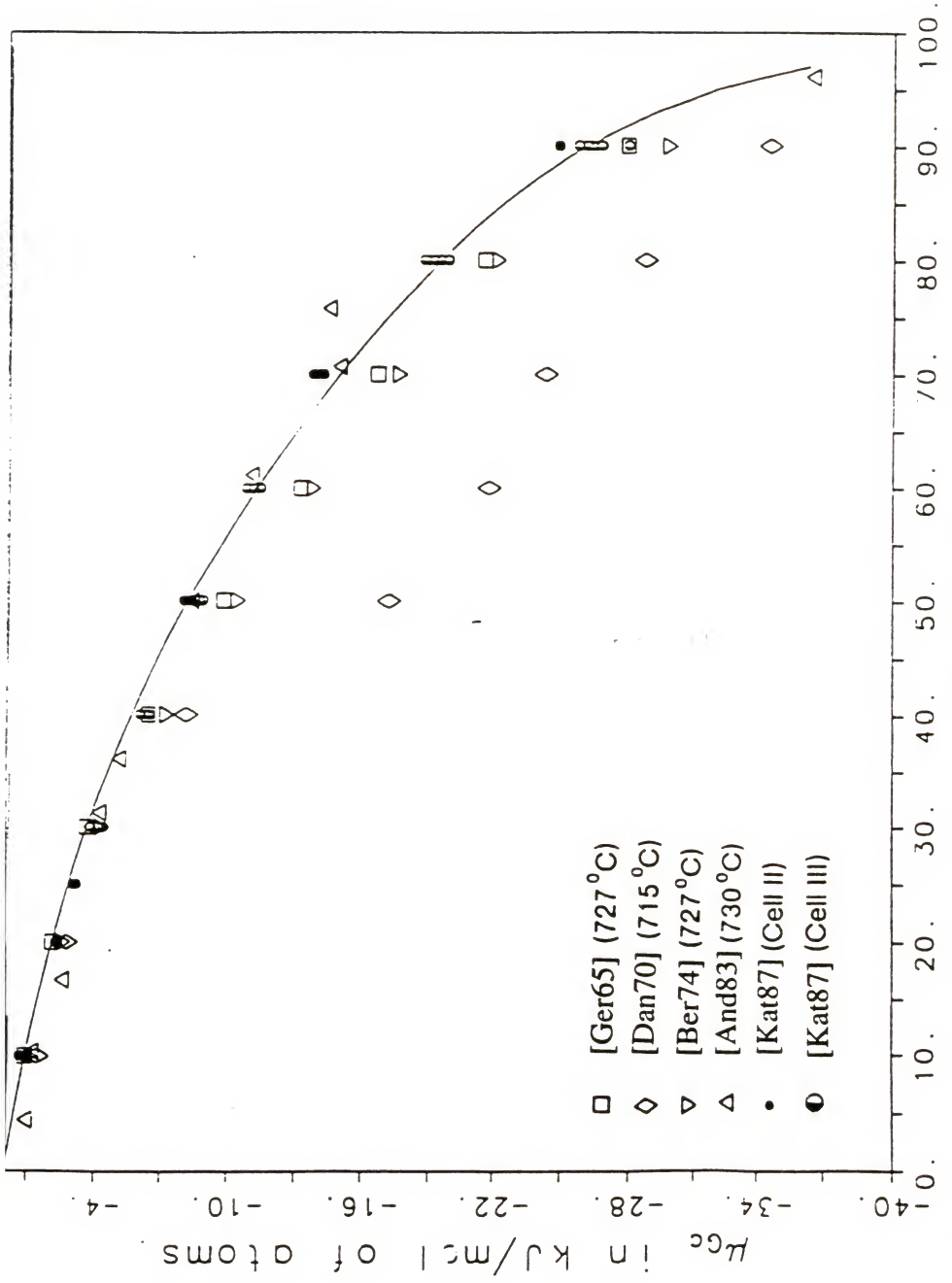

Figure 3-16. Optimized liquid phase Ga activity in the Ga-Sb system.

Assessments of Ternary Systems

Ga-Sb-As Assessment

The Ga-Sb-As system exhibits a eutectic valley extending from the Sb-rich region side of the binary Ga-Sb phase diagram to the As-rich region of the GaAs phase diagram. Given the high vapor pressure of As, the phase diagram determinations have been limited to As-dilute compositions [Ant70, Woo58, Ino70, Fos72, Gra73, Nah77, Sug77, Gra80, Pes83, Man86 and Mik65].

The pseudobinary section GaAs-GaSb in the ternary phase diagram is a region of extended solid solution with a large region of immiscibility in the solid phase. There exists significant disagreement, however, regarding the solid phase behavior in this pseudobinary section. A eutectic-type phase diagram has been proposed [Ino71] in the GaAs-GaSb section, though more recent measurements have indicated a miscibility gap in the solid solution [Gra73, Pes83, Man86 and Ish88].

Measurements of the liquidus have generally been made using differential thermal analysis (D.T.A.), while those on the solidus have been made using microprobe analysis on solid solutions of GaAs-GaSb deposited on GaAs substrates by liquid phase epitaxy (LPE) or by X-ray analysis.

Binary systems. The binary systems Ga-As, Ga-Sb and As-Sb [Ans93, Nga88] have been assessed previously, and the optimized coefficients for the Gibbs energy expressions for the contained phases have been used as the limiting values for assessment of the ternary system Ga-Sb-As. The binary systems Ga-Sb and Ga-As were assessed [Ish88, Sha89 and Lee92] as also by this work. For the As-Sb system, the thermodynamic parameters were taken from Ishida et al. [Ish89a].

Solid phases. There has been no evidence for the formation of a ternary compound in this system. For the pseudobinary solid solution, Straumanis and Kim [Str65] showed that Vegard's law was obeyed to 34 at. % GaAs from their measurements on samples of alloys obtained by annealing quenched melts. In contrast, Muller and Richards [Mul64] observed complete solid solution over the entire composition range in flash evaporated samples and lattice parameter measurements indicated that Vegard's law was obeyed to 50 at. % GaAs composition. Later, Gratton and Woolley [Gra73] determined the variation of lattice parameter with composition. They confirmed the validity of Vegard's law to 38 at. % GaAs compositions. At compositions greater than 61 at. % GaAs, they observed slight negative deviations from Vegard's Law, which was consistent with the predicted results of Straumanis and Kim [Stra65]. A summary of lattice parameters is given in Table 3-27.

Pseudobinary section. The liquidus in the pseudobinary section has been fairly well characterized [Ino71, Fos72, Ish88, Mik65] and the data are in agreement. The solid solutions in the pseudobinary section, however, have been the subject of controversy. Inoue et al. [Ino71] reported a eutectic type behavior at a composition of 3.0 mole % GaAs composition and temperature of 981 K, while other investigators [Gra73, Pes83,

Man86, Ish88] found that a solid solution occured over the entire composition range. The critical temperature for the miscibility region lay near the solidus curve. Given the difficulty in achieving equilibrium in the solid solution, it was not surprising that the range of immiscibility varied significantly in the authors' works. Pessetto et al. [Pes83], Stringfellow [Str83], and Cooper et. al. [Coo82] determined a symmetric miscibility gap, while Gratton and Woolley [Gra80], Mani et al. [Man86] and Ishida et al. [Ish88] suggested an asymmetric miscibility gap.

Invariant equilibria. The invariant reaction from liquid to solid in the As-dilute pseudobinary section has been reported to be peritectic by Stringfellow [Str72], Gratton and Woolley [Gra80] and Ishida et al. [Ish83]; but a eutectic reaction has been proposed by Inoue et al. [Ino71]. A peritectic behavior is accepted in this assessment.

The four phase reaction $L \Leftrightarrow (Ga) + Ga(As,Sb)^{I} + Ga(As,Sb)^{II}$ is degenerate. The calculated monovariant equilibria is shown in Figure 3-17 and the reaction scheme is presented in Figure 3-18. The temperatures and compositions of the various binary or pseudo-ternary reactions are given in Table 3-28.

Liquidus surface. Liquidus data have been reported only for the As-dilute pseudobinary section and the Ga-Sb rich region in the ternary system. A number of calculated phase diagrams using either semi-empirical models or optimized coefficients have appeared in the literature. Antypas [Ant70] calculated the ternary phase diagram using Darken's quadratic formalism for the ternary liquid and a regular solution model for the solid solution and compared the results with the data of Woolley [Woo62]. The

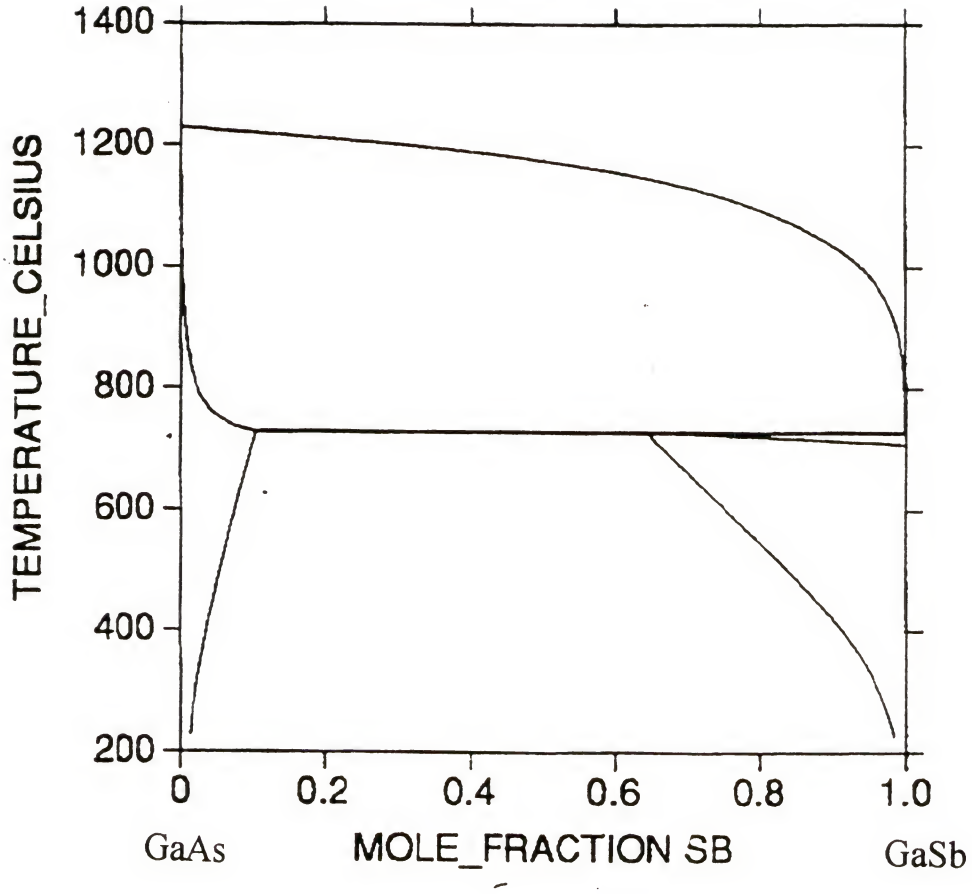

Figure 3-17. Calculated monovariant equilibria in the Ga-As-Sb system.

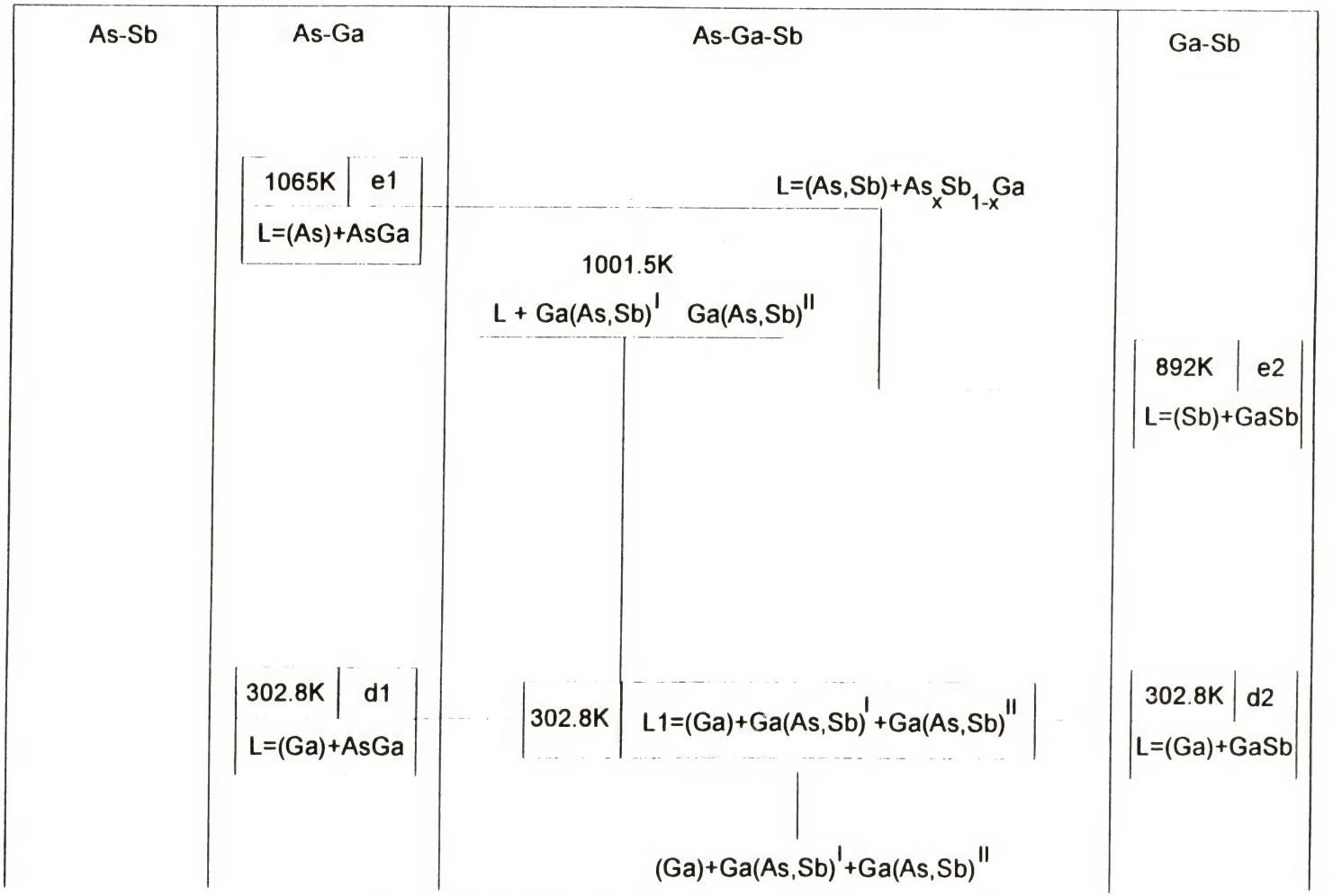

Figure 3-18. Reaction scheme for the Ga-As-Sb system.

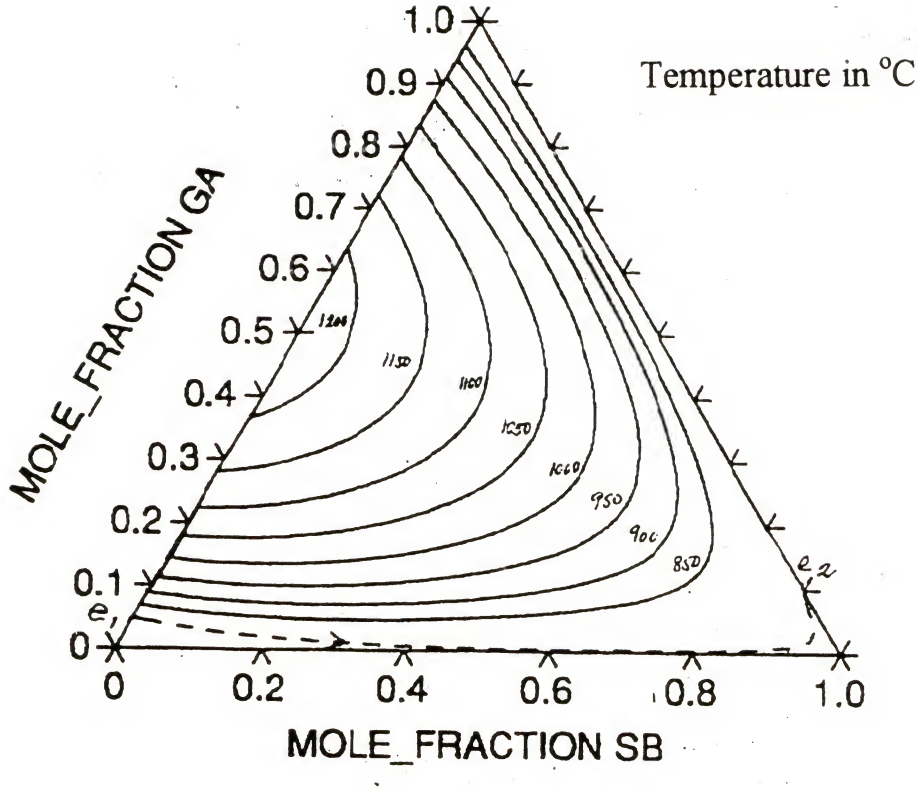

Figure 3-19. Calculated liquidus lines in the Ga-As-Sb system.

analysis of Foster and Woods [Fos72] indicated nearly ideal liquid phase behavior with strong positive deviations in the solid solution. Sugiyama et al. [Sug77] obtained As solubility data from weight loss measurements. Gratton and Woolley [Gra80] found large, three-phase, liquid-solid-solid fields corresponding to the two-phase, solid-solid fields of the pseudobinary section. They also determined the locus of the cusp in the liquidus sheet. Calculated liquidus lines are shown in Figure 3-19.

In-Sb-As Assessment

The phase diagram of the In-Sb-As system is dominated by the pseudobinary solid solution formed between the only contained binary compounds InAs and InSb. These alloys are attractive semiconducting materials due to their narrow and direct bandgap energy (infrared optoelectronic devices) and high electron mobility (high speed electronic devices). Several consistent measurements of the liquidus surface have been reported, however, the variation of the solidus has been controversial, primarily due to the strain energy associated with the size difference between As and Sb atoms, the solid solution exhibits immiscibility. The measured extent of this immiscibility has varied considerably, with both eutectic and isomorphous type phase diagrams reported. Experimental difficulties beyond those normally encountered with temperature and composition measurement include low diffusivities in the solid, As vapor loss, a large As segregation coefficient, and a tendency for supercooling in the liquid.

Table 3-27. Summary of solid phases in the Ga-As-Sb system.

Phase	Pearson Symbol/Prototype	Lattice Parameter (pm)	Comments
$Ga(As_xSb_{1-x})$	cF8 ZnS Sphalerite	565.26 to 609.5	Vegard's Law valid for GaSb-rich compositions and slight negative deviations at GaAs-rich compositions
GaAs	same	565.26	x=1
GaSb	same	609.5	x=0

Table 3-28. Summary of invariant equilibria in the Ga-As-Sb system

T (K) Reaction	Type	Phases	Composition At % As Ga Sb
L = (As) + GaAs	Eutectic	Liquid As GaAs	0.0 0.0
1001.6 L = (Sb) + GaSb	Eutectic	Liquid Sb GaSb	0.0
$L + GaAs_xSb_{1-x}^{I}$ $= GaAs_xSb_{1-x}^{II}$	Peritectic	Liquid $GaAs_xSb_{1-x}$	0.052 0.5 0.321
302.8 L = (Ga) + $GaAs_xSb_{1-x}^{I}$ + $GaAs_xSb_{1-x}^{II}$	Degenerate	Liquid (Ga) $GaAs_xSb_{1-x}$	~0.0 ~1.0 ~0.0

Binary systems. The phase diagrams of the In-As and In-Sb binary systems are centered about the compound InAs or InSb. Simple eutectic type phase diagrams are exhibited on both sides of the compounds. Though little information is available for As-rich solutions, considerable experimental data exists for the compound InAs and In-rich compositions in the In-As system. The In-Sb system has been extensively studied, including several consistent measurements of the liquidus and compound properties as well as the liquid phase enthalpy of mixing and component activities. The As-Sb system shows a continuous solid solution and is less well studied than the other two binary systems. The As-Sb system shows a continuous solid solution and is less well studied than the two other binary systems. The binary systems In-Sb and In-As were assessed by Ishida et al. [Ish88]. For the As-Sb system, the thermodynamic parameters are taken from [Ans94].

Solid phases. No ternary compounds have been reported in the In-Sb-As ternary system. The structural characteristics of the pseudobinary $InAs_xSb_{1-x}$ have been studied by a number of investigators. The solution crystallizes in the zinc blende structure and shows a slight deviation from Vegard's Law. Woolley and Warner [Woo64] improved the accuracy of their original measurements [Woo58] of the lattice parameter by annealing compressed powders for 6 months at a temperature 10 to 15°C below the relevant solidus temperature. Slight negative deviations from Vegard's Law were observed for InAs compositions greater than 70 at. % InAs, while somewhat larger positive deviations were reported for InSb-rich compositions. The cross over composition (~ 30 at. % InAs) corresponds to a minimum in the bandgap energy, suggesting that considerable ordering exists on the group III sublattice [Sem74]. The room temperature lattice parameter

measurement of Muller and Richards [Mul64] on a flash evaporated equimolar film is in good agreement with the results of Woolley and Warner [Woo64]. A summary of the lattice parameters is given in Table 3-29.

Pseudobinary system. The pseudobinary InAs-InSb section of this ternary system has been examined by a number of investigators. Thermal analysis, X-ray, and metallographic studies [Shi53, Shi56] indicated a eutectic-type phase diagram that was nearly degenerate with respect to InSb. The extrapolated InAs-rich solidus gave an estimated 2 at. % InSb maximum solubility at the eutectic temperature. In contrast, the solidus determination by X-ray measurements [Woo58] indicated an isomorphous-type phase diagram with a broad liquidus-solidus gap. This finding was later confirmed by near equilibrium liquid phase epitaxial growth studies at constant temperature [Str71]. With the exception of the solidus data of Shih and Peretti [Shi53, Shi56], the measured values of the more recent solidus data are in good agreement.

Liquidus measurements of the pseudobinary phase field have been reported by several investigators [Woo58, Str71, Shi53 and Gro83]. Although Gromova et al. [Gro83] extrapolated their DTA measurements to zero cooling rate to account for supercooling of the melt, their four liquidus temperatures for Sb-rich melts were somewhat below the values reported by other investigators. Further evidence for the formation of a continuous solid solution is found in the ability to grow the full compositional range of solutions by conventional film growth techniques such as organo-metallic chemical vapor deposition (MOCVD) [Nat81].

Table 3-29. Summary of solid phases in the In-As-Sb system.

Phase	Pearson Symbol/Prototype	Lattice Parameter (pm)	Comments
$In(As_xSb_{1-x})$	cF8 ZnS Sphalerite	605.84 to 647.94	Slight posittive (InSb-rich) and slight negative (InAs-rich) deviations from Vegard's Law
InAs	same	605.84	x=1
InSb	same	647.94	x=0

Table 3-30. Summary of invariant equilibria in the In-As-Sb system.

T (K) Reaction	Type	Phases	Composition At % As In Sb
998.6 L = (As) + InAs	Eutectic	Liquid As InAs	0.85 0.15 0.0
763.0 L = (Sb) + InSb	Eutectic	Liquid Sb InSb	0.0 0.288 0.702
778.0 $InAs_xSb_{1-x}^{I}$ = $InAs_xSb_{1-x}^{II}$	Critical Point	$InAs_xSb_{1-x}$	0.334 0.5 0.166

Part of the reason for the discrepancy in the solidus is related to the difficulty in achieving equilibrium at the relatively low temperatures of solid solution existence. Although no solid solution thermodynamic data are available, semi-empirical and assessment procedures have been used to estimate the interaction energy in the solid solution. Using these procedures, solid solution immiscibility was predicted above room temperature with a calculated critical temperature ranging from well below to just above the solidus curve [Str69, Str72, Kau81, Str82, Ona82a, Ona82b, Pat87, Ich89]. The results of EXFAS measurements show that the In-V bond lengths are close to their binary compound values as the composition varies. On this basis, the stored elastic strain energy has been suggested to be the major contribution to the thermodynamic enthalpy of mixing. The existence of solid solution immiscibility has recently been experimentally confirmed by the electron probe microanalysis of [Ish89]. Their data indicate an asymmetric miscibility gap with the critical temperature located just below the solidus curve at an InAs-rich composition [Ish89].

Invariant equilibria. The four phase reaction $L \Leftrightarrow (In) + In(As,Sb)^{I} + In(As,Sb)^{II}$ is degenerate. The calculated monovariant equilibria is shown in Figure 3-20 and the reaction scheme is presented in Figure 3-21. The temperatures and compositions of the various binary or pseudo-ternary reactions are given in Table 3-30.

Liquidus surface. In addition to the pseudobinary liquidus measurements cited in the previous section, several other determinations of the ternary liquidus have been reported in the literature. Extensive measurements of the constitution of the In-Sb-As system were performed by Shih and Peretti [Shi54, Shi56] using thermal analysis and

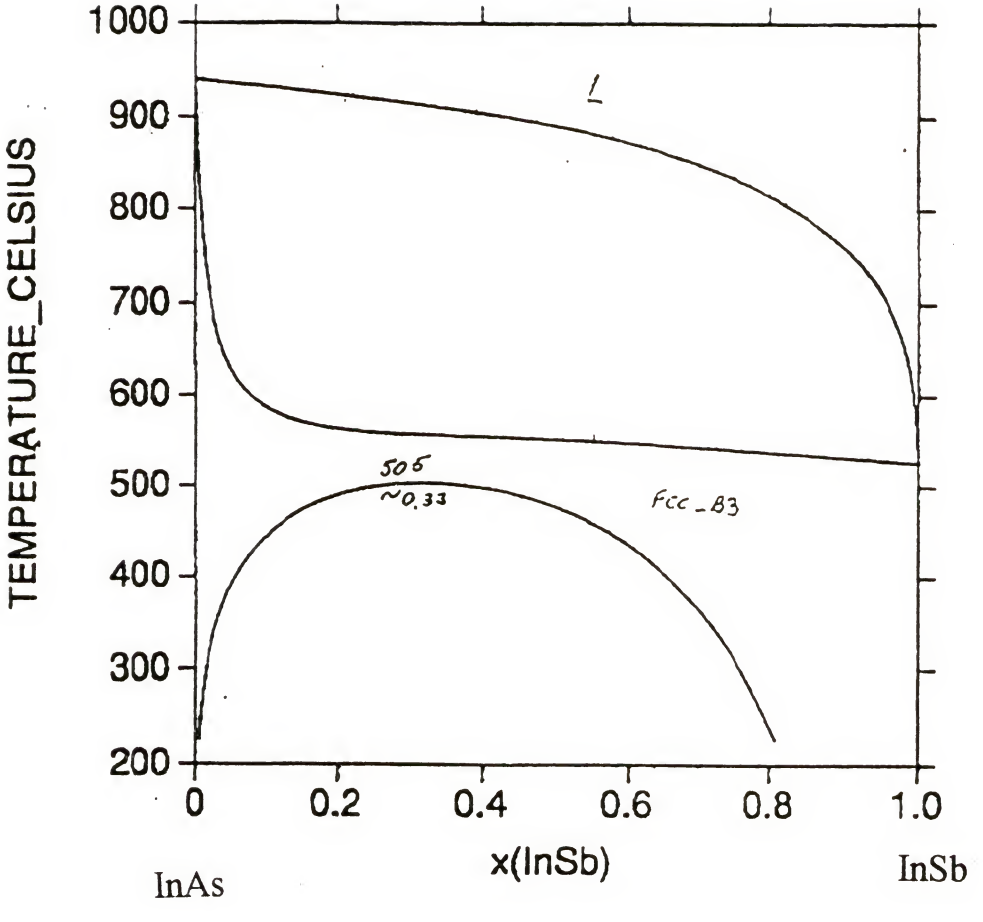

Figure 3-20. Calculated monovariant equilibria in the In-Sb-As system.

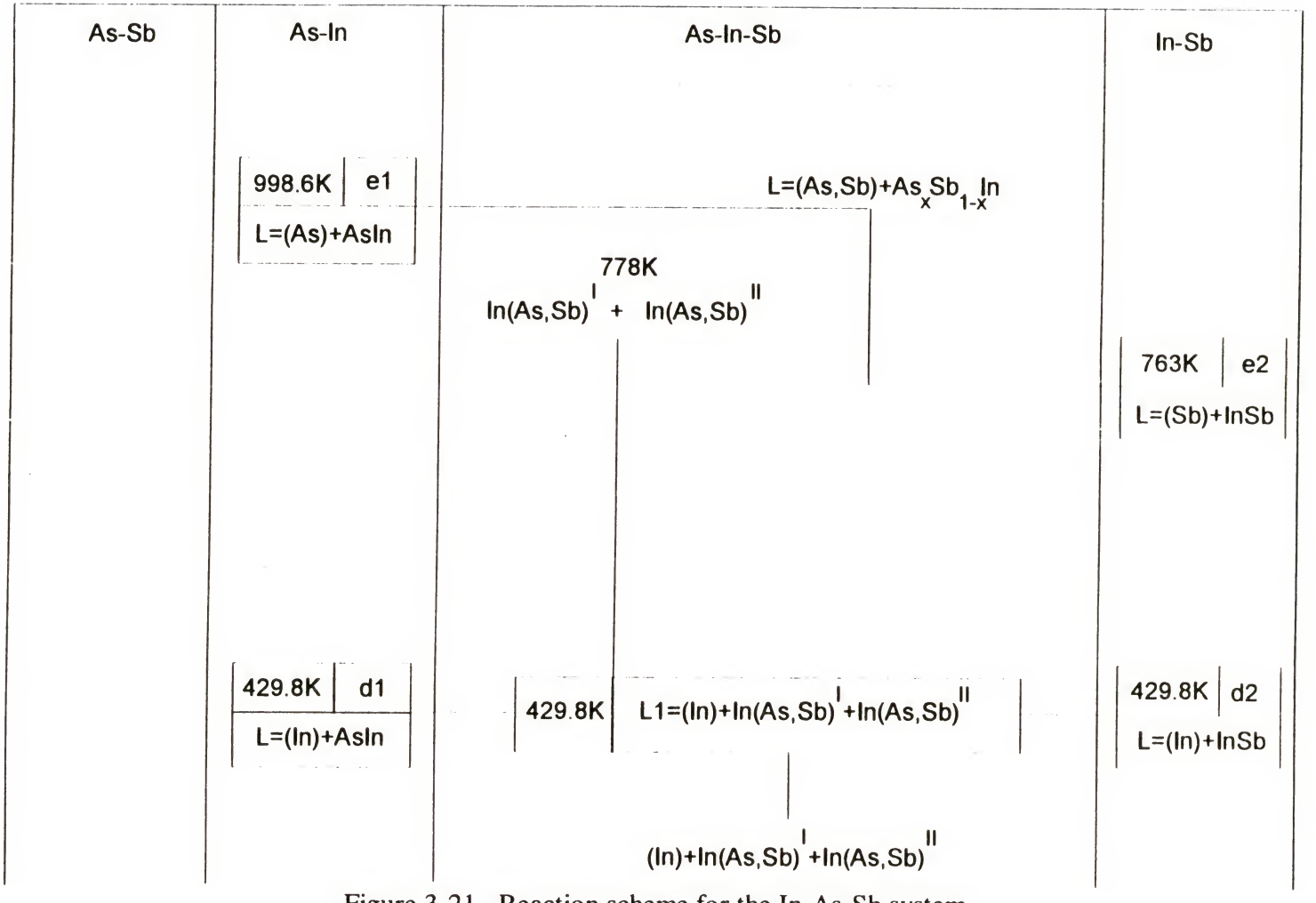

Figure 3-21. Reaction scheme for the In-As-Sb system.

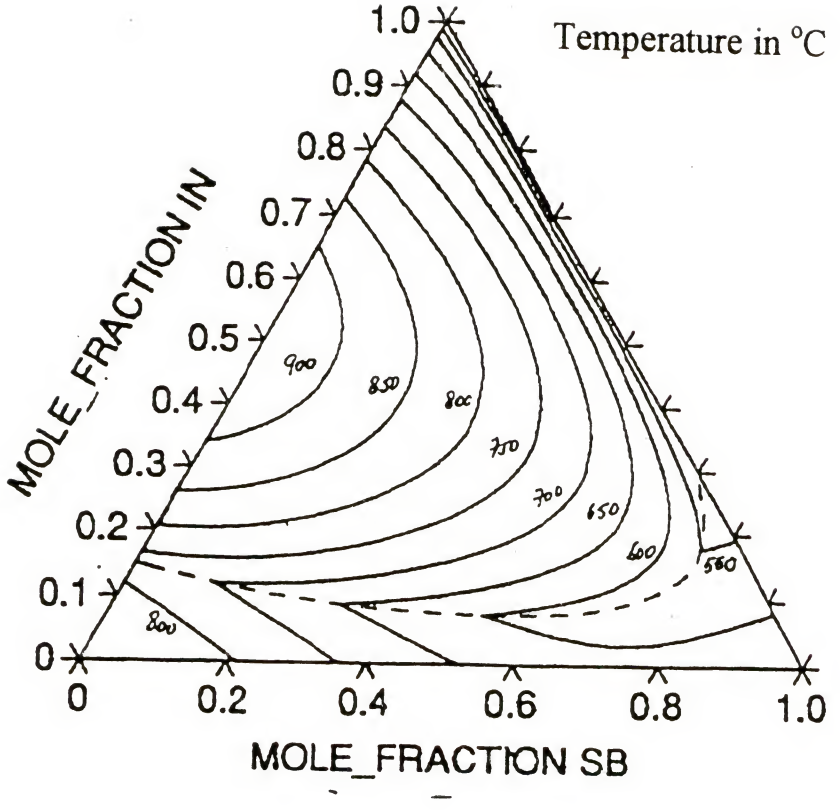

Figure 3-22. Calculated liquidus lines in the In-Sb-As system

metallographic techniques. In these studies [Shi54], the InAs-Sb section as well as three sections in the In-InAs-InSb, four sections in the Sb-InAs-InSb, and two sections in InAs-Sb-As subsystems [Shi56] were examined. Dissolution experiments were performed by Stringfellow and Greene [Str71] for solutions dilute in As at temperatures typically encountered in liquid phase epitaxy (LPE). Liquidus data were also obtained at 773 and 793 K by direct visual observation of the dissolution of a ternary crust [Abr81]. In addition to the pseudobinary liquidus measurements [Gro83], these authors also investigated six compositions dilute in As. It is well established in the literature that a significant amount of supercooling (as great as 50°C) can exist, even when using low cooling rates or a solid substrate as in the LPE experiments. In view of this difficulty, the As-dilute liquidus data are in surprisingly good agreement. Calculated liquidus lines are shown in Figure 3-22.

Solidus surface. Given the relatively low melting temperature of the elements (In: 429.75 K, As: 1090 K, Sb: 903.78 K) and the compounds (InAs: 1211 K, InSb: 800 K) and the high vapor pressure of As, solidus measurements have been difficult. This is apparent from the discussion previously given for the extent of the miscibility gap in the pseudobinary section. A considerable amount of solidus data was collected [Shi54, Shi56], though those data involving the $InAs_xSb_{1-x}$ solid solution might be questioned in view of the subsequent pseudobinary solidus measurements. Strinfellow and Greene [Str71] reported solidus data in the temperature range 793 to 1002 K by measuring the composition of films grown by an isothermal LPE process. Similarly, Abrikosov et al. [Abr81] measured the composition of LPE grown films; the data being in excellent agreement with [Str71].

Solution thermodynamics. There have been no enthalpy measurements in either the liquid or solid solution phases. Sorokina et al. [Sor84] has reported Knudsen effusion vapor pressure measurements for a wide range of compositions. Rather, the solution thermodynamics of this ternary system has largely relied on the results of assessment work or semi-empirical models [Str69, Ste70, Str72, Bat81, Kau81, Ona82a, Ona82b, Str82, Pat87, Ish89a and Ish89b].

CHAPTER 4
CONCLUSIONS

Compound semiconductor systems have been studied experimentally. The binary arsenides and antimonides were the subjects of specific interest to this study. The reason for this was that these systems determine the properties of higher order semiconductor systems to which they form important constituents. Accurate predictions of multicomponent properties are possible only through good understanding of properties in these binary limits.

The present work was successful in conducting direct measurement of thermodynamic properties through the use of solid electrolytic cells. Containment of arsenic vapors was the most difficult part in these experiments. Another problem was due to the long diffusion times required for attaining equilibrium in the solid phases of these systems. However, carefully designed electrochemical cells and the use of B_2O_3 powder in the electrodes were able to achieve this. This was evident through the stability of the electrochemical cells during operation and the return of the cells to equilibrium condition upon applying electrical and thermal perturbation to the experimental cells.

The results indicate negative deviations for Group III activity in the binary liquid melts, which are consistent with theoretical predictions. For the binary systems In-As, Ga-As and Sb-Te, the experimental results on Gibbs energy data are first of their kind.

Activity of In along the liquidus in the binary In-As phase diagram was obtained for the first time up to a temperature of 1150 K.

For Ga-As system, the Gibbs energy of formation of GaAs does not exist above 743 K. In this study, the experiments were successfully extended to temperature of up to 973 K. The values of the Gibbs energy of formation of GaAs at these high temperatures were checked for consistency using the second and third laws. The calculated value of the standard enthalpy of formation of GaAs at 298.15K, $\Delta^{\circ}H_f$(298.15 K), was in good agreement with experimental data [Mar74 and Yam94]. Taking into due consideration the uncertainities involved in the specific heat data, C_p and its thermal dependence, it was concluded that the measured values were consistent and within acceptable limits of experimental errors.

A similar anaysis was done on the Gibbs energy data for InAs in the In-As system. The analysis showed excellent agreement with experimental data for [Sha63, Sch58 and Yam94]. The existing discrepancy between the experimental and calculated values of the standard enthalpy of formation of InAs at 298.15K, $\Delta^{\circ}H_f$(298.15 K), indicates random errors inherent to experimental measurement, and systematic errors inherent to the choice of specific heat, Cp, data used in the calculations by numerous aouthors. The error analysis as presented in chapter 2 shows that the dominant effect is that of the temperature dependence of the specific heat, Cp, data.

The results obtained from experiment were analysed for consistency with other thermochemical and phase diagram data. The systems, Ga-As, In-As, In-Sb and Ga-Sb were thermodynamically assessed in the present study. Such data was utilized to perform phase equilibria calculations and predict data in the relatively difficult region of

experimentation, namely the Group V-rich region of the phase diagram. Optimizations of this nature were able to define the necessary binary limits for ternary and higher order semiconductor systems, for which data is usually scarce or non-existent. Such predictions were successfully demonstrated in two ternary systems, namely Ga-As-Sb and In-As-Sb.

Another aspect of this study was to understand the pseudobinary section GaAs-InAs. Thermodynamic study of the GaAs-InAs pseudobinary phase diagram and the Ga-In-As system provides reliable data for use in different processes such as liquid phase epitaxy, molecular beam epitaxy, and chemical vapor deposition, employed for production of multilayer devices with $Ga_xIn_{1-x}As$ solid solutions. In fact, near equilibrium epitaxial growth conditions are proven to yield devices of optimum electrical properties. A discussed in chapter 2, the existence of a miscibility gap in the GaAs-InAs pseudobinary solid phase region has been debated in the past. The experiments in the present work support the existence of a miscibility gap, and estimate the critical temperature to be between 950 K and 1050 K. More experiments in the solid phase, however, are required to characterize the solid solution of the alloys in terms of the miscibility range through activity measurements at different alloy compositions.

REFERENCES

[Abb64] Abbasov, A.S., Nikol'skaya, A.V., Gerasimov, Y.I., & Vasilev, V.P., Dokl. Akad. Nauk. SSSR, 156, 1399 (1964).

[Abb66] Abbasov, A.S., Mamedov, K.N., Nikol'skaya, A.V., Gerasimov, Y. I., & Vail'ev, V.P., Dokl. Akad. Nauk SSSR, 170, 1238 (1966).

[Abb70] Abbasov, A.S., & Mamedov, K.N., Isz. Akad. Nauk Azerb. SSR Ser. Fiz Mt. Tekhr. Nauk. 3, 86 (1970).

[Abr59] Abrikosov, N.K., Poretskaya, L.V., & Ivanova, I.P. Zh. Neorg. Khim. 4, 2525, (1959).

[Abr75] Abrikosov, N.K., Bankina, V.F., Poretskaya, L.V., Skudnova, E.V., & Chizheskaya, S.N., Semiconducting Chalcogenides & Their Alloys [in Russian], Nauka, Moscow (1975).

[Abr81] Abrokwah, J.K. & Gershenzon, M., J. Electron. Mater. 10, 2 (1981).

[Alq83] Alqasmi, R. & Egan, J.J., Ber. Buns. Phys. Chem. 87, 815, (1983).

[And75] Anderson, T.J., University of California, Berkeley, Report LBL-4148 (1975).

[And83] Anderson, T.J., Aselage, T.L., & L.F. Donaghey, J. Chem. Thermo. 15, 927 (1983).

[And84] Anderson, T.J., & Donaghey, L.F., J. Electrochem. Soc. 131, 3006 (1984).

[Ans79] Ansara, I., Int. Met. Rev. 24 (1), 20 (1979).

[Ans84] Ansara, I., & Dutartre, D., CALPHAD, 8(4), 323 (1984).

[Ans94] Ansara, I., Chatillon, C., Lukas, L., Nishizawa, T., Ohtani, H., Ishida, K., Hillert, M., Sundman, B., Argent, B.B., Watson, A., Chart, T.G., & Anderson, T.J., CALPHAD, 18(2), 177 (1994).

[Ant70] Antypas, G.A., & James, L.W., J. Appl. Phys. 41, 2165 (1970).

[Art67] Arthur, J.R., J. Phys. Chem. Solids, 28, 2257 (1967).

[Ase85] Aselage, T.L., Chang, K. M., & Anderson, T.J., CALPHAD, 9, 227 (1985).

[Ban73] Ban, V.S., & Ettenberg, M., Chem. Vap. Deposition, Int. Conf. 4th, Ed. Wakefield, G., Princeton, NJ, USA (1973).

[Bar77] Barin, I., Knacke, O., & Kubaschewski, O., Thermochemical Properties of Inorganic Substances, Springer-Verlag (1977).

[Bat81] Batura, V.P., Vigdorovich, V.N. & Selin, A.A., Diagrammy Sostoyaniya Met. Sistem. Termodinam. Raschety i Eksperim. Metody, M. 138 (1981).

[Ber74] Bergman, C., Laffitte, M., & Muggionu, Y., High Temp.-High Pressure, 6, 53 (1974).

[Bla70] Blachnik, R., & Schneider, A., Z. Anorg. Alleg. Chem. 372, 314 (1970).

[Boo57] van den Boomgaard, J., & Scol, K., Philips Res. Rept. 12, 127 (1957).

[Boo61] van den Boomgaard, J., & Scol, K., Philips Res. Chem. 65, 1275 (1961).

[Bor86] Bordas, S., Clavaguera-Mora, M.T, Legendre, B., & Hancheng, C., Thermochim. Acta, 107, 239, (1986).

[Bre54] Breckenridge, R.G., Blunt, R.F., Hosler, W.R., Fredricks, H.P.R., Becker, J.H., & Oshinsky, W., Phys. Rev. 96, 571 (1954).

[Bre80] Brebrick, R.F., J. Electrochem Soc. 127 (12), 2649 (1980).

[Bro77] Brouwer, N., & Oonk, J.A. J., Z. Phys. Chem. (Neue Folge), 105 (3/4) 113(1977).

[Ceo89] Ceolin, R., Bergman, C., Bellissent, R., Menelle, A., Rouland, J.C., & Gaspard, J.P., Solid State Comm. 71(5), 343 (1989).

[Cha73] Chatterji, D., & Smith, J.V., J. Electrochem. Soc. 120, 770 (1973).

[Cha77] Chang, K.Y., & Pearson, G.L., J. Electrochem. Soc. 124, 753 (1977).

[Cha90] Chang, Y.S., & Li, C.S., Mat. Chem. Phys. 26, 253, (1990).

[Cla82] Clavaguera-Mora, M.T., & Clavaguera, N., J. Phys. Chem.. Solids, 43, 963, (1982).

[Coo82] Cooper, C.B., Saxena, R.R. & Ludowise, M.J., J. Electrochem. Mater. 11, 1001 (1982).

[Cox67] Cox, R.H, & Pool, M.J., J. Chem Eng. Data, 12, 247 (1967).

[Cre81] de Cremaux, B., Inst. Phys. Conf. Ser. 56, 115 (1981).

[Dan70] Danilin, V.N., & S.P. Yatsenko, Tr. Inst. Khem. Akad. Nauk. SSSR, Ural. Finial, 20, 142 (1970).

[Dar53] Darken, L.S., & Gurry, R.W., Physical Chemistry of Metals, McGraw-Hill, New York, (1953).

[Das74] Dash, A.J., Finch, A., & Gardner, P.J., J. Chem. Eng. Data, 19, 113 (1974).

[Deg78] Dedegkaev, T.T., Kryukov, I.I., Lideikis, T.P., Tsorenka, B.V., &Yakovlev, Yu. P., Sov. Phys. Tech. Phys. 23, 350 (1978).

[Del79] Delcet, J., Delgado-Brune, A., & Egan, J.J., Conf. Proc. Metall. Soc. AIME. 275, (1979).

[DeM70] De Maria, G., Malaspina, L., & Piacente, V., J. Chem. Phys. 52, 1019 (1970).

[DeW85] DeWinter, J.C., & Pollack, M.A., J. Appl. Phys. 58(6), 2410 (1985).

[DeW86] DeWinter, J.C., & Pollack, M.A., J. Appl. Phys. 59, 10 (1986).

[Din86] Ding, J., Washburn, J., Sands, T., & Keramidas, V.G., Inst. Phys. Conf., 83, Las Vegas, Nevada (1986).

[Din89] Dinsdale, A.T., N. P. L. Rep. DMA (A), 195, N. P. L. Teddington, U. K. (1989).

[Dro58] Drowart, J., & Goldfinger, P., J. Chim. Physique , 55, 721 (1958).

[Dro78] Drowart, J., Smoes, S., & Vanderauwera-Mahieu, A., J. Chem. Thermodyn. 6, 123 (1978)

[Dut83] Dutartre, D., Thesis, Nr IDI 18326, Institut National des Sciences Appliques, Lyon, France (1983).

[Ega85] Egan, J.J., High Temp. Sci. 19, 111, (1985).

[Feu88] Feutelais, Y., Legendre, B., & Morgant, G., J. Thermal Anal. 34, 1093, (1988).

[Fol58] Folberth, O.G., Z. Naturforsch. 13a, 856 (1958).

[Fos72] Foster L.M., & Woods J.F. , J. Electrochem. Soc., 119, 504(1972).

[Fox73] Foxon, C.T., Harvey, J.A., & Joyce, B.A., J. Phys. Chem. Solids, 34, 1693 (1973).

[Fox74] Foxon, C.T., Joyce, B.A., Farrow, R.F.C., & Griffiths, R.M., J. Phys. D. (Appl. Phys.) 7, 2422 (1974).

[Gad61] Gadzhiev, S.N., & K.A. Sharifov, Dokl. Akad. Nauk SSSR, 136, 1339 (1961).

[Gam75] Gambino, N., & Bros, J.P., J. Chem. Thermodyn., 7, 443 (1975).

[Gar77] Garbato, L., & Ledda, F., Thermochim. Acta, 19, 267 (1977).

[Ger61] Gerasimov, Y.I., & Nikol'skaya, A.V., Vopr. Met. Fiz. Polyprov. Akad. Nauk SSSR Tr. 4-go (i.e. Chetvertogo), 30 (1961).

[Ger65] Gerasimenko, L.N., Kirichenko, I.V., Lozhkin, L.N., & Morachevskii, Electrokhim., Akad. Nauk SSSR, Otd. Obshch. i. Tekhn. Kim., Sb. Statei, 236 (1965).

[Gho89] Ghosh, G., Lukas, H.L, &. Delaey, L., Z. Metallkde. 80, 731, (1989).

[Gla58] Glazov, V.M, & Petrov, D.A., Tzv. Akad. Nauk. SSSR, Otd. Tekhn. Nauk. 4, 125 (1958).

[Gla69] Glazov, V.M, Chizheuskaya, S.N., & Glagolera, N.N., Liquid Semiconductors, Plenum Press, New York (1969).

[Glu72] Glushko, V.P., (ed.), Thermal Constants of Materials [in Russian], VINITI, 4, 184, Moscow (1972).

[Gol59] Goldfinger, P., & Jeunehomme, M., Adv. Mass Spectrom. 1, 534 (1959).

[Gor75] Gorbov, S.I., Series on Chemical Thermodynamics and Equilibrium (in Russian), Gerasimov, Ya.I., (ed.), Izd. VINITI Akad. Nauk SSSR, Moscow (1975).

[Gor83] Goryacheva, V.I., Geiderikh, V.A., & Gerasimov, Y.I, Russ. J. Phys. Chem. 57, 1637 (1983).

[Gra73] Gratton M.F., Woolley J.C., J. Electron Mater. 2, 455 (1973).

[Gra80] Gratton, M.F., Woolley, J.C., Electroless Copper Plating, 127.1, 55 (1977).

[Gre55] Greenfield, I.G., & Smith, R.L., Trans. AIME, 203, 351 (1955).

[Gro83] Gromova, T.I., Evgen'ev, S.B. & Borisov, S.R., Izv. Akad. Nauk SSSR, Neorg. Mater., 19(3), 341-343 (1983).

[Gut61] Gutbier, H.B., Z. Naturforsch. 16a, 268, (1961).

[Hal63] Hall, R.N., J. Electrochem. Soc. 110, 385 (1963).

[Hau40] Hauffe, K., & Wagner, C., Z. Electrochem. 46(3), 160 (1940).

[Heg88] Hegewald, S., Hein, K., & John, M., Z. Anorg. Allg. Chem. 564, 148 (1988).

[Hei78] Heime, A., & Pagnia, H., Appl. Phys. 15, 79 (1978).

[Hil85] Hillert, M., Jansson, B., Sundman, B., & Agren, J., Metall. Trans. A, 16A, 261, (1985).

[Hir85] Hirayama, C., Straw, R.D., & Hobgood, H.M., J. Less-Comm. Metals, 109, 331 (1985).

[Hol72] Holste, J.C., Phys. Rev. 6, 2495 (1972).

[Hos65] Hoshino, H., Nakamura, Y., Shimoji, M., & Niwa, K., Ber. Bunsenges. Phys. Chem., 69(2), 114 (1965).

[Hsi66] Hsi-Hsiung, C., Peng-Nien, C., & Mo, C.C., Acta Met. Sinica, 9, 113 (1966).

[Hsi74] Hsieh, J.J., unpublished, Lincoln Laboratory Solid State Research Quarterly Report, Liverpool, 3, 25 (1974).

[Hsi77] Hsieh, J.J., Met. trans. 8A, 403 (1977).

[Hul73] Hultgren, R., Desai, P.D., Hawkins, D.T., Gleiser, M., Kelley, K.K., & Wagman, D.D., American Society for Metals (1973).

[Hur96] Hurle, D.T.J., Emis Datarev. Ser., 16, 557 (1996).

[Ino70] Inoue, J., Osamura, K., & Murakami, Y., Suiyokaishi, 17, 71 (1970).

[Ino71] Inoue, J., Osamura, K., & Murakami, Y., Trans. Japan Inst. Metals, 12, 13 (1971).

[Ish88] Ishida, K., Shumiya, T., Nomura, T., Ohtani, H., & Nishizawa, T., J. Less Common Met. 142, 135 (1988).

[Ish89a] Ishida, K., Nomura, T., Tokunaga, H., Ohtani, H., & Nishizawa, T., J. Less-Common Met., 155(2), 193 (1989).

[Ish89b] Ishimura, M., & Wada, T., J. Crystal Growth, 97, 542 (1989).

[Ita75] Itagaki, K., & Yazawa, A., J. Jpn. Inst. Met. 39, 880 (1975).

[Ita77] Itagaki, K., & Yazawa, A., Trans. Jpn. Inst. Met. 18, 825 (1977).

[Ito82] Itoh, S., Hino, M., & Azakami, T., J. Jap. Inst. Met. 46 (2), 162, (1982).

[Jan85] Janaf Thermochemical Tables, M. W. Chase ed. (third edition), 14, Published by the American Chemical Society and the American Institute of Physics for the National Bureau of Standards, New York, NY 100017, USA (1985).

[Jen67a] Jena, A.K., Bever, M.B., & Banus, M.D., Trans. Metall. Soc. AIME, 239, 725 (1967).

[Jen67b] Jena, A.K., Bever, M.B., & Banus, M.D., Trans. Metall. Soc. AIME, 239, 1232 (1967).

[Jor70] Jordan, A.S., Metall. Trans., 1, 239, (1970).

[Kar73] Karataev, V.V., Mil'vidskii, M.G., Nemtsova, G.A., Rakov, V.V., & Dolgikh, I.A., Izv. Akad. Nauk SSSR, Neorg. Mater. 11, 830 (1973).

[Kar75] Karataev, V.V., Mil'vidskii, M.G., & Nemtsova, G.A., Izv. Akad. Nauk SSSR, Neorg. Mater. 11(5), 830 (1975).

[Kat89] Katayama, I., Nakai, T., Inomoto, T., & Kozuka, Z., Materials Transactions, JIM, 30, 354 (1989).

[Kat87] Katayama, I., Nakayama, J., Nakai, T., & Kozuka, I., Trans. Jpn. Inst. Met. 28, 129 (1987).

[Kau81] Kaufman, L., Nell, J., Taylor, K. & Hayes, F., CALPHAD, 5(3), 185 (1981).

[Khu74a] Khukhryanskii, Yu.P., Kondaurov, V.P., Nikolaeva, F.P., Panteleev, V.I., & Shshevelev, M.I., Izv. Akad. Nauk SSSR Neorg. Mater. 10, 1877 (1974).

[Khu74b] Khkhryanskii, Yu.P., Kondaurov, V.P., Nikolaeva, F.P., & Panteleev, V. I., Russ. J. Phys. Chem. 48, 909 (1974).

[Kle51] Kleppa, O.J., & Weil, J.A., J. Am. Chem. Soc. 73, 4848 (1951).

[Kle55] Kleppa, O.J., J. Am. Chem. Soc. 77, 897 (1955).

[Kno85] Knobloch, G., & Gottschalch, V., Crystal Res. Technol. 20, 1205 (1985).

[Kos55] Koster, W., & Thoma, B., Z. Metallkd. 46, 291 (1955).

[Kot88] Kotchi, K.P., Gilbert, M., & Castanet, R., J. Less-Common Met. L1, 143, (1988).

[Kre71] Krestovnikov, A.N., Ufimtsev, V.B., & Solopai, E.M., Russ. J. Phys. Chem. 45, 1504 (1971).

[Kre71] Krestovnikov, A.N., Solopai, E.M., & Ufimtsev, V.B., Dokl. Akad. Nauk. SSSR, 208(2), 365 (1973).

[Lee92] Lee, H.D., Ph. D. Dissertation, University of Florida, Gainesville (1992).

[Lel81] Lele, S., & Ramachandrarao, P., Metall. Trans. B. 12B, 659 (1981).

[Len81] Lendvay, E., Görög, T., & Tóth, A.L., J. Crystal Growth 53, 591 (1981).

[Lia82] Liao, P.K., Su, C.H., Tung, T., & Brebrick, R.F., CALPHAD, 6, 141 (1982).

[Lic69] Lichter, B.D., & Sommelet, P., Trans. Metall. Soc. AIME, 245, 99 (1969).

[Lit91] Litvak, A.M., & Charykov, N.A., Ivestiya Akad. Nauk SSSR, Neorg. Mater. 2(2), 225 (1991).

[Liu52] Liu, T.S., & Peretti, E.A., Trans. ASM, 44, 539 (1952).

[Luk77] Lukas, H.L., Henig, E.Th., & Zimmermann, B., CALPHAD, 1(3), 225 (1977).

[Lum66] Lumsden, J., Thermodynamics of Molten Salt Mixtures, Academic Press, London (1966).

[Lun63] Lundin, C.E., Pool, M.J., & Sullivan, R.W., Denver Research Report AFORL-63-156 (1963).

[Lyo61] Lyons, V.J., & Silvestri, V.J., J. Phys. Chem. 65, 1275 (1961).

[Mae72] Maekawa, T., Yokokawa, T., & Niwa, K., J. Chem. Thermodyn. 4, 153 (1972).

[Mag68] Maglione, M.H., & Potier, A., J. Chim. Phys. 65, 1595 (1968).

[Mal71] Malinowsky, M., Chem. Zvesti, 25(2), 92 (1971).

[Mal86] Mallika, C., & Sreedharan, O.M., J. Chem. Thermodyn. 18, 727 (1986).

[Man86] Mani H, Joullie A, Karouta F, J. Appl. Phys. 59(8), 2728 (1986).

[Man90] Mani, V.N., Dhanasekaran, R., & Ramasamy, P., J. Crystal Growth, 99, 333 (1990).

[Mar74] Martosudirjo, S., & Pratt, J.N., Thermochim. Acta, 10, 23 (1974).

[Mar90] Marchant, A.B., Optical Recording—A Technical Overview, Addison-Wesley Publishing Company, (1990).

[Mec71] Mechkovskii, L.A., Savitskii, A.A., Skums, V.F., & Vecher, A.A., Russian J. Phys. Chem. 45, 1143 (1971).

[Mik65] Miksovski, M. & Kulwicki, B.M., J. Electrochem., Soc. 112, 149C (1965).

[Mul64] Muller, E.K. & Richards, J.L., J. Applied Phys. 38, 4 (1964).

[Nac58] Nachtrieb, N.H., & Clement, N., J. Phys. Chem. 62, 876 (1958).

[Nah77] Nahory R.E., Pollack M.A., DeWinter J.C., & Williams K.M., J. Appl. Phys. 48, 1607 (1977).

[Nak78] Nakajima, F., & Kobayashi, M., J. Appl. Phys. 17, 149 (1978).

[Nat81] Nataf, G., & Verie, C., J. Crystal Growth, 55(1), 87 (1981).

[Nga88] Ngai, T.L., Sharma, R.C., Chang, Y.A., Bulletin of Alloy Phase Diagrams, 9 (1988).

[Nik59] Nikol'skaya, A.N., Geiderikh, V.A., Gerasimov, Ya. I., Dokl. Akad. Nauk SSSR, 130, 1074 (1959).

[Oeh78] Oehme, G., & Predel, B., Thermochim. Acta, 22, 267 (1978).

[Ona82a] Onabe, K., Jpn. J. Appl. Phys. 21(6), 964 (1982).

[Ona82b] Onabe, K., Jpn. J. Appl. Phys. 21(6), 323 (1982).

[Pan72] Panish, M.B., & Ilegems, M., Progress in Solid State Chemistry, Reis, H., & McCaldin, J.O. (eds.), Pergamon Press, 7(2), 39 (1972).

[Pan74] Panish, M.B., J. Crystal Growth, 27, 6 (1974).

[Pat87] Patrick, R. & Chen, A.B., Phys. Rev. B, 36(6), 6585 (1987).

[Pen65] Perea, E.H., & Fonstad, C.G., J. Electrochem. Soc. 127, 313 (1980).

[Per80] Peng-nien, C., & Chin-chi, M., Acta Netall. Sin. 8, 32 (1965).

[Pes83] Pessetto, J.R., & Stringfellow, G.B., J. Crystal Growth, 62, 1 (1986).

[Pie63] Piesbergen, U., Z. Naturforsch. 18(a), 141 (1963).

[Poe86] van der Poel, C.J., Gravesteijn, D.J., Rippens, W.G.V.M., Stockx, H.T.L.P., & van Uigen, C.M.J., J. Appl. Phys. 59, 1819, (1986).

[Pog49] Pogodin, S.A., & Dubinsky, S.A., Izv. Sektora Fiz. Khim., 17, 204 (1949).

[Pon75] Pong, R., University of California, Berkeley, Report LBL-2785 (1975).

[Pre71] Predel, B., & Stein, D.W., J. Less Common Met. 24, No. 4, 391 (1971).

[Pre76] Predel, B., & Oehme, G., Z. Metallkd. 67, 826 (1976).

[Pro78] Proks, J., Chem. Zvesti, 32(4), 433 (1978).

[Pup74] Pupp, C., Murray, J.J., & Pottie, R.F., J. Chem. Thermodyn. 6, 123 (1974).

[Rak70] Rakov, V.V., Lainer, B.D., & Mil'vidskii, M.G., Russ. J. Phys. Chem. 44, 922 (1970).

[Rau75] Rau, H., J. Chem. Thermodyn. 7, 27 (1975).

[Ric63] Richman, D., J. Phys. Chem. Solids, 24, 1131 (1963).

[Ric65] Richman D., & Hockings, E.F., J. Electrochem. Soc. 112, 461 (1965).

[Ros80] Rosa, C.J., Rupf-Bolz, N., Sommer, F., & Predel, B., Z. Metallkd. 71, 320 (1980).

[Rub66] Rubinshteiin, R.N., & Kozlovskaya, V.M., J. Electrochem. Soc. 113, 752 (1966).

[Rug95] Rugg, B.C., Silk, N.J., Bryant, A.W., & Argent, B.B., CALPHAD, 19(3), 389 (1995).

[Sau86] Saunders, N., & Mioddownik, A.P., Report to the Scientific Group Thermodata Europe, March (1986).

[Sch58] Schottky, W.F., & Bever, M.B., Acta Metallurg. 6, 320 (1958).

[Sch59] Schneider, A., & Klotz, K., Naturwissenschaften, 46, 141 (1959).

[Sch61] Schneider, A., Klotz, H., Stendel, J., & Strauss, G., Pure Appl. Chem. 2, 13 (1961).

[Sem69] Semenkovich, S.A., & Melekh, B.T., Symp. The Chemical Bond in Crystals, Izd. Nauk. Tekhnika: Minsk, USSR, 277, (1969).

[Sem74] Semikolenova, N.A. & Khabarov, E.N., Sov. Phys. Semicond. 8(11), 1459 (1974).

[Sew75] Sewell, H., & Anderson, J.G., Solid State Electron. 18, 641 (1975).

[Sha87] Sharma, R.C., Ngai, T.L., & Chang, Y.A., J. Electron. Mater. 16, 307 (1987).

[Sha63] Sharifov, K.A., Gadzhiev, S.N., & Garibov, I.M., Izv. Akad. Nauk Azer.SSR Ser. Fiz. Mat. Tekhn. Nauk, 2, 53 (1963).

[She95] Shen, J.Y., Chatillon, C., Ansara, I., Watson, A., Rugg, B., & Chart, T., CALPHAD, 19(2), 215 (1995).

[Shi53] Shih, C., & Peretti, E.A., J. Amer. Chem. Soc. 75, 608 (1953).

[Shi54] Shih, C. & Peretti, E.A., Trans. Amer. Soc. Metals, 46, 389 (1954).

[Shi56] Shih, C.H. & Peretti, E.A., Trans ASM, 48, 706 (1956).

[Sir67] Sirota, N.N., & Yushkevich, N.N., Chemical Bonds in Semiconductors, N.N. Sirota, ed., 95, Consultants Bureau, New York (1967).

[Sir68] Sirota, N.N., Semiconductors & Semimetals, 4, ed. Williarson, P.K., & Beer, A.C., Academic Press, New York (1968).

[Sol74] Sol, N., Clariou, J.P., Linh, N.T., & Moulin, M., J Crystal Growth, 27, 325 (1974).

[Som82] Sommer, F., Z. Metallkde. 73, 72, (1982).

[Sor84] Sorokina, O.V., Evgen'ev, S.B. & Zhukov, A.P, Izv. Akad. Nauk SSSR, Neorg. Mater. 20(2), 200 (1984).

[Ste70] Steininger, J., J. of Applied Phys. 41(6), 2713 (1970).

[Str65] Straumanis, M.E., & Kim, C.D., J. Appl. Phys. 112, 112 (1965).

[Str69] Stringfellow, G.B. & Greene, P.E., J. Phys. Chem. Solids, 30, 1779 (1969).

[Str71] Stringfellow, G.B., & Greene, P.E., J. Electrochem. Soc. 118, 805 (1971).

[Str72] Stringfellow, G.B., J. Phys. Chem. Solids, 33, 665 (1972).

[Str82] Stringfellow, G.B., J. Electron. Mater. 11(5), 903 (1982).

[Str83] Stringfellow, G.B., J. Appl. Phys. 54, 404 (1983).

[Sug77] Sugiyama, K. & Oe, K., Japan J. Appl. Phys. 16,197 (1977).

[Sza80] Szapiro, S., J. Phys. Chem. Solids, 41, 279 (1980).

[Ter59] Terpilowski, J., Arch. Hutn. 4, 355 (1959).

[Ter60] Terpilowski, J., & Trzebiatowski, W., Bull. Acad. Poln. Sci. (Chim.) 8, 95 (1960).

[Tma84] Tmar, M., Gabriel, A., Chatillon, C., & Ansara, I., J. Crystal Growth, 69, 421 (1984).

[Tma87] Tmar, M., & Chatillon, C., J. Chem. Thermodyn. 19, 1053 (1987).

[Tma88] Tmar, M., & Chatillon, C., J. Crystal Growth, 89(4), 501 (1988).

[Uij85] van Uijen, C.M.J., SPIE, Proc. 2, 529 (1985).

[Vec74] Vecher, A.A., Voronova, E.I., Mechkovskii, L.A., & Skoropanov, A.S., Russ. J. Phys. Chem. 48, 584 (1974).

[Vig73] Vigdorovich, E.N., Popov, V.V., Artamanou, M.M., & Andreev, V.M., Izv. Akad. Nauk SSSR Neorg. Mater. 9, 771 (1973).

[Vor76] Voronin, G.F., Dokl. Akad. Nauk SSSR, 196(1), 133 (1971).

[Wag57] Wagner, C., Thermodynamics of Alloys [Russian Translation], Metallurgizdat, Moscow (1957).

[Was82] Wasai, K., & Mukai, K., J. Jpn. Inst. Metals, 46, 266 (1982).

[Wel52] Welker, H., Z. Naturforsch. 7a, 744 (1952).

[Wel53] Welker, H., Z. Naturforsch. 89, 248 (1953).

[Wit67] Wittig, F.E., & Gehring, E., Ber. Bunsenges. Phys. Chem., 71, 29 (1967).

[Woo58] Woolley, J.C. & Smith, B.A., Proc. Phys. Soc. 72, 214 (1958).

[Woo62] Woolley, J.C., Compound Semiconductors, Williamson, R.K., & Goering, H., (eds.) Reinhold Publishing, New York (1962).

[Woo64] Woolley, J.C. & Warner, J., J. Electrochem. Soc. 111, 1142 (1964).

[Wyp88] Wypartowicz, J., & Fitzner, K., J. Less-Comm. Metals, 138, 289 (1988).

[Yam88] Yamaguchi, K., Itagaki, K., & Yazawa, A., J. Jap. Inst. Metals, 52, 966 (1988).

[Yam91] Yamada, N., Ohno, E., Nishiuchi, K., & Akahirat, N., J. Appl. Phys. 69, 2849, (1991).

[Yam94] Yamaguchi, K., Takeda, Y., Kameda, K., & Itagaki, K., Materials Transactions, J. Jpn. Inst. Metals, 35, 9 (1994).

[Yaz68] Yazawa, A., Kawashima, T., & Itagaki, K., J. Jpn. Inst. Metals, 32, 1288 (1968).

[Yos75] Yoshido, T., Miyazaki, K., & Fujisawa, K., Jpn. J. Appl. Phys. 14, 1987 (1975).

BIOGRAPHICAL SKETCH

The author, Sudhanshu Misra was born in Allahabad in India on November 4, 1964. His interest in science and engineering together with the inspiration from his father, a professor and a well known researcher in chemistry, led him to pursue a career in chemical engineering. He joined the chemical engineering program at the Indian Institute of Technology, Bombay, in India for a bachelor's degree in 1983. After graduating with a bachelor's degree in 1987, he joined Colorado State University, Fort Collins, in the U.S.A for an M.S. in chemical engineering. He graduated with an M.S. degree in chemical engineering in 1989. Immediately thereafter he joined the chemical engineering department at the University of Florida for a doctoral degree. In early 1994, he took up a job as a Quality Engineer at Altatron, Inc., in Fremont, California after which he joined IMP, Inc., in San Jose, California as a process engineer. In 1995, he joined the flash memory development group at Texas Instruments, Inc., as a process development engineer. He is currently a senior process development engineer at Lucent Technologies in Orlando, Florida, working on chemical mechanical polishing (CMP) for intermetal planarization.

I certify that I have read this study and that in my opinion it conforms to acceptable standards of scholarly presentation and is fully adequate, in scope and quality, as a dissertation for the degree of Doctor of Philosophy.

Timothy J. Anderson, Chairman
Professor of Chemical Engineering

I certify that I have read this study and that in my opinion it conforms to acceptable standards of scholarly presentation and is fully adequate, in scope and quality, as a dissertation for the degree of Doctor of Philosophy.

Ranga Narayanan
Professor of Chemical Engineering

I certify that I have read this study and that in my opinion it conforms to acceptable standards of scholarly presentation and is fully adequate, in scope and quality, as a dissertation for the degree of Doctor of Philosophy.

Mark E. Orazem
Professor of Chemical Engineering

I certify that I have read this study and that in my opinion it conforms to acceptable standards of scholarly presentation and is fully adequate, in scope and quality, as a dissertation for the degree of Doctor of Philosophy.

Rolf E. Hummel
Professor of Materials Science and Engineering

I certify that I have read this study and that in my opinion it conforms to acceptable standards of scholarly presentation and is fully adequate, in scope and quality, as a dissertation for the degree of Doctor of Philosophy.

Fan Ren
Associate Professor of Chemical Engineering

This dissertation was submitted to the Graduate Faculty of the College of Engineering and to the Graduate School and was accepted as partial fulfillment of the requirements for the degree of Doctor of Philosophy.

December, 1998

Winfred M. Philips
Dean, College of Engineering

M. J. Ohanian
Dean, Graduate School